This thesis

is submitted for the

Degree of Doctor of Philosophy

in

the Faculty of Engineering

at

the University of Glasgow.

September, 1962.

ProQuest LLC.
789 East Eisenhower Parkway
P.O. Box 1346
Ann Arbor, MI 48106 – 1346

Acknowledgements.

The author wishes to express his appreciation for the continuous assistance and encouragement given by Mr.J.H. Collins throughout this work.

The constant interest and helpful suggestions of Profs. I.N. Sneddon and J. Lamb are gratefully acknowledged.

The helpful advice given by Mr.R. McLean and Mr.F. Aitken of Ferranti Ltd., Edinburgh on the experimental side of the work has been most valuable.

Many others in the Electrical Engineering Department have helped in several ways. Particular thanks are due to Mr.J. Richter and Mr.H.J.J. Seguin for many helpful discussions and to Mr.G. Boyle who skilfully constructed most of the test pieces.

Thanks are also due to Dr.D.C. Gilles of the Computing Laboratory and his staff for their assistance and for the use of DEUCE computer.

The work has been done under a Research Studentship awarded by D.S.I.R., to whom thanks are given for providing a maintenance grant.

Contents.

1. Introduction.

Since Polder[1], in 1949, first discovered the gyromagnetic nature of magnetisation in a ferrite medium, large-scale investigations have taken place into the behaviour of guided electromagnetic wave propagation in ferrites and numerous devices have been built which depend for their existence on the reciprocal and non-reciprocal nature of the propagation. Included in this category are the isolator, circulator and non-reciprocal phase-shifter. Before proceeding to discuss the particular interest in ferrite propagation in this thesis, an account of the fundamental nature of propagation in ferrites is given.

Polder's initial discovery was that, in order to relate the magnetic flux density and field intensity in a ferrite medium, a tensor permeability is required, i.e.,

$$\underline{B} = \tilde{\mu} . \underline{H}.$$

where $\tilde{\mu}$ is the ferrite tensor permeability.

At low frequencies ($\sim$ 100 Mc/s), the off-diagonal component of the tensor becomes negligibly small and $\tilde{\mu}$ reduces to a scalar. The discussion in this thesis is confined to ferrites operating in the microwave region, (1 - 100 Gc/s) where the off-diagonal component is significant. The total magnetisation vector of a magnetised ferrite has associated with it, an angular momentum arising from the aggregate of the angular momenta of all the unpaired electron spins. Because of this angular momentum, the magnetisation behaves as a gyroscope, i.e. if the magnetisation vector is displaced from its equilibrium position under the influence of a uniform d.c. magnetic field, it will precess like a top round the axis of the d.c. magnetic field at a

frequency determined by the magnitude of the d.c. magnetic field. Due to the damping mechanism in the ferrite crystal structure, the magnetisation vector tends to line up with the d.c. field after an interval of time which is typically 10^{-8} sec. However, the precession can be maintained by forced oscillations which take the form of an applied r.f. magnetic field at right - angles to the d.c. biassing field. If the precession frequency, determined by the magnitude of the d.c. magnetic field, coincides with the frequency of the driving field, a large precession angle is possible and a large amount of power is absorbed from the driving field and dissipated in the ferrite crystal lattice. This situation is described as ferromagnetic resonance. When the magnetisation precesses, a component of magnetisation and hence, magnetic flux density is set up at right-angles to the d.c. field. The tensor nature of the permeability follows from this fact. When the d.c. field acts in the z-direction, the tensor is given by:-

$$\tilde{\mu} = \begin{bmatrix} \mu & -j\kappa & 0 \\ +j\kappa & \mu & 0 \\ 0 & 0 & \mu_o \end{bmatrix}$$

where μ and κ are related to the d.c. field, H, the saturation magnetisation, M and the operating frequency, f.

In an infinite magnetised ferrite medium, two types of propagation are normally considered[2] - in the direction of the d.c. field and normal to the d.c. field. In the former case, it has been shown[3] that the normal modes have circularly polarised magnetic fields and that the tensor permeability reduces to a scalar which is different for the two senses of

polarisation. For the positive sense, where the magnetic field rotates in the same direction as the precession, the permeability is $\mu - \kappa$, and in the opposite sense, $\mu + \kappa$. Owing to the different propagation constants for opposite senses of circular polarisation, the electric field vector of a linearly-polarised wave is rotated as the wave passes through the ferrite medium. This rotation has been termed Faraday rotation. In the case of propagation normal to the direction of the d.c. field, the ferrite behaves as a dielectric medium when the magnetic field is parallel to the d.c. field and possesses an effective scalar permeability when the electric vector is parallel to the d.c. field.

Although analyses of wave guide configurations using ferrites would be valuable, it is usually sufficient to consider the propagation of plane waves together with a physical reasoning for a working explanation.

In this thesis, an attempt is made to discover means of broadbanding the microwave resonance isolator, using uniform field biassing. A description of the operation of the three main types of isolator and a brief history of the resonance isolator is given as an introduction.

When an energy source operates into a mismatched load, a certain amount of power is reflected back into the generator. Apart from the fact that the energy is lost from this load, this effect is undesirable because it may have serious effects on the output of the source. The source frequency may be shifted - this effect is called frequncy - pulling -, the output power is also affected and the reflected energy is dissipated in the source. Previous attempts to prevent the reflected power from reaching the source have been to insert an attenuating pad between source and load. The pad, of course, not only attenuates the reflected energy but also reduces the

energy transmitted to the load. The latter effect is always undesirable. However, the isolator is a device which overcomes this difficulty. It absorbs large amounts of reflected power without significantly affecting the power travelling from the source to the load. The isolator is, by nature, non-reciprocal. The loss in db suffered by a reflected wave travelling through the isolator is called reverse loss and the small loss occuring in the opposite direction of propagation is called forward loss. The three common types of isolator used in pratice are discussed.

The Faraday rotation isolator[4] consists of a circular waveguide holding an axially-magnetised ferrite rod together with resistive vanes orientated at 45° at either end of the circular section. When the d.c. field and frequency are adjusted to produce 45° of rotation of a linearly-polarised wave, the device works as an isolator. The input and output waveguides are rectangular and this necessitates transitions into the circular waveguide. The non-reciprocal nature of the rotation insures that waves travelling in opposite directions have their electric vectors parallel and normal respectively to the attenuating vanes. Thus, the wave travelling in one direction is absorbed by the vane and the wave in the opposite direction is left unattenuated. The bandwidth of this isolator is narrow and is operation is critically dependent on temperature.

The field-displacement isolator,[5,6,7] using rectangular waveguide has a thin ferrite strip, transversely magnetised, with a resistive card placed against one side of the ferrite. When the d.c. biassing field and the ferrite position are suitably fixed, an electric field null appears at the ferrite face where the card is located for one direction of propagation but

not for the other. A high reverse loss occurs in the resistive card whilst the forward loss remains low. The field-displacement isolator operates far from resonance so that the size of the biassing magnet can be small. However, the isolator is difficult to build because of the sensitivity of the isolation ratio with respect to the position of the strip, the d.c. field amplitude and the low-field loss in the ferrite. Furthermore, the field-displacement isolator is limited to low-power operation as there is no good heat sink from the ferrite.

The most widely-used isolator is the resonance type. The earliest isolators[8] employed a thin strip of transversely-magnetised ferrite assymetrically-positioned in a rectangular waveguide. The ferrite biassed to resonance and absorbs power from the travelling wave in the waveguide. If the r.f. magnetic field is circularly-polarised in the same sense as the elctron spin precession, a large amount of power is absorbed. For the other sense of polarisation, the wave passes almost intact. The ferrite is placed in a position of circular polarisation and non-reciprocal attentuation results. This is because a wave polarised in one sense and travelling in the +z-direction looks to the ferrite like a wave polarised in the other sense when travelling in the -z-direction. The loss in the +z-direction is called the reverse loss and in the -z-direction, the forward loss. In general, the magnetic field in the rectangular waveguide is elliptically- polarised causing the isolation to have a finite bandwidth. (The linewidth of the ferrite resonance also affects the bandwidth).

High reverse losses were obtained with the full-height ferrite slab

but the isolation ratio, (the ratio of reverse-to-forward loss), was disappointingly low. Fox[8] found that making the ferrite slab very thin to avoid the variation of circular polarisation with position across the ferrite, did not entirely eliminate the presence of considerable forward loss. It was also observed that by using a ferrite of less than full guide height, the isolation ratio was much improved over the full-height case. This occured at the expense of reverse loss per unit length. Weiss[9] has investigated the isolation properties of the H-plane and E-plane isolators. In the H-plane isolator, two ferrite slabs were placed on the top and bottom faces of the wave-guide, respectively, with the broad slab dimension parallel to transverse H. The broad face was parallel to transverse E in the E-plane isolator. In both cases the isolator ratio was much improved on the performance of earlier isolators - isolation ratios of 75 to 1 for H-plane and 60 to 1 for the E-plane isolators to be compared to 25 to 1 for earlier isolators.

Weiss also showed that dielectric loading of the waveguide results in generally-improved performance. The reverse loss was increased due to the energy concentration in the dielectric. Also the reverse-to-forward loss was improved.

The bandwidth of the isolation can be increased by using different types of ferrite[10], tapering of the d.c. magnetic field by means[11] of tapered pole pieces or using different thicknesses and heights of ferrites in tandems. A broadband resonance isolator[12] with a bandwidth of 4.5Gc/s has been built at S band in parallel-plate transmission line by using dielectric concentration effects in conjunction with a narrow-linewidth ferrite biassed with an inhomogeneous magnetic field.

The broadbanding effect can also be achieved by using waveguide structures where the dependence of the position of circular polarisation with frequency is made small. This can be arranged by removing, as far as possible, the variation with frequency of the axial propagation constant. two such structures as the dielectric loaded rectangular waveguide[13] and the ridged waveguide. A coaxial line resonance isolator which uses dielectric loading to create regions of circularly-polarised field at the dielectric face, has been reported in the literature. Also, resonance isolators[14] working at C- and S band have been reported which use ridged waveguide with dielectric loading between the ridge and the top waveguide wall.

With uniform field biassing, the bandwidth of the resonance isolator depends on (a) the linewidth[15] of the ferrite and (b) the degree to which the r.f. magnetic field remains circularly polarised with respect to frequency at the ferrite location. The linewidth may suitably be dealt with by a suitable choice of ferrite material and by field tapering mentioned earlier. The second factor is more serious than the first, in the present state of the art, and the discussion in this work on resonance isolators is exclusively concerned with the behaviour of the circular polarisation of the r.f. magnetic field.

The conventional approach to problems of this kind has been to investigate the fields in structures which are expected to have the necessary conditions of circular polarisation and to place the ferrite in the position of the circular polarisation predicted by theory. This procedure has the obvious limitation that, if the perturbation of the fields by the ferrite is

large, the theoretical results are invalid. Fortunately, the ferrite perturbation does not seem to be serious when its cross-section is small. From a mathematical point of view, this is very convenient because the derivation of the electromagnetic fields in most ferrite configurations in waveguides is exceptionally difficult. Thus an analysis is made of the waveguide structure without the ferrite and the ferrite properties used to determine the behaviour in the presence of the ferrite.

Basically, problems concerning the propagation of electromagnetic waves in waveguides are solved by finding the appropriate solutions of Maxwell's equations which satisfy the prescribed boundary conditions on the waveguide walls. In a loss-less and source-free region of space, Maxwell's equations are[6]:-

$$\text{curl } \underline{E} = \dot{\underline{B}}$$

$$\text{curl } \underline{H} = \dot{\underline{D}}$$

$$\text{div } \underline{B} = 0$$

$$\text{div } \underline{D} = 0$$

$$\text{where } \underline{D} = \epsilon \underline{E} \quad \text{and} \quad \underline{B} = \mu \underline{H}$$

Eliminating either $\underline{E}$ or $\underline{H}$ from the above equations we obtain the vector wave equation:

$$\underline{\nabla}^2 \underline{H} + \omega^2 \mu \epsilon \underline{H} = 0$$

$$\underline{\nabla}^2 \underline{E} + \omega^2 \mu \epsilon \underline{E} = 0$$

In a rectangular cartesian coordinate system, each component of $\underline{E}$ or $\underline{H}$ satisfies the wave equation,

$$\nabla^2 \phi + \omega^2 \mu \epsilon \phi = 0$$

where ϕ is any component of $\underline{E}$ or $\underline{H}$.

When the waveguide being considered has circular boundaries, it is possible to find a wave equation through which all the propagating field components may be derived. Assuming that propagation takes place in the waveguide, in the axial z-direction with dependence $e^{-j\beta z}$, the wave equation may be written in its two-dimensional form,

$$\nabla_t^2 \phi + k^2 \phi = 0$$

where 't' denotes transverse coordinates.

$$k^2 = \omega^2 \mu e - \beta^2$$

The fields in waveguide structures are found on solution of the wave equation in the particular configuration being considered. The normal method of solution is to separate the wave equation into two ordinary differential equations and to find the solutions of these which satisfy the boundary conditions. In many cases, however, this procedure is not simple especially when the boundary conditions are complicated, e.g. the ridged waveguide. The resulting mathematical complexity of the solution makes the preparation of programmes for an automatic digital computer a difficult task. A numerical method seems to be more suited to the problem of finding particular solutions in waveguide structures. Young and Hohmann[17] have used a relaxation procedure to determine the cut-off frequencies of single and double ridged waveguides. In this work, a finite difference method is used which allows both the eigen-vectors and eigenvalues of the wave equation to be determined simultaneously. Although

most of the problems discussed in this work are concerned with resonance isolators, it must be stressed that the finite-difference method is quite separate and a powerful tool in dealing with waveguide problems in general.

The first part of the thesis is concerned with a definition of the polarisation factor and the analytical solution of the wave equation for dominant mode propagation in the dielectric loaded waveguide, (section 3) and the ridged waveguide, (section 4). Section 5 begins with an introduction to finite-differences and proceeds to show the application of the theory to the simple problem of dominant mode propagation in the rectangular waveguide, for which the solution is already known. The section ends by dealing with the ridged waveguide by finite-differences and comparing the results to those of section 4. Certain inhomogeneous waveguides are discussed in section 6, also by finite-differences. The experiments performed are described in section 7 and the results given. Calculations of loss in dielectric and ferrite samples in waveguides are given in section 8 and further applications of the finite-difference method to problems involving cylindrical geometries, in section 9.

2. Polarisation Characteristics of Waveguide Structure.

The discussion in this section is limited to waveguide structures excited in the dominant H-mode, whose field components are expressed in rectangular cartesian coordinates. The y-axis is taken as the direction of the d.c. magnetic field, and the z-axis as the direction of propagation in the absence of the ferrite. The unloaded fuide fields are assumed to be perturbed negligibly by the ferrite sample. Shapes of sample for which this procedure is valid are discussed by Soohoo.[18]

The x and y components of microwave magnetic field may be related through the equation

$$H_x = jP\,(x,y,f)\,H_z \qquad 2.1.$$

The quantity, P, is defined as the polarisation factor at frequency f, at a point x,y, in the waveguide cross-section. When the r.f. magnetic field is circularly polarised

$$P\,(x_o,y_o,f_o) = 1 \qquad 2.2.$$

The object of the investigation into the behaviour of P in certain waveguide structures is to find how the deviation of $P\,(x_o,y_o,f)$ from unity can be minimised. A suitable standard for comparison purposes is the rectangular waveguide, operating in the H_{01} mode, of broad dimension A, cut-off frequency f_c, which has a value of P given by

$$P = \left((f/f_c)^2 - 1 \right)^{\frac{1}{2}} \tan \frac{\pi x}{A} \qquad 2.3.$$

where $f_c = \dfrac{c}{\lambda_c}$, $\lambda_c = 2A$

This formula indicates that $\dfrac{\partial P}{\partial f}$ is minimised in the neighbourhood

of unity P by taking $f \gg f_c$. This criterion is limited by the onset of propagation of the H_{02} mode at $f = 2f_c$. However, $\frac{\partial P}{\partial f}$ may also be minimised by reducing f_c. This may be accomplished by (a) introducing a dielectric slab into the waveguide or (b) inserting a ridge into the waveguide cross-scetion. The effect of these alterations is discussed in sections 3 and 4 respectively. It is also feasible to obtain the minimising effect by increasing A, thereby lowering f_c. The main objection to this is that the problem of matching the section of waveguide with increased width to ordinary waveguide of width A, is considerable, especially when the match is required over the whole operating frequency range. For this reason, the idea of increasing A is abandoned and in all cases where X band waveguide is mentioned, A is the standard 0.90".

3. Dielectric Slab Loaded Waveguide.

3.1. Indroduction.

The relation between free-space wavelength, λ_o, and guide wavelength λ_g, in a rectangular waveguide is given by[19]

$$\lambda_g^2 = \frac{\lambda_o^2}{1 - (\frac{\lambda_o}{\lambda_c})^2} \qquad 3.1.1.$$

where λ_c is the cut-off wavelength.

However, when the rectangular waveguide is partially filled with a dielectric slab, there is no such simple relation between λ_o and λ_g. This is because the transverse wavenumber (equal to $\frac{2\pi}{\lambda_c}$ in the case of the rectangular waveguide) is no longer constant, but is frequency-dependent, and has separate values in air, k_A, and in dielectric, k_D. In fact

$$k_A^2 = \beta_o^2 - \beta^2 = (\frac{2\pi}{\lambda_o})^2 - (\frac{2\pi}{\lambda_g})^2 \qquad 3.1.2.$$

$$k_D^2 = \beta_o^2 e_r - \beta^2 = (\frac{2\pi}{\lambda_o})^2 e_r - (\frac{2\pi}{\lambda_g})^2 \qquad 3.1.3.$$

where e_r is the dielectric permittivity.

The relation betwenn k_A and k_D is determined from the characteristic equation which is derived by applying the continuity conditions at the dielectric face to the field expressions in the two media. From the characteristic equation, the dispersion curve may be drawn, i.e. the variation of λ_g with λ_o. Only then is it possible to calculate the dependence of P with frequency and with position in the cross-section.

The characteristic equation, derived by Lewin[20], is obtained in the following section.

3.2. Characteristic Equation.

The geometry of the dielectric slab loaded waveguide is shown schematically in the Fig. 3.1. The dominant H-mode is assumed to propagate along the z-axis with longitudinal field dependence $e^{-j\beta z}$. The field expressions in regions 1, 2, and 3 may be written down, omitting the dependence $e^{+j(\omega t - \beta z)}$:

Region 1

$$E_y = \sin k_A x.$$

$$H_x = \frac{\beta}{\omega\mu} \sin k_A x. \qquad 3.21.$$

$$H_z = \frac{jk_A}{\omega\mu} \cos k_A x.$$

Region 2

$$E_y = M \sin k_D x + N \cos k_D x$$

$$H_x = \frac{\beta}{\omega\mu} (M \sin k_D x + N \cos k_D x) \qquad 3.2.2.$$

$$H_z = \frac{jk_D}{\omega\mu} (M \cos k_D x - N \sin k_D x)$$

Region 3

$$E_y = L \sin k_A (A - x)$$

$$H_x = \frac{\beta L}{\omega\mu} \sin k_A (A - x) \qquad 3.2.3.$$

$$H_z = \frac{-jk_D}{\omega\mu} L \cos k_A (A - x)$$

We define the non-dimensional quantities, s_1 and s_2 to be

$$s_1 = \frac{d}{A} \qquad s_2 = \frac{D}{A}$$

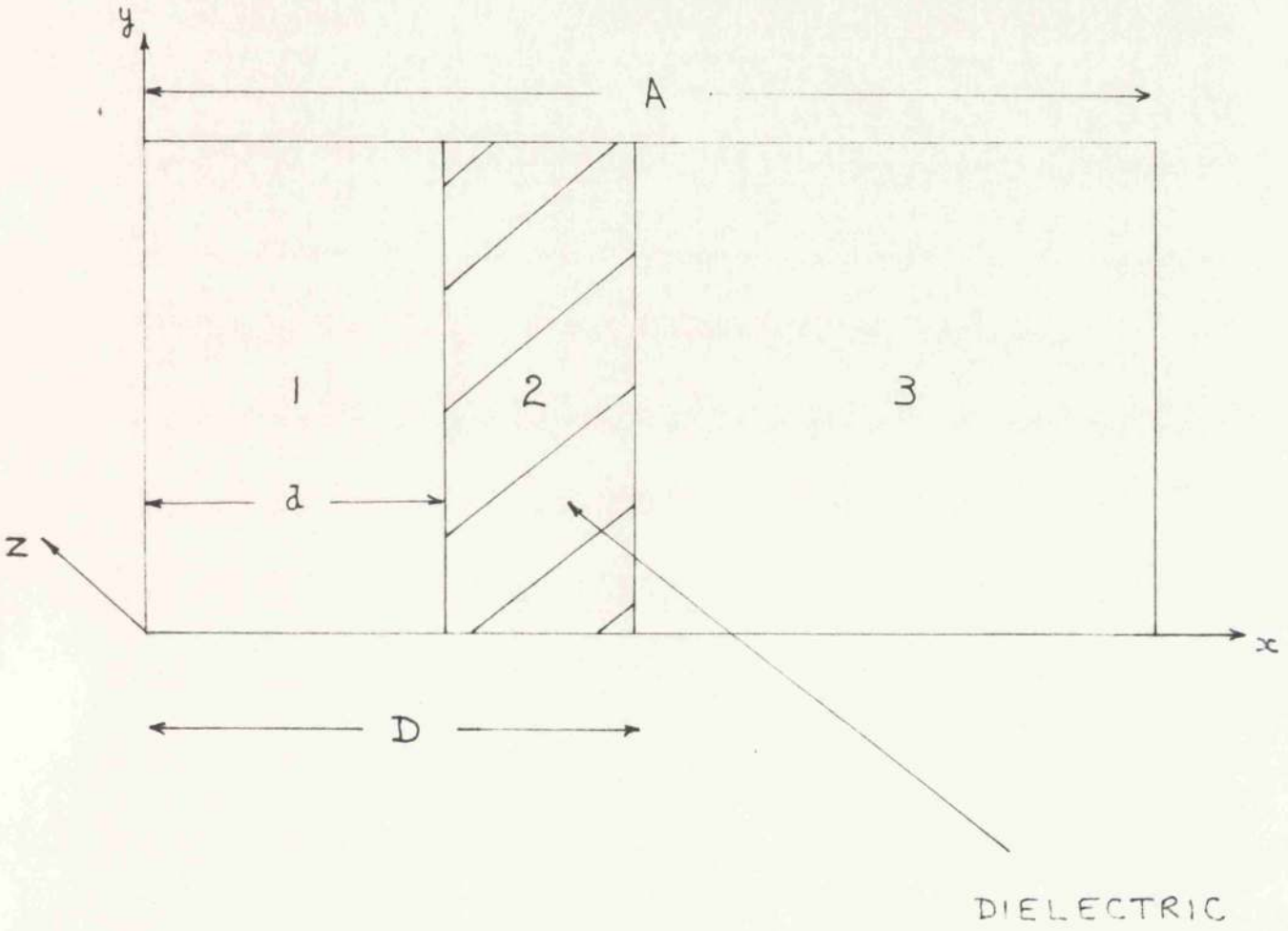

DIELECTRIC THICKNESS = t

" CONSTANT = ϵ_T.

FIGURE 3.1.

As previously mentioned, the characteristic equation is found by applying the continuity conditions at $x = s_1A$ and $x = s_2A$.

1. $(E_y)_1 = (E_y)_2$ at $x = s_2A$

$$\sin k_A A s_2 = M \sin k_D A s_2 + N \cos k_D A s_2 \qquad 3.2.4.$$

2. $(H_z)_1 = (H_z)_2$ at $x = s_2A$

$$k_A \cos k_A A s_2 = k_D (M \cos k_D A s_2 - N \sin k_D A s_2) \qquad 3.2.5.$$

3. $(E_y)_2 = (E_y)_3$ at $x = s_1A$

$$L \sin k_A A (1 - s_1) = M \sin k_D A s_1 + N \cos k_D A s_1 \qquad 3.2.6.$$

4. $(H_z)_2 = (H_z)_3$ at $x = s_1A$

$$- L \cos k_A A(1 - s_1) = k_D (M \cos k_D A s_1 - N \sin k_D A s_1) \qquad 3.2.7.$$

Dividing 3.2.4. by 3.2.5. and 3.2.6. by 3.2.7., there results the following pair of equations for $\frac{M}{N}$:-

$$\frac{M}{N} = \frac{\frac{k_A}{k_D} \tan k_D A s_2 - \tan k_D A s_2}{1 + \frac{k_D}{k_A} \tan k_D A s_2 \tan k_A s_2} \qquad 3.2.8.$$

$$\frac{M}{N} = \frac{\tan k_D A s_1 + \frac{k_D}{k_A} \tan k_A A(1 - s_1)}{\frac{k_D}{k_A} \tan k_A A(1 - s_1) \cdot \tan k_D A s_1 - 1} \qquad 3.2.9.$$

Equating the right-hand sides of equations 3.2.8. and 3.2.9. and rearranging, we have : -

$$\tan k_D A(s_1 - s_2) + \frac{k_D}{k_A} \frac{\tan k_A A (1 - s_1) + \tan k_A A s_2}{1 - (\frac{k_A}{k_D})^2 \tan k_A A(1 - s_1) \tan k_A A s_2} = 0 \quad 3.2.10.$$

Equation 3.2.10. is the characteristic equation mentioned in section 3.1. For the purpose of convenience, the characteristic equation is written in the following form:-

$$\tan F + \tan (G_1 + G_2) = 0 \quad 3.2.11.$$

$$F = k_D A (s_1 - s_2) \quad 3.2.12.$$

$$\text{where } \tan G_1 = \frac{k_A}{k_D} \tan k_A A s_2 \quad 3.2.13.$$

$$\text{and } \tan G_2 = \frac{k_A}{k_D} \tan k_A A(1 - s_1) \quad 3.2.14.$$

3.3. Solution of the Characteristic Equation.

The parameters of equation 3.2.11. are s_1, s_2 and e_r. The variable, $u = \frac{\lambda_o}{\lambda_g}$ is introduced and inserted into equation 3.2.11. The only unknown remaining is $\frac{2A}{\lambda_o}$ which may be found by trial-and-error or by iteration. The iteration procedure is admirably suited to automatic computation and, for this reason a programme in alphacode interpretive scheme has been written for the DEUCE computer. An outline of the procedure involved is described at this juncture.

The solution of equation 3.2.11. is: -

$$F + G_1 + G_2 + m\pi = 0 \qquad 3.3.1.$$

where m is zero for the dominant mode.

Having specified all the parameters of the waveguide and the variable, u, a guess is assumed for the value of F which satisfies equation 3.3.1.

According to Taylor's theorem, the true value of the left-hand side of equation 3.3.1., (f(F)), may be expanded in terms of the value obtained from the guess and its derivatives, i.e.

$$f(F_o) = f(F_1) + hf^1(F_1) \qquad 3.3.2.$$

where $h = F_1 - F_o$

Therefore, since $f(F_o)$ is zero,

$$h = - \frac{f(F_1)}{f^1(F_1)} \qquad 3.3.3.$$

A better approximation to the true value of F is now obtained by adding h to the previous value of F. The whole process is repeated until the value of F is close enough to F_o so that

$$f(F) \leqslant \delta \qquad 3.3.4.$$

where δ is an arbitrarily small number. At this point the iteration is stopped and the value of $\frac{2A}{\lambda_o}$ calculated algebraically from F by means of equations 3.1.2. and 3.2.11. Thus, one point on the dispersion curve is located - usually the cut-off condition (u = 0) is obtained first. Other points on the dispersion curve are obtained

by increasing the value of u and repeating the iteration procedure described above using the old value of F as the first approximation to the new F. On the digital computer, the dispersion curve is obtained automatically by prescribing a set interval in u.

At any point on the curve, the unknown field coefficients L, M and N may be calculated, enabling the field components over the whole cross-section to be worked out. Also the polarisation factor, P, and the ratio of the transverse magnetic field strength to the square root of the total power flow are simply deduced. This last quantity is of importance in deciding the axial length of the ferrite material to be placed in the position of circular polarisation because the attenuation per unit length of the ferrite depends on the magnitude of the r.f. field presented to it. The overall power flow is calculated from the complex Poynting vector, $E \times H^*$,

$$W = \int_S (\underline{E} \times \underline{H}^*)_z \cdot d\underline{S} \qquad 3.3.5.$$

where S is the waveguide cross-section.

The integral in equation 3.3.5. is split into three parts - W_1 and W_3 to give the power flow in regions 1 and 3, and W_2 to give the power flow in the dielectric, (Fig. 3.1.).

On evaluation of the integrals we find that

$$W_1 = \frac{e_o}{\mu_o} u R \left(s_2 - \frac{\sin 2k_A A s_2}{2k_A A}\right) \qquad 3.3.6.$$

$$W_2 = \frac{e_o}{\mu_o} u R(M^2 + N^2)\left[(s_1 - s_2) - \frac{\sin 2(k_D A s_1 + \theta)}{2 k_D A} + \frac{\sin 2(k_D A s_2 + \theta)}{2 k_D A} \right] \qquad 3.3.6.$$

$$W_3 = \frac{e_o}{\mu_o} u R L^2 \left[(1 - s_1) - \frac{\sin 2k_A A(1 - s_1)}{2k_A A} \right]$$

$$\text{where } R = \frac{bA}{+2} \left(\frac{\mu_o}{e_o} \right)^{1/2} \qquad \theta = \tan^{-1} \left(\frac{M}{N} \right) \qquad 3.3.7.$$

The ratio of H_x to $W^{\frac{1}{2}}$ introduced earlier in this section may beworked out for region 1 by means of equations 3.2.1. and 3.3.6. This expression, however, is not dimensionless and a dimensionless form is defined by the following equation

$$\bar{H}_x = H_x \left(\frac{R}{W} \right)^{\frac{1}{2}} \quad \text{where } \bar{H}_x \text{ is dimensionless}$$

$$= \frac{(u)^{\frac{1}{2}}}{g} \sin k_A x \qquad 3.3.8.$$

where $g =$

$$\left\{ \left(s_2 - \frac{\sin 2k_A A s_2}{2k_A A} \right) + (M^2 + N^2) \left[(s_1 - s_2) - \frac{\sin 2(k_A A s_1 + \theta)}{2k_A A} + \frac{\sin 2(k_A A s_2 + \theta)}{2k_A A} \right] + L^2 \left[(1 - s_1) - \frac{\sin 2k_A A (1 - s_1)}{2k_A A} \right] \right\}^{\frac{1}{2}} \qquad 3.3.9.$$

The corresponding expression for $\bar{H}_x$ in a rectangular waveguide propagating the dominant H-mode is

$$(\bar{H}_x)_A = (u)^{\frac{1}{2}} \sin \frac{\pi x}{A} \qquad 3.3.10.$$

The maximum value of $(\bar{H}_x)_A$ is $\frac{1}{2}$ when $\frac{x}{A}$ is $\frac{1}{2}$ and $u = 1$. A comparison of $\bar{H}_x$ with the maximum value of $(\bar{H}_x)_A$ is useful in deciding the ratio of the axial lengths of ferrite to be used in the case of the rectangular waveguide and the dielectric slab loaded waveguide.

3.4. Discussion of results.

The following quantities have been computed for a series of parameters, s_1, s_2 and e_r as a function of u :-

1. $2A/\lambda_o$
2. $P(s_2A,y,f)$
3. M
4. N.
5. L.
6. $\overline{H}_x$ at $x = s_2A$.
7. H_x at $x = s_2A$.

These quantities are presented as a function of u in Table 3.1. for a typical dielectric loaded waveguide, ($e_r = 12$, $t/A = 0.20$) The cut-off wavelength is sharply increased when the dielectric is introduced into a rectangular waveguide. The dispersion curve rises rapidly at values of $2A/\lambda_o$ near cut-off but levels off for larger values. In X band, ($1.28 \leqslant 2A/\lambda_o \leqslant 1.86$), the values of u are all greater than unity, (see Table 3.1.). Consequently, for this particular loading, the phase velocity of the travelling wave is less than that of light throughout X band and the air-filled section of the waveguide is transversely cut-off, i.e. k_A is imaginary. The energy in the wave tends to concentrate in the dielectric, setting up a high field strength at the dielectric face, (see $\overline{H}_x$ in Table 3.1.) This situation should be compared with that of the empty rectangular waveguide where the phase velocity is always greater than that of

Table 3.1. Dispersion curve and fields; $s_1 = 0.6$ $s_2 = 0.4$ $e_r = 12$

u	$\frac{2A}{\lambda_o}$	P	$\bar{H}_x$	M	N	$\bar{L}_x$	$\overline{H_x}$
0.0	0.4212	0.0000	0.0000	0.4229	-0.3718	1.0000	0.0000
0.4	0.4269	0.2337	0.6274	0.3906	-0.3543	1.0000	0.1889
0.8	0.4453	0.4653	0.8900	0.2611	-0.2620	1.0000	0.2636
1.2	0.4816	0.6896	1.0969	0.2953	-0.3627	1.0000	0.4948
1.6	0.5476	0.8916	1.2810	0.5368	-0.9860	1.0000	1.5510
2.0	0.6732	1.0377	1.4605	0.3725	-2.4509	1.0000	4.0972
2.4	0.9228	1.0862	1.6326	-3.8415	-7.3885	1.0000	14.970
2.8	1.4179	1.0702	1.6880	-84.657	-14.504	1.0000	147.88
3.2	2.7815	1.0527	1.3638	-24062.	45462.	1.0000	65839.

light and the field dependence is sinusoidal.

The field coefficient,L, which is theoretically unity when the dielectric is symmetrical about the centre of the waveguide is calculated by means of equation 3.2.6. from M and N. The closeness of the computed value of L to unity determines the accuracy of the solution of the transcendental equation and provides a check that no error exists in the computer programme.

The effect of slab thickness and permittivity on the polarisation factor,P, is shown in Figs.3.2a. and 3.2b.,(the variation of P with y is zero since the fields are independent of y for the dominant mode). In Fig.3.2a., $P(s_2A,y,f)$ is plotted over X band for three dielectric slabs having permittivity, $e_r = 12$, but different thicknesses. On the same Figure, P is drawn over X band for the case of the rectangular waveguide in the guide position where P is unity at $2A/\lambda_o = 1.60$. In Fig.3.2b., the variation of $P(s_2A,y,f)$ is plotted for three dielectric slabs having the same thickness, but different permittivity.

In Fig.3.2a., The curve of polarisation factor against frequency rises very sharply, in the case of the rectangular waveguide, on either side of the centre frequency. Defining the bandwidth of circular polarisation as the range in frequency for which P is less than 1.10, it is apparent that, as compared with the dielectric loaded guides, the rectangular waveguide is narrow-band. From the curves referring to the dielectric loaded waveguides, it is observed that the minimum value of P over the band is obtained for the dielec-

FIGURE 3.2a.

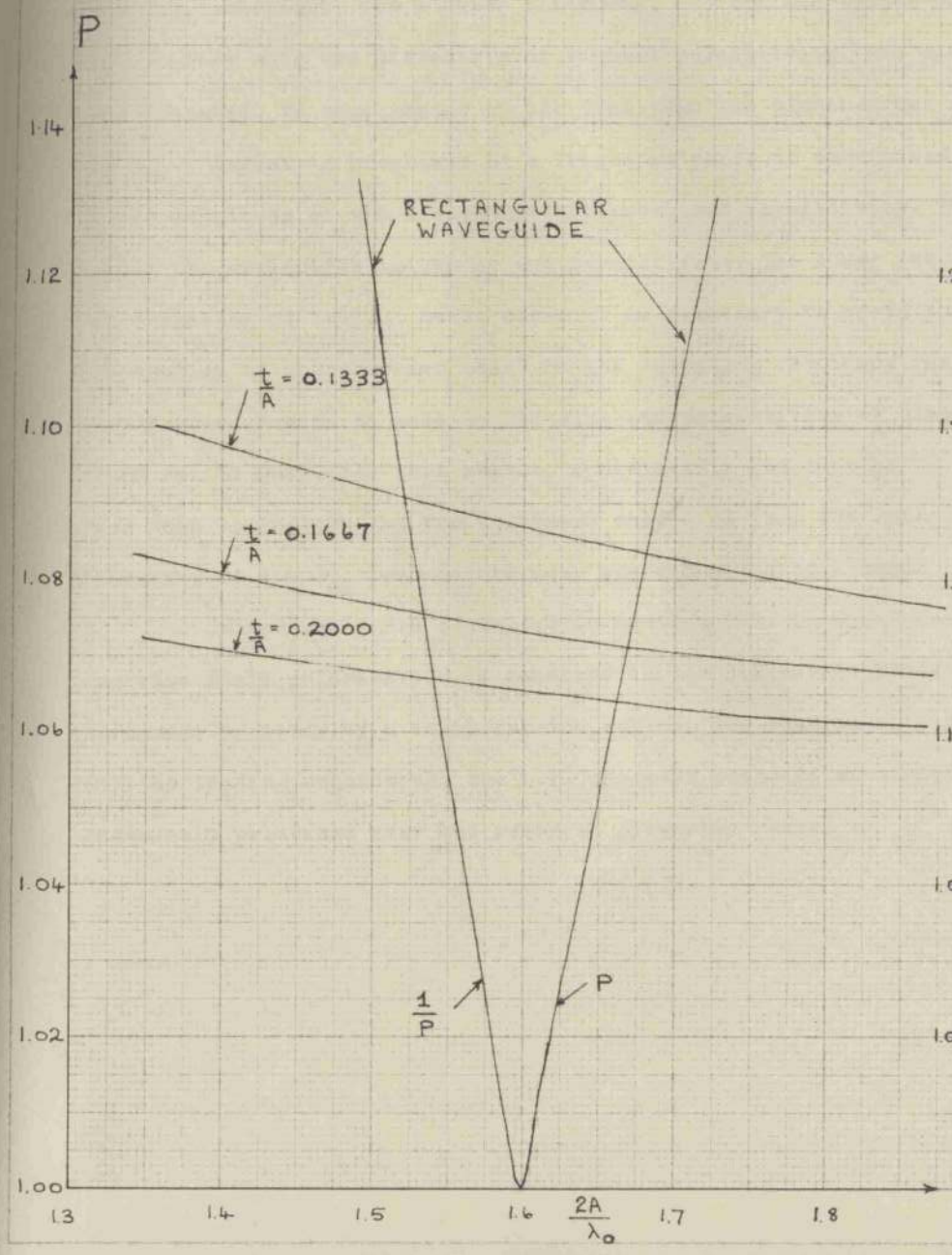

FIGURE 3.2b.

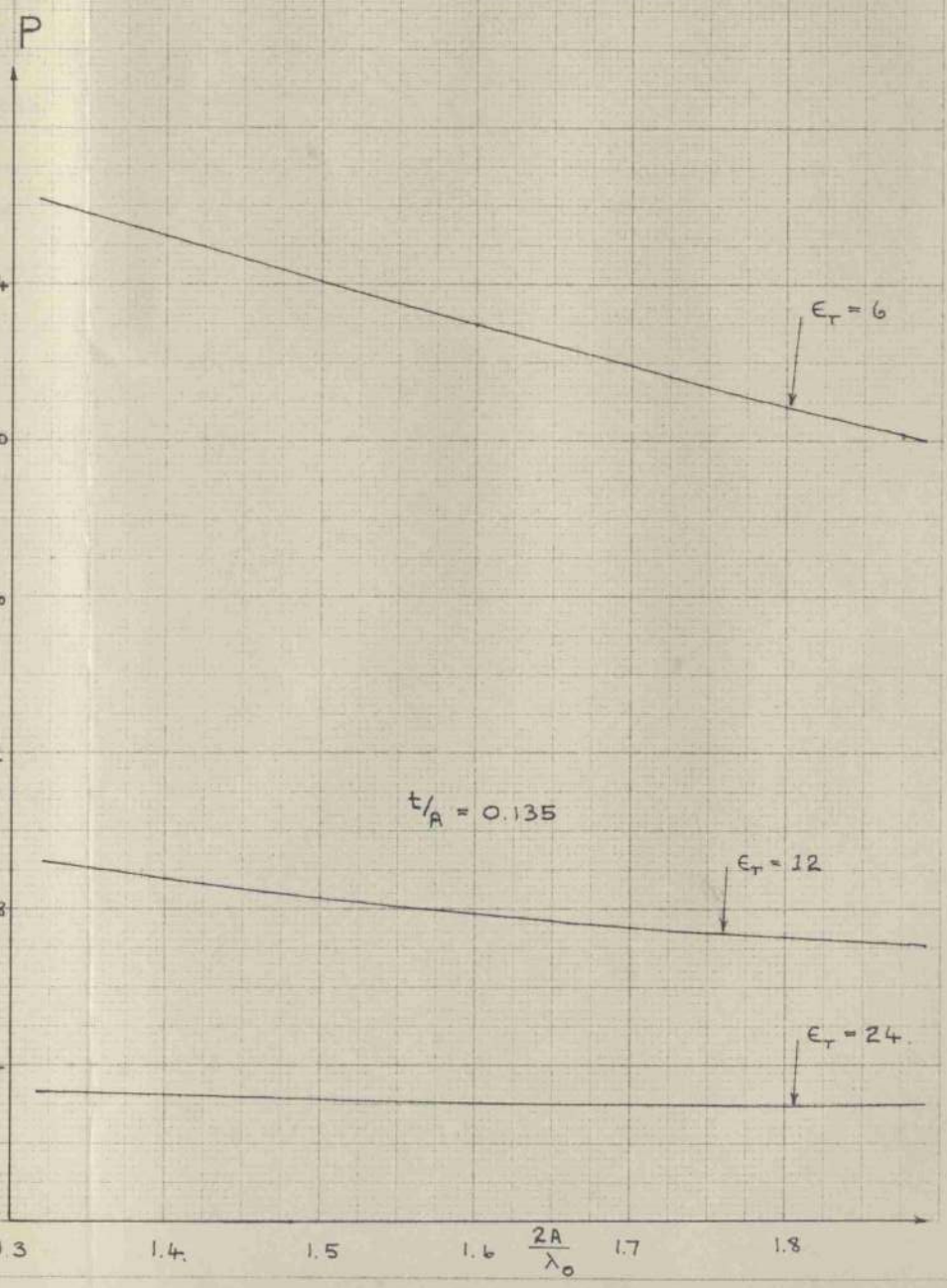

tric with the largest thickness and that, in each case, the bandwidth of circular polarisation covers the whole of X band. It is observed from Fig.3.2b. that, for a given thickness, the minimum values of P are obtained with the dielectric of highest permittivity. The situation, however, is complicated by the fact that the higher-order mode, the H_{02} , begins to propagate at a frequency which is determined by the magnitude of the dielectric thickness and permittivity. The larger the dielectric thickness and permittivity, the lower the cut-off frequency of the H_{02} mode. Since it is necessary to avoid the propagation of higher-order modes in the operating frequency range, a compromise has to be made in the size and permittivity of slab which can be used. For this reason, a dielectric constant of 12 has been used throughout and the thickness chosen so that the cut-off frequency of the H_{02} mode occurs near the upper end of X band.

Experiments are described in section 7.2. in which the magnetic field polarisation is measured in the dielectric loaded waveguide by means of a small ferrite sphere. The results show that, for the loading considered, the r.f. magnetic field is substantially circularly polarised over the measured frequency range.

4. Ridged Waveguide - Orthogonal Modes.

4.1. Introduction.

Cohn[21] and other authors have shown that the introduction of a ridge into a rectangular waveguide depresses the cut-off frequency of the dominant mode whilst having little effect on the cut-off frequencies of the higher-order modes. The difficulty which may be met with in the use of dielectric slab loaded waveguides for isolator applications - the propagation of unwanted modes at higher frequencies - is thus avoided in the ridged waveguide. To the present author's knowledge no published figures have been presented for the field expressions in the ridged waveguide. In the present section the cut-off relations and the field expressions are found by orthogonal mode approach similar to that used by P.N. Butcher[22] on the slotted ridged waveguide. The complicated set of boundary conditions on the ridged waveguide walls are satisfied by expressing the field components as infinite Fourier series in terms of fundamental solutions of the wave equation. Satisfaction of the boundary conditions results in an infinite number of linear equations in the coefficients of the Fourier series. The determinant of these equations must be zero for a non-trivial solution. It is necessary to use an approximation to the doubly-infinite determinant and a 2 x 2 determinant is chosen as a reasonable approximation. The solution of the determinantal equation provides the cut-off wavelength, and the field expressions and circular polarisations factor, P, may be deduced.

4.2. Solution of the Wave Equation.

The transverse cross section of a typical single-ridged waveguide

is chosen in Fig. 4.1. The air-filled region, in which solutions to the two dimensional wave equation are sought, is divided into two rectangular regions, 1 and 2.

$$\text{Region 1.} \quad \left(\frac{A}{2} - a\right) \leqslant x \leqslant \frac{A}{2}, \quad -(B + b) \leqslant y \leqslant -B$$
$$\text{Region 2.} \quad 0 \leqslant x \leqslant \frac{A}{2}, \quad -B \leqslant y \leqslant 0. \qquad 4.2.1.$$

Solutions of the wave equation satisfying the boundary conditions on the metal walls and the axis of symmetry, are written down as infinite series whose coefficients are determined by applying the remaining boundary condition on the line of continuity of the two regions:

$$y = -B, \quad \frac{A}{2} - a \leqslant x \leqslant \frac{A}{2} \qquad 4.2.2.$$

Thus in region 1,

$$\phi_1 = e^{-j\beta z} \sum_{m=0} \phi_{1m} \sinh p_{1m} \frac{y+B+b}{A} \cos \frac{m}{a}\left(x - \frac{A}{2}\right). \qquad 4.2.3.$$

In region 2,

$$\phi_2 = e^{-j\beta z} \sum_{m=1} \phi_{2m} \cosh p_{2m} \frac{y}{A} \sin \frac{m x}{A} \qquad 4.2.4.$$

$$p_{1m}^2 = (\beta^2 - \beta_o^2) A^2 + \left(\frac{m\pi A}{a}\right)^2$$
$$p_{2m}^2 = (\beta^2 - \beta_o^2) A^2 + (m\pi)^2 \qquad 4.2.5.$$
$$\text{where } (\beta^2 - \beta_o^2) = \left(2\frac{\pi}{\lambda_c}\right)^2$$

The electromagnetic field components are derived from ϕ through equations 5.1.1.

On the line of continuity between regions 1 and 2, all field components are continuous.

In the case of E_x,

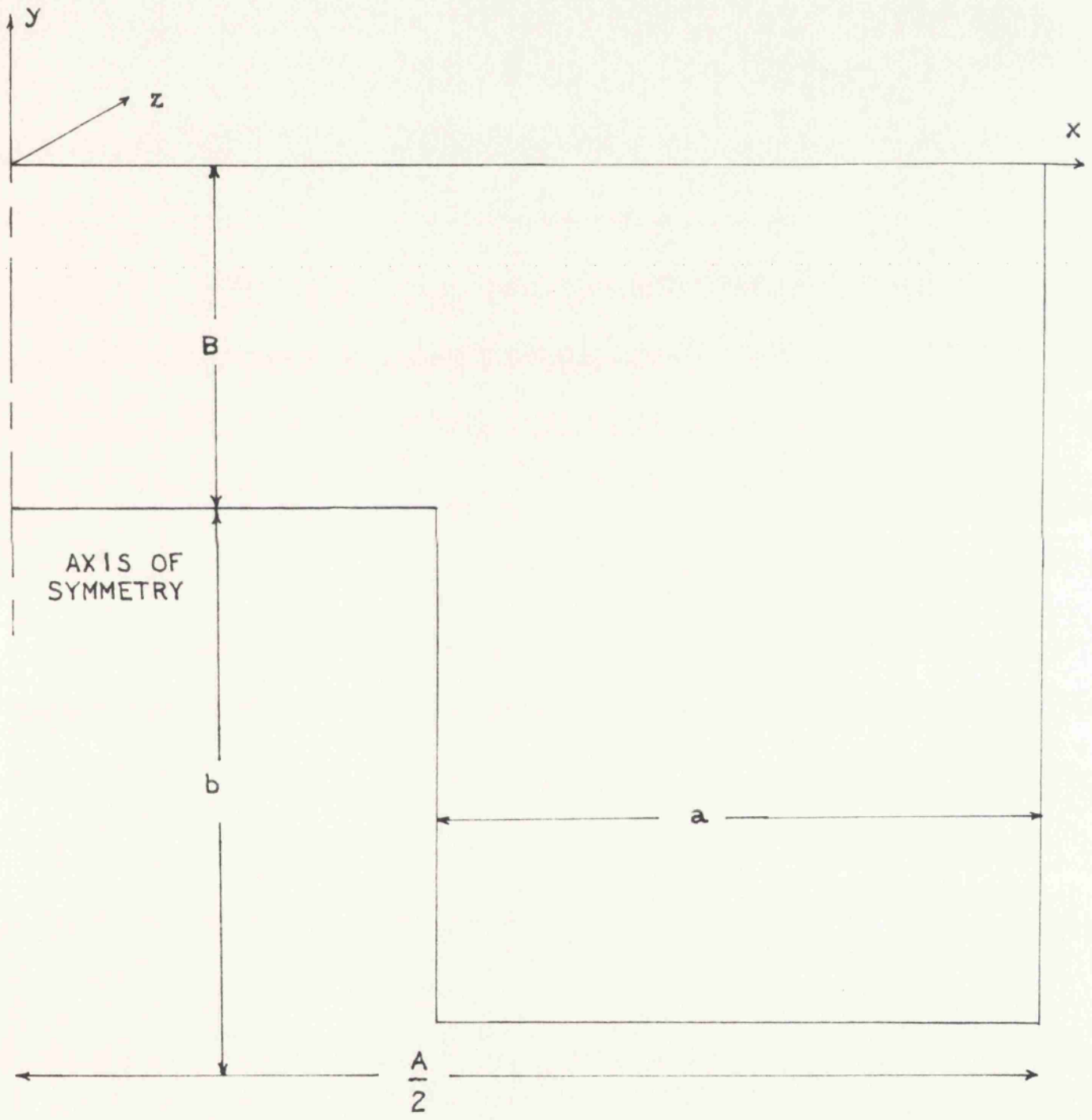

FIGURE 4.1.

$$-\sum_{\substack{m=1\\(odd)}}^{\infty} \phi_{2m} \sinh p_{2m}\frac{B}{A} \sin m\pi\frac{x}{A}\, p_{2m} = 0 \quad 0 \leqslant x \leqslant \left(\frac{A}{2}-a\right) \qquad 4.2.6.$$

$$= \sum_{m=o}^{\infty} \phi_{1m}\, p_{1m} \sinh p_{1m}\frac{b}{A} \cos m\frac{\pi}{a}\left(x-\frac{A}{2}\right), \frac{A}{2}-a \leqslant x \leqslant \frac{A}{2}.$$

and in the case of Hz,

$$\sum_{\substack{m=1\\(odd)}}^{\infty} \phi_{2m} \cosh \phi_{2m}\frac{B}{A} \sin \frac{m\pi x}{A} = \sum_{m=0} \phi_{1m} \cosh p_{1m}\frac{b}{A} \cos \frac{m\pi}{a}\left(x-\frac{A}{2}\right) \qquad 4.2.7.$$

Multiply 4.2.6. by $\sin \frac{n\pi x}{A}$ and integrate from 0 to $\frac{A}{2}$.

$$-p_{2m}\phi_{2m} \sinh p_{2m}\frac{B}{A} = \sum_{m=o}^{\infty} \phi_{1m}\, p_{1m} \sinh p_{1m}\frac{b}{A}\, K_{nm} \qquad 4.2.8.$$

$$K_{nm} = \frac{4}{A}\int_{\frac{A}{2}-a}^{\frac{A}{2}} \sin n\frac{\pi x}{A} \cos m\frac{\pi}{a}\left(x-\frac{A}{2}\right) dx \qquad 4.2.9.$$

$$= \frac{4}{\pi}\left(\frac{a}{A}\right)^2 (-1)^{m+1} \frac{\sin n\frac{\pi}{2} \sin n\frac{\pi a}{A}\cdot n}{m^2 - n^2\left(\frac{a}{A}\right)^2} \qquad (n \text{ odd}) \qquad 4.2.10.$$

Multiply 4.2.7. by $\cos r\frac{\pi}{a}\left(x-\frac{A}{2}\right)$ and integrate from $\frac{A}{2}-a$ to $\frac{A}{2}$

$$\sum_{\substack{r=1\\(odd)}}^{\infty} \phi_{2r} \cosh p_{2r}\frac{B}{A}\, K_{rm} = \phi_{1m}\left(\frac{a}{A}\right)\Delta_m \cosh p_{1m}\frac{b}{A} \qquad 4.2.11.$$

$$\Delta_m = 2 \quad m = 0$$

$$\Delta_m = 1 \quad m \neq 0$$

Substituting in 4.2.8. for ϕ_{1m} from 4.2.11,

$$-\phi_{2n} \sinh p_{2n}\frac{B}{A} = \sum_{m=0}^{\infty} \sum_{\substack{r=1\\(odd)}}^{\infty} \phi_{2r} \cosh p_{2r}\frac{B}{A}\, \frac{p_{1m}}{p_{2n}}\, \frac{K_{nm}\cdot K_{rm}\cdot \tanh p_{1m}\frac{b}{A}}{2\Delta_m\left(\frac{a}{A}\right)}$$

$$= \sum_{\substack{r=1 \\ (odd)}}^{\infty} \phi_{2r}\, p_{nr} \cosh p_{2r} \frac{B}{A} \qquad 4.2.12.$$

Therefore:

$$\sum_{\substack{r=1 \\ (odd)}}^{\infty} \phi_{2r} \cosh p_{2r} \frac{B}{A} \left(P_{nr} + \delta_{nr} \tanh p_{2n} \frac{B}{A} \right) = 0 \qquad 4.2.13.$$

$$P_{nr} = \frac{A}{2a} \frac{1}{p_{2n}} \sum_{m=0} p_{1m} \tanh p_{1m} \frac{b}{A} \frac{K_{nm} K_{rm}}{\Delta_m} \qquad 4.2.14.$$

For a non-trivial solution, the doubly infinite determinant of the function in the brackets of equation 4.2.13. is zero, i.e.

$$\text{Det} \left(P_{nr} + \delta_{nr} \tanh p_{2n} \frac{B}{A} \right) = 0 \qquad 4.2.15.$$

However since P_{nr} tends to zero as n,r, become large, and tanh $p_{2n} \frac{B}{A}$ tends to one as n becomes large, then a reasonable approximation to equation 4.2.15. is a two-by-two determinant

$$\begin{vmatrix} P_{11} + \tanh p_{21} \frac{B}{A} & P_{13} \\ P_{31} & P_{33} + \tanh p_{23} \frac{B}{A} \end{vmatrix} = 0 \qquad 4.2.16.$$

Solutions of equations 4.2.16 were found by means of a digital computer, DEUCE. A brief description of the method of solution is given in section, 4.4.

An alternative method of finding the cut-off wavenumber and field components is to sub-divide the waveguide cross-section into two rectangles whose intersection is defined by the straight line

$$x = \frac{A}{2} - a, \qquad 0 \leqslant y \leqslant -B \qquad \text{(Fig. 4.1.)}$$

and repeat the orthogonal mode analysis applied above.

4.3. Alternative Solution of the Wave Equation.

The following analysis is introduced principally to provide a suitable comparison for the calculations of cut-off wavelength performed in the previous section. The fields found by the two approaches could also be compared, but it is assumed that if substantial agreement exists between the cut-off wavelengths, then the fields are likely to be in agreement also.

The two regions in which the cross-section is divided are defined by the equations,

$$\begin{aligned} &\text{Region 3,} \quad \tfrac{A}{2} - a \leqslant x \leqslant \tfrac{A}{2}, \quad 0 \leqslant y \leqslant -(B+b) \\ &\text{Region 4,} \quad 0 \leqslant x \leqslant \tfrac{A}{2} - a, \quad 0 \leqslant y \leqslant -B \end{aligned} \qquad 4.3.1.$$

The solutions to the wave equation in regions 3 and 4 satisfying the boundary conditions on the waveguide walls are written as follows:-

$$\phi_3 = e^{-j\beta z} \sum_{m=0}^{\infty} \phi_{3m} \cosh p_{3m} \frac{(x - \frac{A}{2})}{A} \cos \frac{m y}{B+b} \qquad 4.3.2.$$

$$\phi_4 = e^{-j z} \sum_{m=0}^{\infty} \phi_{4m} \sinh p_{4m} \frac{x}{A} \cos \frac{m y}{B} \qquad 4.3.3.$$

$$\begin{aligned} p_{3m}^2 &= (\beta^2 - \beta_o^2) A^2 + \frac{(m\pi A)^2}{B+b} \\ p_{4m}^2 &= (\beta^2 - \beta_o^2) A^2 + \frac{(m\pi A)^2}{B} \end{aligned} \qquad 4.3.4.$$

The remaining boundary condition to be satisfied is the continuity of all the field components along the line

$$x = \frac{A}{2} - a, \quad 0 \leqslant y \leqslant -B$$

For the continuity of H_z, we have that

$$\sum_{m=0}^{\infty} \phi_{3m} \cosh p_{3m} \frac{a}{A} \cos \frac{m\pi y}{B+b} = \sum_{m=0}^{\infty} \phi_{4m} \sinh p_{4m} (\tfrac{1}{2} - \tfrac{a}{A}) \cos \frac{m\pi y}{B}$$

$$0 \leqslant y \leqslant -B \qquad 4.3.5.$$

In the case of E_y, we have that

$$-\sum_{m=0}^{\infty} \phi_{3m}\, p_{3m} \sinh p_{3m} \frac{a}{A} \cos \frac{m\pi y}{B+b} = 0 \qquad -B \leqslant y \leqslant -(B+b) \qquad 4.3.6.$$

$$= \sum_{m=0}^{\infty} \phi_{4m}\, p_{4m} \cosh p_{4m} \left(\frac{1}{2} - \frac{a}{A}\right) \cos \frac{m\pi y}{B} \qquad 0 \leqslant y \leqslant -B$$

Multiply 4.3.5. by $\cos \frac{r\pi y}{B}$ and integrate from 0 to $-B$

$$\sum_{r=0}^{\infty} \phi_{3r} \cosh p_{3r} \frac{a}{A} C_{rm} = -\frac{1}{2} \phi_{4m} \sinh p_{4m} \left(\frac{1}{2} - \frac{a}{A}\right) \Delta_m \qquad 4.3.7.$$

Multiply 4.3.6. by $\cos \frac{n\pi y}{B+b}$ and integrate from 0 to $-(B+b)$.

$$\frac{B+b}{2B} \phi_{3n}\, p_{3n} \sinh p_{3n} \frac{a}{A} \Delta_n = \sum_{m=0}^{\infty} \phi_{4m}\, p_{4m} \cosh p_{4m} \left(\frac{1}{2} - \frac{a}{A}\right) C_{nm} \qquad 4.3.8.$$

$$C_{mr} = \frac{1}{B} \int_0^{-B} \cos \frac{r\pi y}{B} \cos \frac{m\pi y}{B+b}\, dy.$$

$$= \frac{B.\ m.\ \cos r\pi .\ \sin \frac{m\pi B}{B+b}}{B + B.\ r^2\pi .\ 1 - \left(\frac{B}{B+b} \frac{m}{r}\right)^2} \qquad 4.3.9.$$

Combining 4.3.6. and 4.3.8., we have

$$\phi_{3n}\, p_{3n} \sinh p_{3n} \frac{a}{A} \Delta_n = 4 \sum_{m=0}^{\infty} \sum_{r=0}^{\infty} \phi_{3r} \cosh p_{3r} \frac{a}{A} p_{3m} \frac{C_{rm}\, C_{nm}}{\Delta_m} \coth p_{3m} .\left(\frac{1}{2} - \frac{a}{A}\right)$$

Thus

$$\sum_{r=0}^{\infty} \phi_{3r} \cosh p_{3r} \frac{a}{A} \left(Q_{nr} + \delta_{nr} \tanh p_{3r} \frac{a}{A}\right) = 0 \quad \text{(cf. equ. 4.2.13)} \qquad 4.3.10$$

$$Q_{nr} = 4 \sum_{m=0}^{\infty} \frac{p_{4m}\, C_{rm}\, C_{nm} \coth p_{4m} \left(\frac{1}{2} - \frac{a}{A}\right) .\ B}{p_{3r}\ \Delta_m\ \Delta_r\ B+b} \qquad 4.3.11.$$

As in the previous section, a 2 X 2 approximation to the

doubly-infinite determinant of equation 4.3.10 is taken,

$$\begin{vmatrix} Q_{00} + \tanh p_{30} \frac{a}{A} & Q_{10} \\ Q_{01} & Q_{11} + \tanh p_{31} \frac{a}{A} \end{vmatrix} = 0 \qquad 4.3.12.$$

Since $C_{0m} = 0 \quad m \neq 0$

$= 1 \quad m = 0$, then

$$Q_{00} = \frac{B}{B + b} \coth p_{40} \left(\frac{1}{2} - \frac{a}{A} \right)$$

Also

$$Q_{01} = 0 \quad \text{unless} \quad m = 0$$

$$= \frac{2}{\pi} \frac{p_{40}}{p_{11}} \sin \frac{\pi B}{B + b} \coth p_{40} \left(\frac{1}{2} - \frac{a}{A} \right). \quad (m = 0)$$

and

$$Q_{10} = \frac{1}{\pi} \cdot \frac{p_{40}}{p_{30}} \sin \frac{\pi B}{B+b} \coth \left(\frac{1}{2} - \frac{a}{A} \right) \qquad (m = 0)$$

Q_{11} is the only term in equation 4.3.12. for which the infinite series of equation 4.3.11 must be evaluated. The other 'Q' terms reduce to the simple forms shown above. Consequently the solution of equation 4.3.12. is very much more simple to find than the solution of equation 4.2.16., in which each of the 'P' terms involves an infinite series.

The solutions of equations 4.3.12. and 4.2.16 are presented for the same set of ridged waveguide parameters in Table 4.1. The results which refer to sections 4.2. and 4.3. are labelled with the subscript P and Q respectively.

Table 4.1. Cut-off Wavelength - $\frac{a}{A} = \frac{1}{4} \quad B + \frac{b}{A} = \frac{4}{9}$

$\frac{b}{A}$	0.10	0.15	0.20	0.25	0.30
$(2\frac{A}{\lambda_c})_P$	0.911	0.847	0.768	0.686	0.601
$(2\frac{A}{\lambda_c})_Q$	0.902	0.838	0.766	0.686	0.600

In table 4.1., there is good agreement between the two separate calculations for $2\frac{A}{\lambda_c}$ which is more pronounced for larger values of $\frac{b}{A}$, i.e., when the ridge height is large. It may be deduced that the employment of the 2 X 2 approximation to the doubly-infinite determinant in both cases considered, is justified as long as the $\frac{b}{A}$ is greater than 0.10.

Once $2\frac{A}{\lambda_c}$ has been determined, it is possible to find the field distribution over the ridged cross-section through equations 4.2.3. and 4.2.4. Since a 2 X 2 approximation has been taken for the determinantal equation, only the first two terms in the series expansion for the field components need be considered. Accordingly,

$$\phi_1 = e^{-j\beta z}\left(\phi_{10} \sinh p_{10}\frac{y+B+b}{A} + \phi_{11}\sinh p_{11}\frac{y+B+b}{A}\cdot\cos\frac{\pi}{a}\left(x-\frac{A}{2}\right)\right) \qquad 4.2.17.$$

$$\phi_2 = e^{-j\beta z}\left(\phi_{21}\cosh p_{21}\frac{y}{A}\sin\frac{\pi x}{A} + \phi_{23}\cosh p_{23}\frac{y}{A}\sin\frac{3\pi x}{A}\right) \qquad 4.2.18.$$

In section 5.7. the magnetic field components H_x and H_z are compared with those found by the finite-difference approach, along the line,

$$y = 0 \qquad 0 \leqslant x \leqslant \frac{A}{2}$$

By setting $y = 0$ in equation 4.2.18. and using equation 5.1.1. the H_z and H_x expressions are found to be:-

$$H_{z2} = \phi_{21}\left(\sin\frac{\pi x}{A} + \frac{\phi_{23}}{\phi_{21}}\sin\frac{3\pi x}{A}\right)$$

$$H_{x2} = j \frac{\beta A}{(kA)^2} \phi_{21} \left(\cos \frac{\pi x}{A} + 3 \frac{\phi_{21}}{\phi_{23}} \cos \frac{3\pi x}{A}\right)$$

The ratio, $\frac{\phi_{21}}{\phi_{23}}$, is determined from equation 4.2.13 when the solution of the determinantal equation is complete.

P (x,0,f,) is determined from the ratio of H_x to H_z. In region (2),

$$P(x,0,f) = j \frac{\beta A}{(kA)^2} \left(\frac{\cos \frac{\pi x}{A} + 3 \frac{\phi_{21}}{\phi_{23}} \cos \frac{3\pi x}{A}}{\sin \frac{\pi x}{A} + \frac{\phi_{21}}{\phi_{23}} \sin \frac{3\pi x}{A}} \right)$$

A discussion of the field distribution in the ridged wvarguide is left over until section 5.7.

4.4. Numerical Computations.

The determinantal equation 4.2.16. being trancendantal, is best suited to solution by iteration. Since one of the ridge parameters, $\frac{B}{A}$, occurs in a simple form in the equation, it was decided to make $\frac{B}{A}$ the 'unknown'. In order to evaluate the 'P' terms, it is nesessary to specify $\frac{a}{A}$, $\frac{b}{A}$, and $\frac{2A}{\lambda_c}$. From the physical point of view, it would be better to prescribe all the ridge parameters and to determine the cut-off from these. However, since $\frac{2A}{\lambda_c}$ occurs in all the 'P' terms and 'tanh' terms in equation 4.2.16., it is more convenient to approach the solution in a roundabout way. Having evaluated all the expressions in the determinantal equation, it is relatively simple to find $\frac{B}{A}$ by trial-and-error or iteration. The infinite series involved in the expression for P_{nr}

converges quite rapidly. For, as m increases, the mth term varies as $\frac{1}{m^3}$. It is quite sufficient only to evaluate the first five terms in the series, to obtain P to within 0.1% The iteration procedure was carried out on a DEUCE computer using a Tabular Interpretive Programme (T.I.P.) in which computations for thirty values of $2\frac{A}{\lambda_c}$ are dealt with simultaneously. The values for a given set of ridged parameters are then found by linear interpolation.

Since only a few results were required for the solution of equation 4.3.12., the computations were carried out by trial-and-error using a desk calculation machine.

5. Finite Differences.

5.1. Defining Equations.

In a lossfree and uniform, homogeneous waveguide, only uncoupled H- and E-modes can exist.[23] The electromagnetic field components are then defined, for a periodic time dependence, $e^{j\omega t}$ and axial dependence $e^{-j\beta z}$ by the following equations:-[24]

H-modes

$$\begin{aligned} k^2 \underline{H}_t &= -j\beta \underline{\nabla}_t \phi \\ k^2 \underline{E}_t &= +j\omega\mu(\underline{u}_z \times \underline{\nabla}_t \phi) \\ H_z &\equiv \phi \end{aligned} \qquad 5.1.1.$$

E-modes

$$\begin{aligned} k^2 \underline{E}_t &= -j\beta \underline{\nabla}_t \psi \\ k^2 \underline{H}_t &= -j\omega\epsilon(\underline{u}_z \times \underline{\nabla}_t \psi) \\ E_z &\equiv \psi \end{aligned} \qquad 5.1.2.$$

where $k^2 = \omega^2\mu\epsilon - \beta^2$, is the axial propagation constant, $\underline{u}_z$ is a unit vector in the z-direction and the subscript 't' refers to the transverse (x and y) components of the vector.

The functions ϕ and are solutions of the wave equation:-

$$(\nabla_t^2 + k^2)\phi = 0 \qquad 5.1.3.$$

subject to the boundary condition:

$\frac{\partial \phi}{\partial n} = 0$; $\psi = 0$ on the perfectly conducting waveguide walls.

Further boundary conditions may arise in particular modes due to symmetry conditions.

5.2. Finite differences in two Dimensions.

This section begins with a brief account of the basic idea of the finite-difference method which may be found in the standard texts.[25]

Consider a function ϕ of the transverse Cartesian coordinates x and y which is analytic in a region of the xy-plane. A particular point O in the region is surrounded by four equidistant points as in Fig. 5.1. The separation between O the four points 1 - 4 is labelled 'h'. By means of a Taylor series expansion, the values of ϕ at the points 1 - 4 may be written down in terms of h, ϕ and its derivatives at the point O:-

$$\phi_1 = \phi_o + h\phi_o^x + \frac{h^2}{2!}\phi_o^{x^2} + \frac{h^3}{3!}\phi_o^{x^3} \ldots\ldots \quad 5.2.1.$$

$$\phi_3 = \phi_o - " + " - " + \ldots\ldots\ldots \quad 5.2.2.$$

$$\phi_2 = \phi_o + h\phi_o^y + \frac{h^2}{2!}\phi_o^{y^2} + \frac{h^3}{3!}\phi_o^{y^3} + \ldots\ldots \quad 5.2.3.$$

$$\phi_4 = \phi_o - " + " - " + \ldots\ldots\ldots \quad 5.2.4.$$

where $\phi_o^{x^n} = \left(\frac{\partial^n \phi}{\partial x^n}\right)$ at the point O

$\phi_o^{y^n} = \left(\frac{\partial^n \phi}{\partial y^n}\right)$ at the point O

Adding equations 5.2.1., 5.2.2., 5.2.3., and 5.2.4., neglecting all terms in $(h)^4$ and higher order, we obtain the following equation:-

$$\sum_1^4 \phi_s - 4\phi_o = h^2(\phi_o^{x^2} + \phi_o^{y^2}) = h^2(\nabla_t^2 \phi)_o \quad 5.2.5.$$

Equation 5.2.5. shows the basic representation, in terms of surrounding function values, of $\nabla_t^2 \phi$ at any point in the region. If ϕ satisfies the wave equation, equation 5.2.5. may be written as:-

$$\sum_1^4 \phi_s - 4\phi_o = -h^2 k^2 \phi_o \quad 5.2.6.$$

To apply the finite-difference method to propagation in rectilinear waveguides, the waveguide cross-section is sub-divided into a number of square sub-regions of side length 'h', the intersections of which are

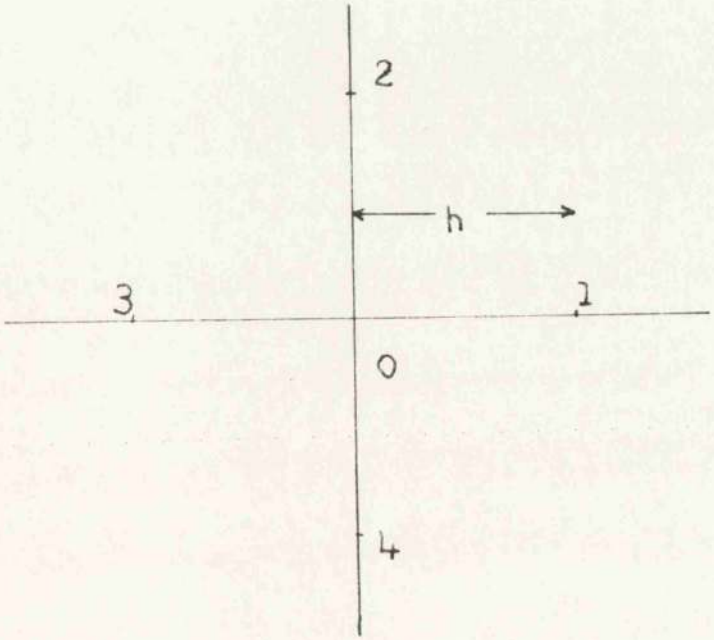

FIGURE 5.1.

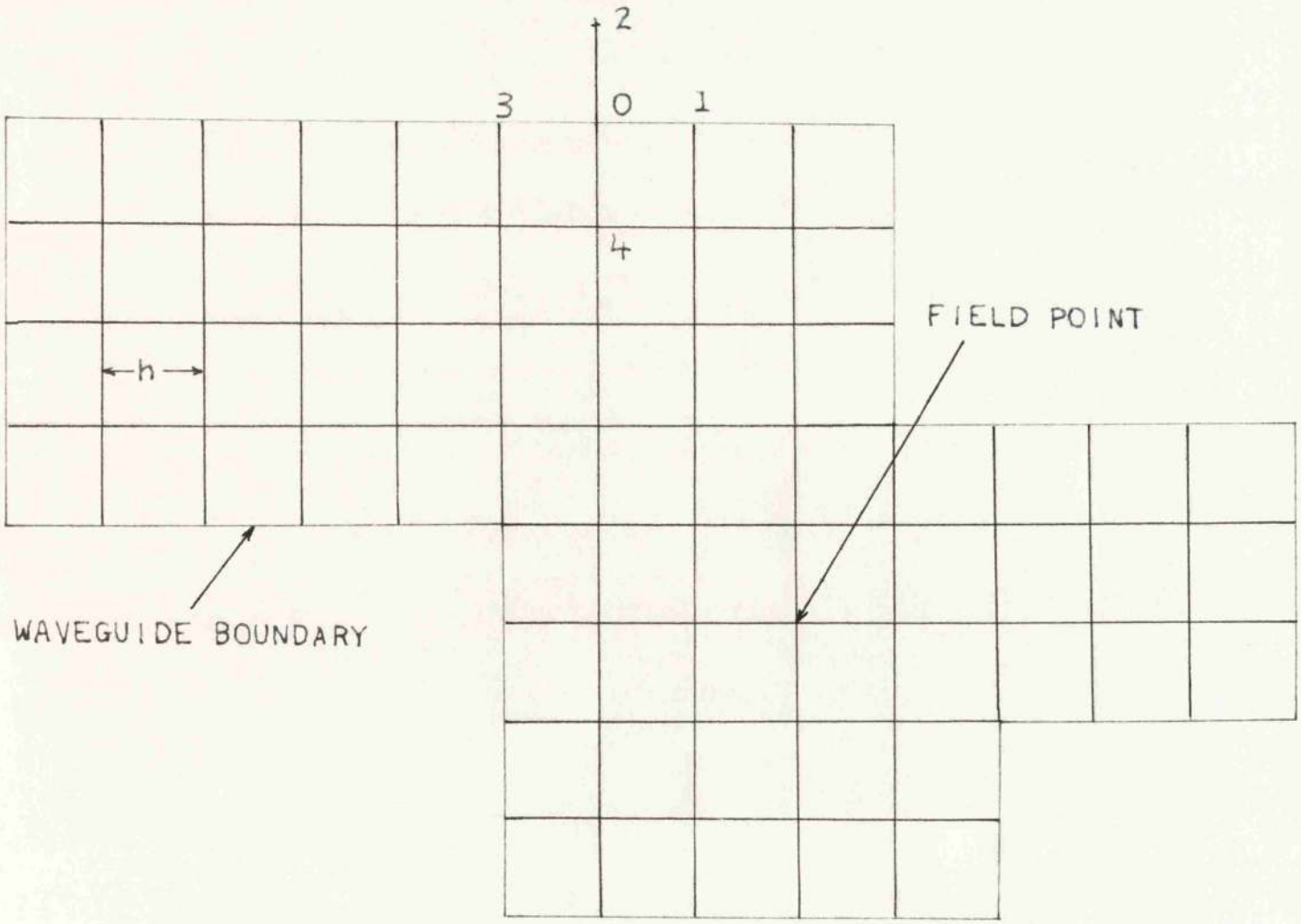

FIGURE 5.2.

labelled field-points (Fig. 5.2.). The waveguide shown has, for the purpose of generality, boundaries which are rectilinear but otherwise arbitrary. At each point in the waveguide cross-section, equation 5.2.6. is applied, points on the boundary being dealt with in the following way:- The point O, in Fig. 5.2. lies on the waveguide boundary. Since the boundary condition on the waveguide wall for H-modes is:-

$$\frac{\partial \phi}{\partial n} = 0$$

then, to a first approximation, the value of ϕ at the point 2 is equal to the value of ϕ at the point 4, i.e.

$$\phi_2 = + \phi_4$$

Therefore, in this case, equation 5.2.6. becomes

$$\phi_1 + \phi_3 + 2\phi_4 - 4\phi_o = -h^2k^2\phi_o \qquad 5.2.7.$$

In the case of E-modes, $\Psi = 0$ on the boundary so that

$$\Psi_2 = -\Psi_4$$

Therefore, for E-modes, equation 5.2.6. becomes

$$\Psi_1 + \Psi_3 - 4\Psi_o = -h^2k^2\Psi_o \qquad 5.2.8.$$

Difference equations at points on the remaining boundaries are dealt with in the same manner.

It is sometimes advisable to have field-points not on the waveguide boundary but rather, half a mesh length away from the boundary. This may be visualised by considering all the points O - 4 in Fig. 5.2. moved down half a mesh length. In this case, the difference equation 5.2.6. for ϕ and Ψ becomes:-

$$\phi_1 + \phi_3 + \phi_4 - 3\phi_o = -h^2 k^2 \phi_o \qquad 5.2.9.$$

$$\Psi_1 + \Psi_3 + \Psi_4 - 3\Psi_o = -h^2k^2\Psi_o \qquad 5.2.10.$$

When equation 5.2.6. has been written down at all the interior points of the cross-section with the relevant modifications made for points next to the boundary, a system of 'n' linear equations is obtained (n is the total number of points in the cross-section). These may be written conveniently in the form:-

$$B\,\phi = \lambda\,\phi \qquad 5.2.11.$$

Where B is a n x n band matrix of known integer elements, ϕ is a 1 x n vector of 'n' unknown values of ϕ and λ is the unknown latent root of matrix B, which, from equation 5.2.6., is identically $-h^2k^2$. The 'n' latent roots of matrix B correspond to the first 'n' cut-off wavenumbers of the waveguide for the particular type of mode in question (H or E). Each latent root, λ_r has a latent vector, ϕ_r, which is automatically obtained together with λ_r when equation 5.2.11. is solved.

5.3. Finite Differences in One Dimension.

Certain waveguide propagation problems are, by nature, one-dimensional, e.g. dominant H-mode propagation in rectangular waveguide. In order to deal with problems which are one-dimensional, it is necessary to derive a one-dimensional analogue of equation 5.2.6. Since the function ϕ introduced at the beginning of section 5.2. depends in this case on only one transverse coordinate, say x, the equation is simply derived by adding equations 5.2.1. and 5.2.2.:-

$$\phi_1 + \phi_3 - 2\phi_o = h^2(\phi_o^{x^2}) = h^2(\nabla_t^2\phi)_o = -h^2k^2\phi_o \qquad 5.3.1.$$

Equation 5.3.1. is the one-dimensional analogue of equation 5.2.6.

Instead of dividing the waveguide cross-section into square sub-regions as in the previous section, the x-axis (along which ϕ varies)

is subdivided into a number of equal lengths, h, from one waveguide wall to the other. At each point of subdivision, equation 5.3.1. is applied, with no suitable modifications at the ends of the line. As in section 5.2., all the equations are written in the matrix from of equation 5.2.11.

It is advisable to use the one-dimensional representation of equation 5.1.3. wherever possible since, for a given number of points n, it is possible to obtain a very much finer mesh of points in this case.

The methods used for obtaining the numerical solution of equation 5.2.11. are discussed in the following section.

5.4. Solutions to the Matrix Equation.

The solution of equation 5.2.11. is accomplished by means of an automatic digital computer, in this case, DEUCE. Three separate programmes have been used for finding the latent roots and vectors of matrix B.

(1) Lanczos-Wilkinson. $n \leqslant 31$

This programme finds all the latent roots and vectors of a n x n square matrix, where $n \leqslant 31$. The method involved uses pivotal condensation and back substitution. The matrix data has to be punched in binary, with 12 elements per card and a parameter card giving the dimensions of the matrix and the number of binary places. A square matrix of order 20 requires 41 cards to be prepared for the computer. The computer takes about 30 minutes to punch out all the latent roots and vectors of the matrix. Owing to the fact that this programme is slow and cannot deal with matrices of large order, it was found necessary to use another method of calculation.

(2) Inversion and Iteration.[26] $n \leqslant 83$

This programme is in two sections, (1) inversion of a square matrix by the standard LVO1 programme, and (2) iteration with a guess vector until the machine arrives at the lowest latent root and vector.

The theory underlying the operation is as follows:-

Multiply equation 5.2.11. by the inverse of matrix B.

$$B^{-1} B \phi = \lambda B^{-1} \phi$$

$$\phi = \lambda B^{-1} \phi \quad \text{since} \quad B B^{-1} = 1 \qquad 5.4.1.$$

Suppose the 'n' latent roots of matrix B, $\lambda_1, \lambda_2, \lambda_3, \ldots \lambda_n$, are arranged in order of ascending modulus. An arbitrary vector x_o is taken and two sequences of vectors x_i and y_i are formed from

$$y_{i+1} = B^{-1} x_i \qquad 5.4.2.$$

$$x_{i+1} = y_{i+1} \; / \; \text{maximum element of vector } y_{i+1} \qquad 5.4.3.$$

Each member of the sequence x_i has as its largest element, unity. The initial vector x_o may be written in terms of the 'n' latent vectors, $\phi_1, \phi_2, \ldots \phi_n$

$$x_o = \sum_1^n a_i \phi_i \qquad 5.4.4.$$

If equation 5.4.2. has been applied 'k' times, then

$$Cx_k = \sum_1^n a_i \phi_i \Big/ {}^{k}_{i} = \frac{1}{\lambda_1^k} a_1 \phi_1 + \sum_{i=2}^n a_i \left(\frac{\lambda_1}{\lambda_i}\right)^k \phi_i \qquad 5.4.5.$$

where C is the largest element of y_k

Since λ_1 is the smallest latent root,

Hence $$Cx_k \rightarrow \frac{1}{\lambda_1^k} a_1 \phi_1 \qquad 5.4.6.$$

Which means that y_k tends to ϕ_1. The speed at which convergence takes place depends on the ratio λ_1 / λ_2. When the iteration has been carried out often enough that successive values of x_k agree to as many places as is required, the iteration is stopped and the last values of $^1/C_k$ and x_k taken as the smallest latent root, λ_1 and latent vector, ϕ_1, of matrix B.

A General Interpretive Programme (G.I.P) for the DEUCE computer has been written to carry out the above iteration procedure and is described in the Appendix.

(3) Solution of Linear Equations and Iteration. $n \leqslant 256$.

The method of solution in this programme is again iteration as in (2). However, the laborious process of inverting a large matrix is avoided and instead a very fast programme, LEO 7B, is used which solves directly the equation

$$B\phi = b \qquad 5.4.7.$$

where the right hand side, b, is known and matrix B is in band form. LEO 7B is restricted to dealing with matrix of order less than 256 and whose band may not exceed 29. The iteration is carried out as in (2) with the only exception that the step involved in equation 5.4.2. is replaced by the solution of

$$By_{i+1} = x_i \qquad 5.4.8.$$

In (2) the inversion procedure is carried out only once and successive steps involve multiplication of matrix B^{-1} with a vector. However, here the solution of linear equations involved in equation 5.4.7.

is performed during every iteration. Although there may seem to be a disadvantage involved in solving equation 5.4.7. on each iteration this is not so, because the inversion procedure takes about $1\frac{1}{2}$ - 2 hours on DEUCE for a matrix of order 80 whereas the solution of linear equations takes only about 9 minutes, for a matrix of the same order. Also the limit on the order of matrix which can be dealt with in (2) makes (3) the more attractive method.

When the convergence of the iteration is slow, it is possible to speed it up. If p is an approximation to the lowest latent root, λ_1, equation 5.2.11. is written as

$$(B - pI) \phi = (\lambda_1 - p) \phi$$

The iteration is carried out using the matrix $(B - pI)$ in place of matrix B. Equation 5.4.5. becomes

$$Cx_k = \frac{1}{(\lambda_1 - p)^k} \left(a_1\phi_1 + \sum_{i=2} a_i \left(\frac{\lambda_1 - p}{\lambda_i - p}\right)^k \phi_i\right) \qquad 5.4.9.$$

The rate of convergence now depends on

$$\frac{\lambda_1 - p}{\lambda_2 - p}$$

Since $\frac{\lambda_1 - p}{\lambda_2 - p}$ has been arranged to be smaller than $\frac{\lambda_1}{\lambda_2}$, the rate of convergence is improved.

Occasionally, it is necessary to find the second lowest latent root of matrix B (see section 6). If the required latent root is known to first order, then improved convergence procedure described above is

carried out with p as the approximation to λ_2. This step is equivalent to shifting the origin of the latent roots so that λ_2 is the smallest. The iteration procedure automatically produces the latent root, λ_2, and vector, ϕ_2. The G.I.P. programme which has been used on DEUCE to perform the iteration is described in the Appendix.

5.5. Higher approximations to the Laplacian.

The accuracy of the one and two-dimensional representations of the Laplacian depends mainly on the fineness of the subdivision of the waveguide region. If the mesh length, h, is not small, then higher approximations to the Laplacian involving more neighbouring points than used in equation 5.2.6., are available in the literature.[27] Three approximations for the two-dimensional wave equation have been used and these are summarised below. The numbering of the points refers to Fig.5.3.

1. FD_4 formula

$$\sum_{1}^{4} \phi - 4\phi_o = -h^2k^2\phi_o \qquad 5.5.1.$$

Error is of order $(hk)^4$

2. FD_{20} formula.

$$4\sum_{1}^{4} \phi + \sum_{5}^{8} \phi - 20\phi = (-6h^2k^2 + \tfrac{1}{2} h^4k^4)\phi \qquad 5.5.2.$$

Error is of order $(hk)^6$

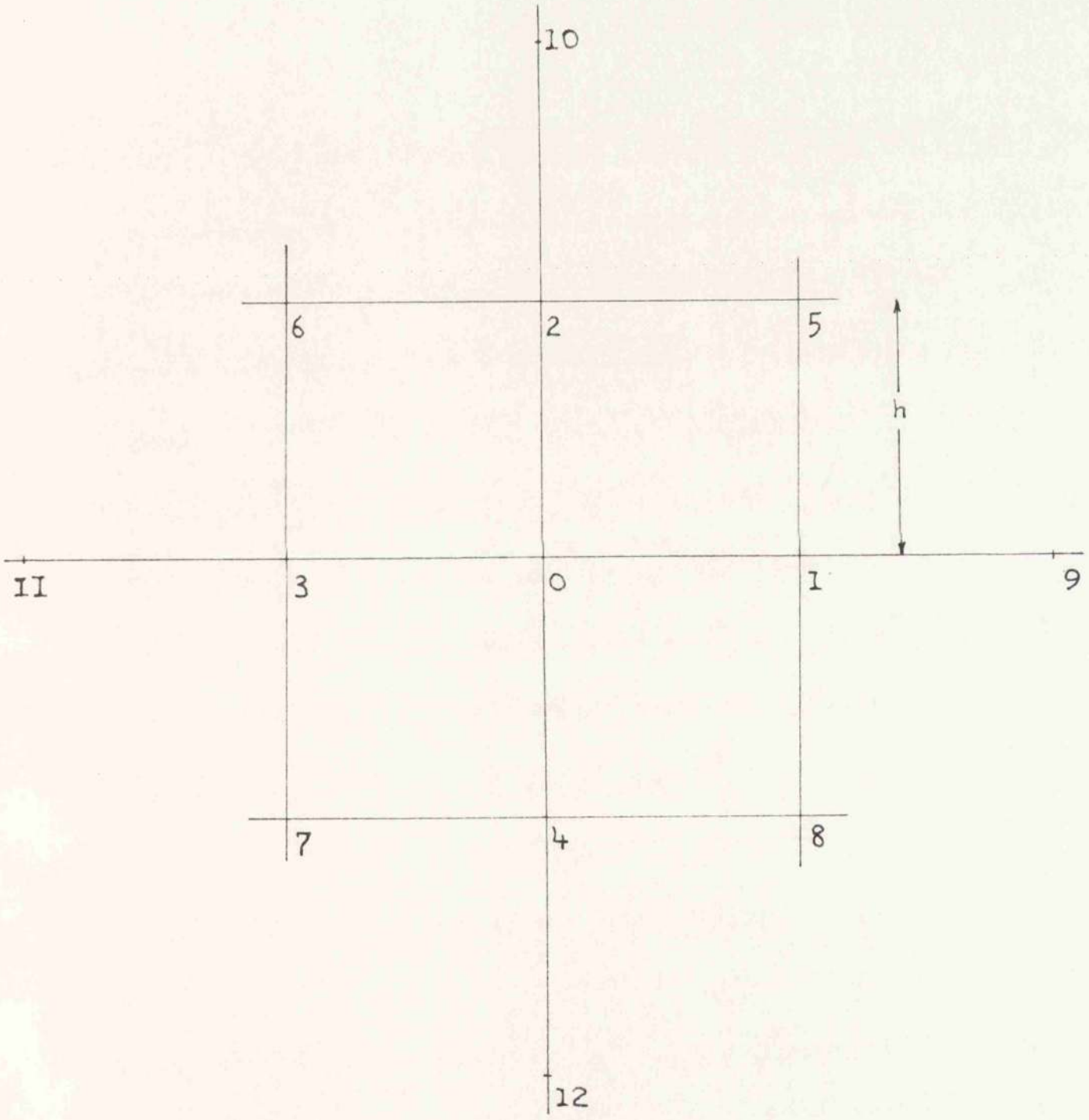

FIGURE 5.3.

3. FD_{180} formula.

$$32\sum_{1}^{4}\phi + 12\sum_{5}^{8}\phi + \sum_{9}^{12}\phi - 180\,\phi_o = (-60\,h^2k^2 + 6\,h^4k^4 - \frac{1}{3}\,h^6k^6)\,\phi_o \qquad 5.5.3.$$

Error is of order $(hk)^8$

In the case of the one-dimensional wave equation, it is usually unnecessary to use higher approximations. This is because it is possible to obtain a very fine mesh so that the error involved in using the first approximation to the Laplacian is negligible. The one-dimensional formula is requoted for neatness :-

4 FD_2 formula

$$\phi_1 + \phi_3 - 2\,\phi_o = -\,h^2k^2\phi_o \qquad 5.5.4.$$

Error is of the order $(hk)^4$.

5.6. Rectangular waveguide.

The conventional rectangular waveguide provides a very simple example of the application of the finite-difference procedure. For the lowest order mode, there is no field dependence on the y-coordinate. This allows the one-dimensional form of the difference formulae, FD_2 , to be used. Since ϕ is zero for this mode at x zero (the symmetry plane of the waveguide), only the region $0 \leqslant x \leqslant \frac{A}{2}$ need be considered. Results are given in Table 5.1. for values of $(kA)^2$ and of ϕ at certain of the field points when the value of 'n' is taken as 5, 25, and 50 respectively. The formula FD_2 has been used in conjunction with programme 3. These results are comparde

in the same Table with the values obtained from the well-known formulae :-

$$(kA)^2 = \pi^2 \quad ; \quad \phi = \sin \frac{\pi x}{A} \qquad 5.6.1.$$

For the purposes of clarity, the matrix for the case, $n = 5$, is written down in square and band form. The five field points lie on the line - $y = 0$; - at $\frac{x}{A} = 0.1\ (\ 0.1)\ 0.5$. The matrix elements are obtained from equation 5.5.4.

Square Matrix, $n = 5$.

Row	Column 1	2	3	4	5
1	-2	2	0	0	0
2	1	-2	1	0	0
3	0	1	-2	1	0
4	0	0	1	-2	1
5	0	0	0	1	-2

Band matrix, $n = 5$.(bandwidth = 3)

Row	Column. 1	2	3
1	0	-2	2
2	1	-2	1
3	1	-2	1
4	1	-2	1
5	1	-2	0

Table I.

	FIELD POINTS			EXACT	$\frac{X}{A}$
	5	25	50		
$(kA)^2$	9.78870	9.86635	9.86878	9.86961	
	1.0000000	1.0000000	1.0000000	1.0000000	0.50
		.9921147	.9921147	.9921147	0.46
	.9510565	.9510565	.9510565	.9510565	0.40
		.9048270	.9048271	.9048271	0.36
ϕ	.8090170	.8090170	.809o171	.8090170	0.30
		.7289686	.7289688	.7289686	0.26
	.5877852	.5877852	.5877854	.5877853	0.30
		.4817537	.4817538	.4817537	0.16
	.3090170	.2090170	.3090171	.3090170	0.10
		.1873813	.1873814	.1873813	0.06
	.0000000	.0000000	.0000000	.0000000	0.00

The results given in Table I show that the field vector, ϕ is accurate to seven decimal places in each of the three cases considered. As expected, the value of $(kA)^2$ is least accurate when the number of points is small. The error in $(kA)^2$ for the case 'n' equal to five is less than 1%. When the number of points is increased to fifty, the error drops sharply to less than 0.01%.

Having obtained k_A and ϕ, the remaining field components Ey and Hx can be determined. Referring to equation 5.1.1., it is seen that these are defined in terms of β and the x-derivative of ϕ. The differentiation is performed numerically on the computer using the formula

$$\left(\frac{\partial \phi}{\partial x}\right)_o = \frac{1}{2h}(\phi_1 - \phi_3) \qquad \text{(see Fig. 5.1.)} \qquad 5.6.2.$$

For n equal to five, the derivative is found to be in error by less that 2% and n fifty by less than 0.1%. Higher order approximations for the derivatives would of course reduce the error. It has been shown how the fields and cut-off wavenumbers of the dominant H-mode in rectangular waveguide may be determined. Higher order H-modes are considered by finding the appropriate latent roots and vectors of matrix B.

E-modes are dealt with by applying the following boundary conditions to the function

$\Psi = 0$ on the waveguide walls

$\frac{\partial \Psi}{\partial n} \neq 0$ on the axis of symmetry (magnetic wall or odd modes)

$\Psi = 0$ " " " " " (electric wall or even modes)

5.7. Magnetic polarisation in ridged waveguide.

Dominant H-mode propagation in ridged waveguides has received considerable attention in recent years. By treating the ridged waveguide at cut-off as a two-dimensional transmission line,Cohn[27] has obtained figures for cut-off wavelength and waveguide impedance.Marcuwitz[28] has published design parameters for ridged waveguides having specified cut-offs.Further work along the same lines has been published by Hopfer[29] and Chen.[30] However,by their nature, the methods normally used to calculate cut-off wavelength have only been capable of giving limited information on the electromegnetic field configuration. The ridged waveguide is of interest as a broadband propagating structure which is easily matched to coaxial line owing to its low wave impedance, and also in the design of broadband resonance isolators.Since the cut-off wavelength of the ridged waveguide is higher than that of a rectangular waveguide having the same broad dimension,then the variation of guide wavelength with frequency is reduced,(see equation 3.1.1.).

The dependence of the circular polarisation of the r.f. magnetic field on frequency is reduced if the cut-off frequency is depressed.One advantage the ridged waveguide possesses over the dielectric loaded waveguide is that the cut-off frequencies over higher-order H-modes are not depressed in the same way as the dominant mode.In the design of a ferrite resonance isolator,it is advisable to locate the region in the waveguide cross-section at which the function,P,defined in section 2, is close to unity. Assuming that P is unity at a position (x_o, y_o) for a frequency f_o,it is useful to plot (a) the variation with frequency,f, of $P (x_o, y_o, f)$ and (b) the variation with position (x,y) of $P (x, y, f_o)$

The result of step (a) determines the bandwidth over which the ellipticity of the r.f. magnetic field is not greater than a specified value, δ. The calculation in (b) gives an indication of the dimensions of the ferrite which can be used, while ensuring that the ellipticity of the r.f. magnetic field over the ferrite cross-section does not exceed δ.

It will be shown that by use of finite-difference methods, it is possible to derive the cut-off wavelength and the longitudinal magnetic field in the ridged waveguide simultaneously. The remaining field components are derived through the axial field from equation 5.1.1.

The geometry of half the cross-section of a single-ridged waveguide is shown schematically in Fig.5.4., the field points of the subdivided cross-section being identified by a column letter A-J, and row number 1-9. The boundary conditions for the symmetric H-modes under consideration are also shown. As in the case of the rectangular waveguide the difference equations are applied at each point in the cross-section from A1 to J5. The matrix form of these equations is as defined in equation 5.2.11.

The solution of the matrix equation yields both λ_r and ϕ_r and hence the cut-off wavelength and longitudinal magnetic field are determined for 'n' modes of the structure. The difference equation for the derivatives of the function ϕ is employed in the derivation of the rest of the field components. Since the relation between βA and the frequency is uniquely determined by a knowledge of kA, the field components as a function of frequency are now known.

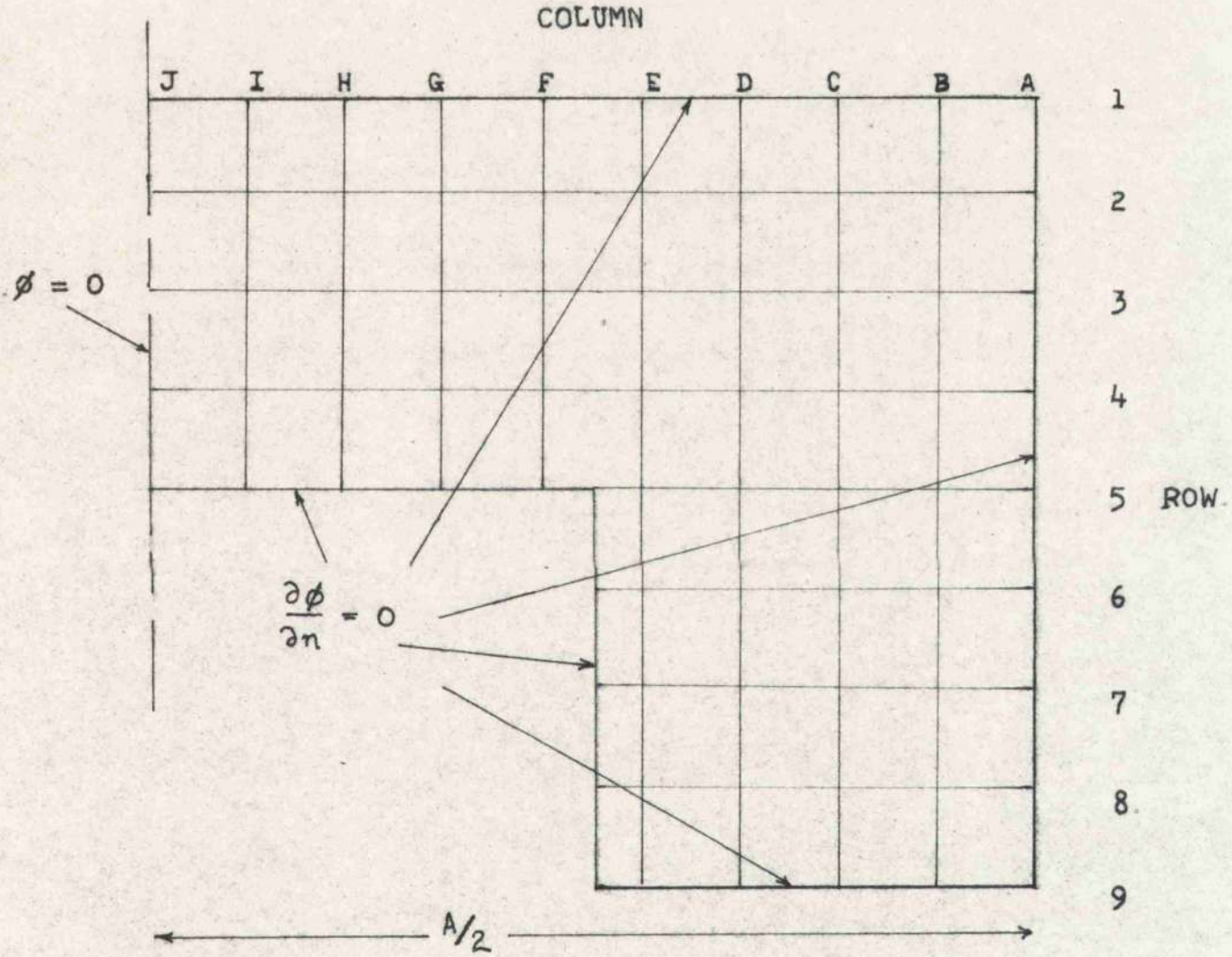
COLUMN
J
I
H
G
F
E
D
C
B
A
1
2
3
4
5
ROW
6
7
8
9
$\phi = 0$
$\frac{\partial \phi}{\partial n} = 0$
A/2

FIGURE 5.4.

Since all the field components satisfy the two-dimensional wave equation, it is possible to employ an alternative procedure from the one mentioned above, for determining the field components other than H_z. For instance, the component H_x satisfies the wave equation and it follows that the difference equations listed in section 5.5. hold when ϕ is identified as H_x. The matrix equation 5.2.11. also holds but the elements are slightly different from those for the 'H_z' matrix. This fact arises from the different boundary conditions which apply to H_z and H_x on the waveguide walls and the axis of symmetry, viz.,

$$\frac{\partial H_z}{\partial n} = 0 \text{ on } \underline{\text{all}} \text{ perfectly conducting walls}$$

$$H_x = 0 \text{ if the waveguide wall is parallel to the y-axis}$$

$$\frac{\partial H_x}{\partial n} = 0 \text{ if the waveguide wall is parallel to the x-axis.}$$

With these restrictions in mind, it is possible to construct the matrix B for H_x which only differs from the H_z matrix in rows which refer to points on the waveguide boundary where the conditions on H_z and H_x differ. The solution of the matrix equation thus obtained for the magnetic field component H_x, gives (a) the cut-off wavelength and (b) the distribution of H_x over the cross-section. Theoretically, the latent roots corresponding to dominant mode propagation of the H_x and H_z matrices, are identical and equal to $-h^2k^2$, and the H_x field distribution may be derived from H_z by taking the numerical x-derivative of H_z at each point in the cross-section. However, it is found in practice,

that when a matrix of order 140 is used, the two latent roots differ by a significant factor for the ridged waveguide whose parameters are given in Table 5.2. The latent root of the H_z matrix lies very close to the value given by other authors and to the experimental value. The error in the H_x latent root may be due to the different boundary condition holding at the two faces of the ridge causing a discontinuity in the value of the field at the ridge edge. The latent vector for H_x lies within 5% of the vector calculated from the x-derivative of H_z. Due to the anomaly in the two latent roots, the alternative method, (H_x) for finding the latent roots and vectors has not been used. The field components other than H_z are derived by point-to-point numerical differentiation in the cross-section.

Calculated results are given for dominant mode propagation in a ridged waveguide whose dimensions are given in Table 5.2. The effect of higher approximations and variable mesh length, h, on the computed value of cut-off wavelength is also shown in Table 5.2. together with the results obtained by other authors.

Table 5.2. Cut-off wavenumber.

$\frac{a}{A} = \frac{1}{4}$		$\frac{B+b}{A} = \frac{4}{9}$	$\frac{b}{A} = \frac{2}{9}$	
n	Matrix band	Difference formula	$\frac{h}{A}$	$(kA/\pi)^2 = (2A/\lambda_c)^2$
21	13	FD_{20}	1/9	0.638
65	21	FD_{20}	1/18	0.585
65	36	FD_{180}	1/18	0.580
140	27	FD_4	1/27	0.558
140	29	FD_{20}	1/27	0.551
	Cohn[21]			0.585
	Orthogonal modes(section 4)			0.535
	Young and Hohmann[17]			0,533
	Experimental (by interpolation)			0.527

It is seen that the use of 21 field points leads toa a rather inaccurate result.This may be accounted for by the fact that the mesh length,h, is not sufficiently small for the number of points on the boundary to be sufficient to describe the boundary conditions accurately.

The two calculations carried out for the 65 and 140 field points indicate that higher approximations to the Laplacian do not significantly affect the result.As might be expected,the crucial factor affecting the accuracy is the number of mesh points in the cross-section. Since the experimental value of $(kA)^2$ differs by about 5% from the value given for both matrices of order 140,and by about 10% for both matrices of order 65, it is reasonable to expect that the error would be reduced to less than 2% by using a matrix of order 300. A computer large enough to deal with such a matrix is,unfortunately,not available.

Field distribution.

Values of the magnetic field components at selected points in the cross-section are given in Table 5.3. The field points refer to the drawing in Fig.5.4. The transverse components of field are normalised so that

$$H_t = \frac{\beta A}{(kA)^2} \frac{A}{2h} \overline{H}_t \qquad 5.7.2.$$

The transverse electric field,E_t, is obtained from H_t through the H-mode wave impedance, $\frac{\omega\mu}{\beta}$. The figures in Table 5.3. are found for the case, n = 65, the difference formula used being FD_{20}.

Table 5.3. Magnetic field components - ridged waveguide.

Point	H_z	$\overline{H}_x$	$\overline{H}_y$
A1	0.8476561	0.0000000	0.0000000
A3	0.8666364	0.0000000	0.0363394
A5	0.9164984	0.0000000	0.0567317
A7	0.9710453	0.0000000	0.0428127
A9	0.9945004	0.0000000	0.0000000
C1	0.7979906	0.0990417	0.0000000
C3	0.8188906	0.0968947	0.0418506
C5	0.8802867	0.0770311	0.0744891
C7	0.9541842	0.0295533	0.0576786
C9	0.9851966	0.0148273	0.0000000
E1	0.6509737	0.1912215	0.0000000
E3	0.6704992	0.1988041	0.0430714
E5	0.7550565	0.2377621	0.1540593
E7	0.9228579	0.0141920	0.1070004
E9	0.9715302	0.0055723	0.0000000
G1	0.4223191	0.2572361	0.0000000
G3	0.4304988	0.2671818	0.0140347
G5	0.4432416	0.2979094	0.0000000
I1	0.1456591	0.2913182	0.0000000
I3	0.1472892	0.2945784	0.0024334
I5	0.1491116	0.2982232	0.0000000

At this point a comparison is made between the magnetic field components H_x and H_z along the top waveguide wall, calculated by finite-differences and by the orthogonal mode approach described in section 4. In both cases the component H_z is normalised to be unity at the side wall and the component H_x to be unity at the centre plane of symmetry. The fields are drawn in Fig.5.5. There is close agreement between the two calculations for both H_x and H_z, the difference never exceeding 5%.

Circular polarisation.

For the case, n = 65, the points on the top waveguide wall, (y = 0), at which $P (x_0, 0, f_0)$ is unity, are found for three values of frequency, f, in X band - one at either extreme, and the third in the centre. The variation at $x = x_0$ of P over the X band frequency range, (8.4. - 12.4 Gc/s), is defined as δP_f. If x_1, x_2, and x_3 are such that

$$P (x_1, 0, 8.4 \text{ Gc/s}) = 1$$

$$P (x_2, 0, 10.4 \text{ Gc/s}) = 1$$

$$P (x_3, 0, 12.4 \text{ Gc/s}) = 1$$

then $x_1 - x_3$ is defined as δx_P at x_2.

The quantity δx_P is the shift in the position of circular polarisation as the frequency moves from one end of X band to the other. The calculated values of δP_f and δx_P for three ridged waveguides having the same width, a, but different heights, b, are compared in Table 5.4. with

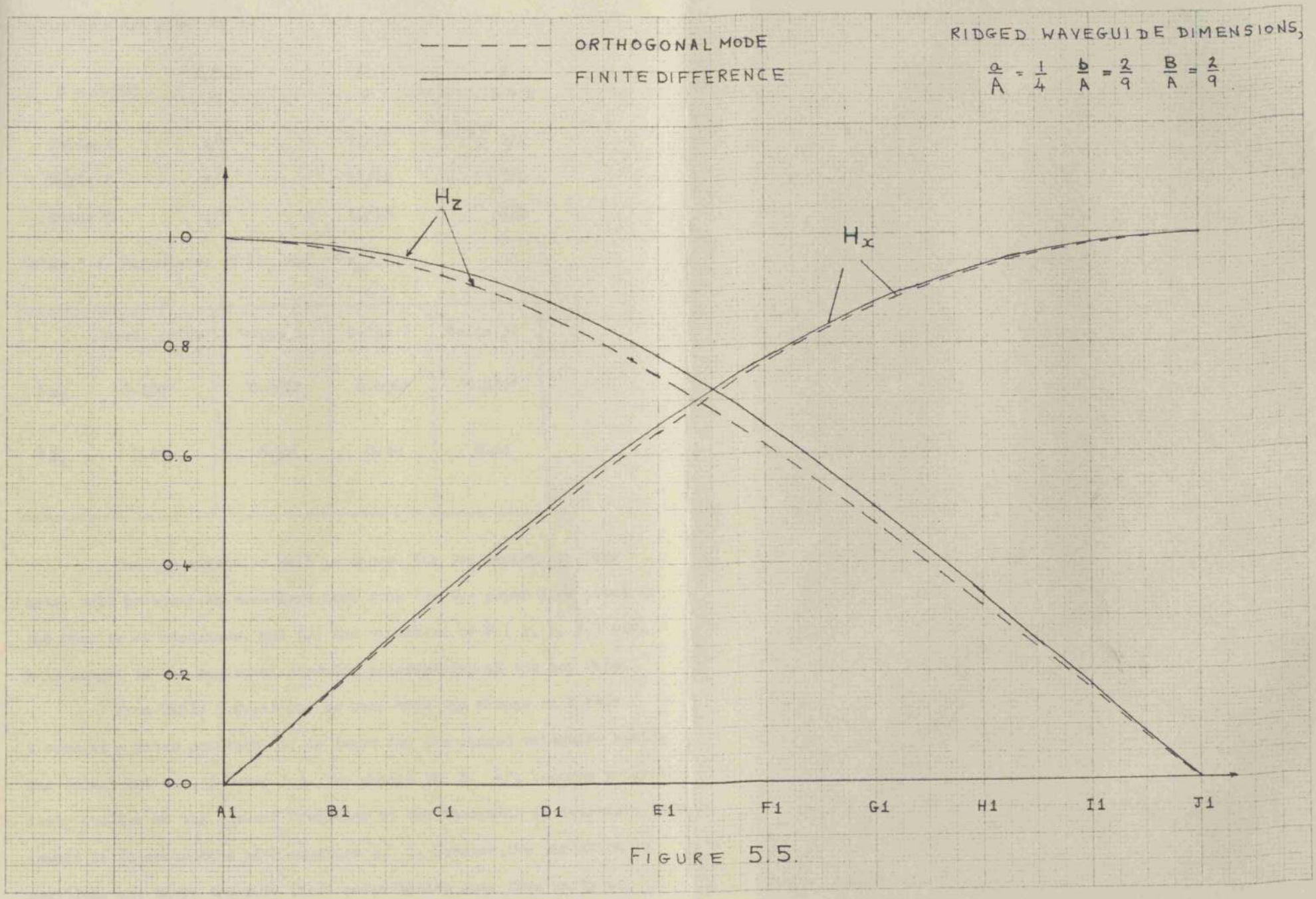
ORTHOGONAL MODE
FINITE DIFFERENCE
RIDGED WAVEGUIDE DIMENSIONS,
a/A = 1/4 b/A = 2/9 B/A = 2/9
Hz
Hx
1.0
0.8
0.6
0.4
0.2
0.0
A1
B1
C1
D1
E1
F1
G1
H1
I1
J1

FIGURE 5.5.

the corresponding values in rectangular waveguide. The ridged waveguide parameters are given by :-

A = 0.90"	$\frac{B + b}{A}$	$\frac{2a}{A}$	$\frac{b}{B + b}$
Guide 1	4/9	11/18	1/2
Guide 2	4/9	11/18	3/8
Guide 3	4/9	11/18	1/4

Table 5.4. Dependence of δP_f and δx_p.

	Rect. guide	Guide 1	Guide 2	Guide 3.
δx_p	0.106"	0.061"	0.050"	0.037"
δP_f	0.65	0.52	0.48	0.44

The top waveguide wall is chosen for two reasons,(1) the metal wall provides an excellent heat sink for the power dissipated in the ferrite at resonance, and (2) the variation of P (x, y, f) with y is slight in the region of circular polarisation at the top face.

From Table 5.4.,it may be seen that the change in P over X band,at a given position, x, is least for the ridged waveguide having the lowest cut-off, (Guide 3). The change in P, δP, becomes progressively smaller as the cut-off frequency of the waveguide is decreased.This result is in accordance with equation 5.7.1. However,the variation in position, x_p, where the r.f. field polarisation goes from unity at

8.4 Gc/s to unity at 12.4 Gc/s also becomes smaller. This means that although the frequency bandwidth is enhanced by using a ridged waveguide with a large ridge, the effect may be lost by a sharp increase of the dependence of P on x. Comparing the rectangular waveguide with the ridged waveguide, the frequency bandwidth is increased in the latter case, but at the expense of reduced ferrite cross-section brought about because δx_p is smaller. In order to achieve the same overall loss as in the rectangular waveguide, it is necessary to increase the proposed axial length of the ferrite. This is because the position of near-unity P in the ridged waveguide is much closer to the side wall than in the rectangular waveguide. Nearer the side wall, the electromagnetic fields are weaker and the attenuation in the ferrite is reduced.

Experimental results are presented in page 93 which show the maximised reverse and forward loss in a slab of ferrite located at the position of circular polarisation on the top waveguide wall. For a given slab position, the results indicate that at one frequency, the forward loss passes througha a minimum while the forward-to-reverse loss ratio remains small. On either side of the centre frequency which agrees well with the calculated value, the forward loss rises rapidly. This situation should be compared with that of the dielectric loaded waveguide where the forward loss remains small throughout the frequency band, see Fig. 7.3. These results are in accordance with the calculations of circular polarisation of the r.f. magnetic field which are given in graphical form in Fig.3.2a. in the

the centre frequency, the forward loss rises rapidly and increases to 1.5 times its minimum value over a range of 2.9.Gc/s when D = 0.13". It is concluded that the dependences of P on position, x, and frequency, f, tend to cancel and, in consequence, the bandwidth of the ridged waveguide as measured above, is not a great improvement on the rectangular waveguide. The situation is improved, however, if dielectric loading techniques are used,(see section 6.4.). This follows because (a), the field strength at the ferrite location is increased, (b), the region of circular polarisation is locked to the ferrite position and (c), the effect of the ridge keeps the cut-off frequency of higher-modes from intruding into X band.

6. Inhomogeneously-loaded waveguides - finite differences.

6.1. Introduction.

It is proposed to show how the finite-difference method is applied to the investigation of mode propagation in dielectric slab loaded waveguide, and later on, to H-mode propagation in a ferrite loaded rectangular waveguide, section 6.3.

The air-dielectric interface is assumed to lie parallel to the coordinate axis, y. The waveguide cross-section is subdivided as before, into square sub-regions of side length 'h', such that certain field points lie on the interface. In the presence of the dielectric, the transverse wavenumber, kA, is not constant. It has one value in air, $k_A A$, and another, $k_D A$, in dielectric, and is also frequency-dependent. In fact

$$k_A A = (\omega^2 \mu_o e_o - \beta^2)^{\frac{1}{2}} \qquad 6.1.1.$$

$$k_D A = (\omega^2 \mu_o e_o e_r - \beta^2)^{\frac{1}{2}} \qquad 6.1.2.$$

where e_r is the dielectric permittivity.

The FD_4 formula, applied at points lying in the air region, gives, by equation 5.2.6.,

$$\sum_1^4 \phi - 4 \phi_o = - h^2 k_A^2 \phi_o \qquad 6.1.3.$$

For ordinary points in the dielectric medium, the corresponding difference equation is written as:-

$$u \left\{ \sum_1^4 \phi - 4 \phi_o \right\} = - h^2 k_A^2 \phi_o \qquad 6.1.4.$$

where $u = (k_A / k_D)^2$.

The difference equations on the interface are more difficult to obtain. This is because the normal derivative of ϕ is always discontinuous at the interface, causing the difference formulae so far obtained to break down. Further, if the derivative of ϕ with respect to y is non-zero on the interface, all the propagating modes are hybrid, i.e. they all have a longitudinal component of both H and E. The situation is first discussed where the derivative of ϕ with respect to y is zero on the interface, allowing pure H-modes to propagate.

6.2. Dielectric slab loaded waveguide.

The field components for propagating H-modes are given in equation 5.1.1. On the dielectric-air interface, Fig. 6.1., H_x is continuous giving the condition that

$$\frac{1}{k_A^2} \left(\frac{\partial \phi}{\partial x} \right)_D = \frac{1}{k_D^2} \left(\frac{\partial \phi}{\partial x} \right)_D \qquad 6.2.1.$$

Since $k_A \neq k_D$, it follows that the notmal derivative of ϕ is discontinuous at the interface. In order to resolve the difficulty of dealing with discontinuous functions, 'image' values of ϕ at points 1 and 3 are introduced which make the normal derivative of ϕ on the interface continuous. In this way, the difference expression of equation 6.2.1. becomes

$$\frac{1}{k_A^2} (\phi_1 - \phi_{3A}) = \frac{1}{k_D^2} (\phi_{1D} - \phi_3) \qquad 6.2.2.$$

where ϕ_{1D} and ϕ_{3A} are the image values of ϕ. These are the

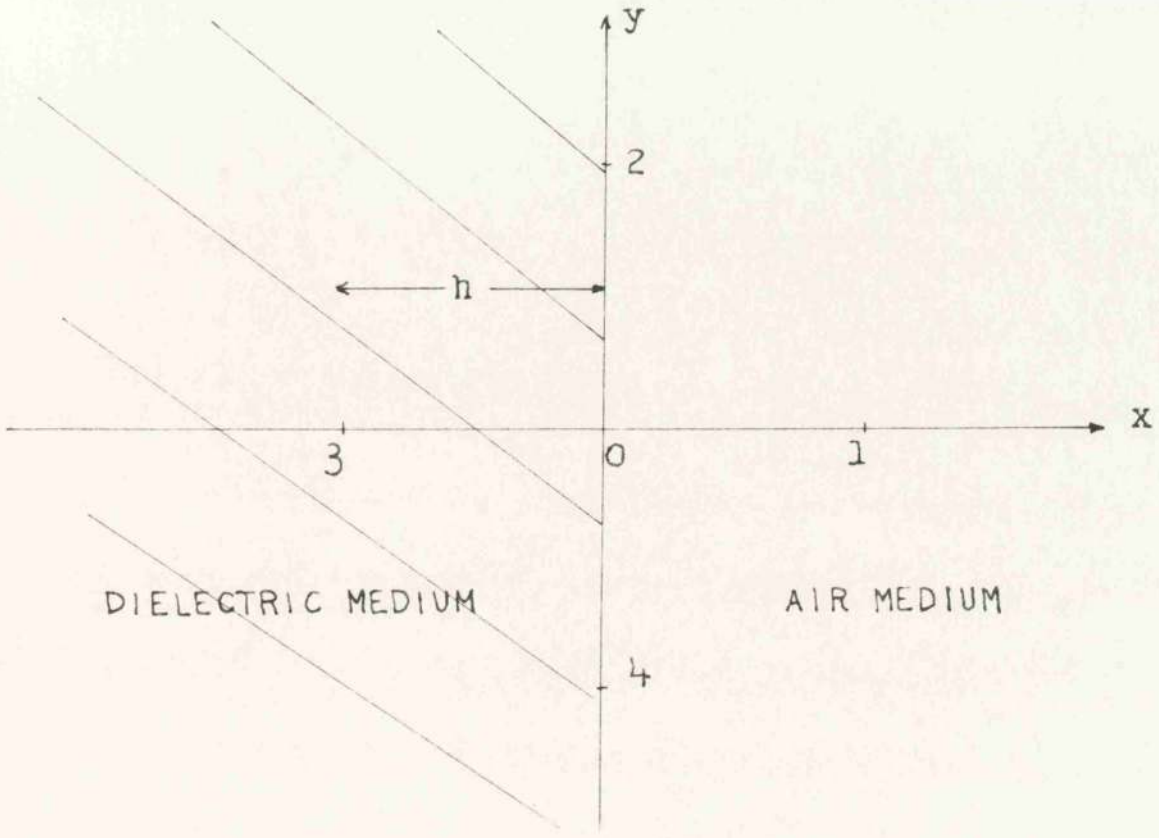

FIGURE 6.1.

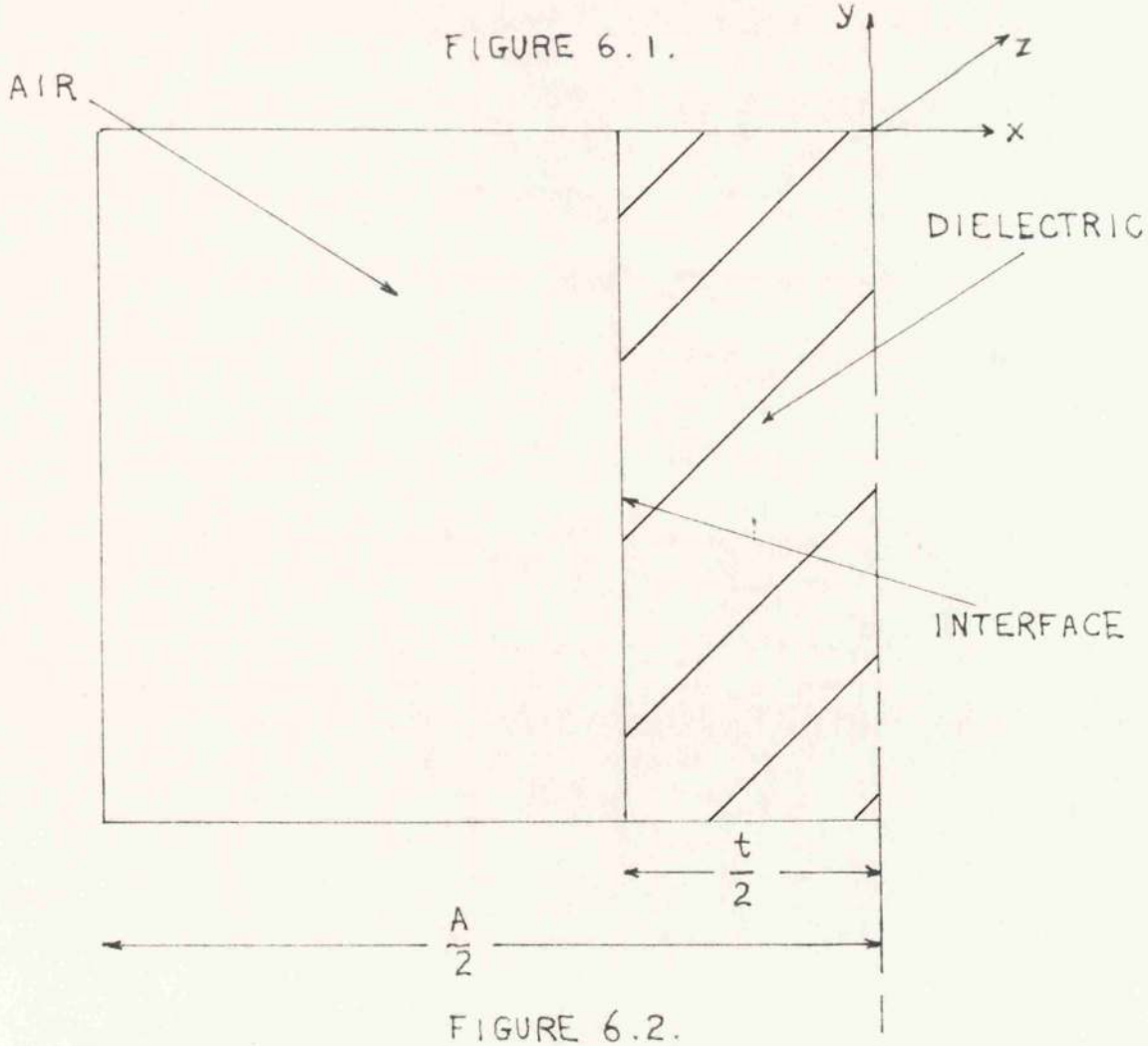

FIGURE 6.2.

values ϕ would have at points 1 and 3 were no air and no dielectric present respectively.With this formulation,equation 5.2.6. is then applied at the point 0,giving separate equations in ϕ_{1D} and ϕ_{3A} :-

$$\phi_{1D} + \phi_2 + \phi_3 + \phi_4 - 4\phi_0 = - h^2 k_D^2 \phi_0 \qquad 6.2.3a.$$

$$\phi_1 + \phi_2 + \phi_{3A} + \phi_4 - 4\phi_0 = - h^2 k_A^2 \phi_0 \qquad 6.2.3b.$$

By eliminating the image functions ϕ_{1D} and ϕ_{3A} between equations 6.2.2. and 6.2.3.,the following equation is obtained for points lying on the interface :-

$$\phi_1 + u\,\phi_3 + \tfrac{1}{2}(1 + u)(\phi_2 + \phi_4 - 4\phi_0) = - h^2 k_A^2 \phi_0 \qquad 6.2.4.$$

Equation 6.2.4. has been obtained by employing the simplest formula for the x-derivative of ϕ together with a double operation of the FD_4 formula. Higher approximations to the derivative and to the difference representation are prohibitively difficult when the 'image' technique is employed for interface points.

The 'n' field points are completely covered by applying equations 6.1.3.,6.1.4.,or 6.2.4.,whichever is relevant at a particular point. The right-hand sides of these equations are identical, $(- h^2 k_A^2 \phi_0)$ and hence the matrix formulation of equation 5.2.11. is again obtained. A complication occurs,however,since some of the elements are frequency-dependent owing to the presence of 'u'.Thus the matrix equation must be solved for discrete values of u corresponding to the investigation of the fields and wavenumbers at selected frequencies in the range of interest.This situation should be compared with that of the rectangular waveguide where equation 5.2.11. need only be solved once to determine

completely the fields and wavenumbers throughout a given frequency band.

A further observation can be made that direct application of equations 6.1.3.,6.1.4., and 6.2.4. to H-mode problems is inefficient since these are one-dimensional in the coordinate 'x'. The one-dimensional analogue of equation 6.2.4. is obtained by setting ϕ_2 and ϕ_4 equal to zero.

$$\phi_1 + u\,\phi_3 - 2\,(1 + u)\,\phi_0 = -\,h^2k^2\phi_0 \qquad 6.2.5.$$

The one-dimensional formulation leads to substantially-increased accuracy in the final results over a two-dimensional treatment,for a given number of field points.It should not be concluded, however,that the two-dimensional equations are unimportant since they are,indeed,essential when discussing hybrid modes,see section 6.4.

A simple illustration of the above theory is obtained by considering the fields and transverse wavenumbers of the dominant H-mode in a rectangular waveguide loaded with a centrally-located dielectric slab parallel to the narrow waveguide wall.One symmetrical half of the waveguide cross-section is shown in Fig.6.2. Calculations were carried out for a waveguide containing a slab of permittivity, $e_r = 12$, and ratio of thickness to waveguide broad dimension, $t/A = 1/5$. Three values of u were taken corresponding to frequencies at the lower end,centre,and upper end of the X band frequency range in X band waveguide.In each case,fifty field points were used at equal intervals in the range $0 \leqslant x \leqslant -A/2$. The one-dimensional difference formula was employed throughout.

The results are drawn up in tabular form. In Tables 6.1. and 6.2.,the transverse wavenumbers at each frequency,and the magnetic field components at the centre frequency,respectively,are compared with those predicted by the separation-of-variables method in section 3.

Table 6.1. Transverse wavenumber.

u	Finite-difference	Separation-of-variables	$\frac{2A}{\lambda_o}$
	$(k_A A)^2$	$(k_A A)^2$	
- 1.50	- 117.4	- 117.8	1.345
- 2.00	- 181.8	- 182.5	1.587
- 2.50	- 252.2	- 252.8	1.807

Table 6.2. Field components ; $u = -2$; $\frac{2A}{\lambda_o} = 1.587$

Point	Finite-differences		Separation-of-variables		$\frac{x}{A}$
	H_z	H_x	H_z	H_x	
1	0.0091	0.0000	0.0091	0.0000	0.50
5	0.0105	0.0055	0.0105	0.0055	0.46
9	0.0150	0.0127	0.0149	0.0126	0.42
13	0.0239	0.0236	0.0238	0.0235	0.38
17	0.0400	0.0415	0.0398	0.0414	0.34
21	0.0589	0.0718	0.0587	0.0717	0.30
25	0.1160	0.1234	0.1158	0.1232	0.26
29	0.1987	0.2119	0.1984	0.2115	0.22
33	0.3404	0.3636	0.3403	0.3630	0.18
37	0.5834	0.6223	0.5828	0.6217	0.14
41	1.0000	1.0680	1.0000	1.0668	0.10
45	0.6640	1.5516	0.6640	1.5497	0.06
49	0.2325	1.8123	0.2326	.8074	0.02

Table 6.3. Magnetic polarisation.

$\frac{2A}{\lambda_o}$	1.350			1.587			1.807		
Point	H_z	H_x	H_x/H_z	H_z	H_x	H_x/H_z	H_z	H_x	H_x/H_z
1	0.0263	0.0000	0.000	0.0091	0.0000	0.000	0.0035	0.0000	0.000
5	0.0288	0.0136	0.438	0.0105	0.0055	0.524	0.0042	0.0025	0.595
9	0.0368	0.0277	0.753	0.0150	0.0127	0.847	0.0067	0.0061	0.910
13	0.0518	0.0480	0.927	0.0239	0.0236	0.987	0.0120	0.0123	1.025
17	0.0766	0.0774	1.010	0.0400	0.0415	1.038	0.0223	0.0235	1.054
21	0.1161	L.1217	1.048	0.0679	0.0718	1.057	0.0420	0.0446	1.062
25	0.1777	1.1891	1.064	0.1160	0.1235	1.065	0.0790	0.0842	1.064
29	0.2732	0.2926	1.071	0.1987	0.2120	1.067	0.1490	0.1588	1.066
33	0.4208	0.4518	1.074	0.3404	0.3634	1.068	0.2811	0.2995	1.066
37	0.6486	0.6972	1.075	0.5834	0.6231	1.068	0.5302	0.5650	1.067
41	1.0000			1.0000			1.0000		
45	0.6543	1.4645	2.238	0.6640	1.5517	2.337	0.6718	1.6373	2.437
49	0.2275	1.6718	7.349	0.2325	1.8123	7.795	0.2365	1.9477	8.236

The magnetic field components and ellipticity at each of three frequencies are presented in Table 6.3. The field components are normalised so that H_z is unity at the dielectric-air interface.

In tables 6.1. and 6.2.,the results obtained by finite-difference methods and the separation-of-variables technique agree to within 1%. In table 6.3.,it may be seen that the fields tend to crowd more into the dielectric at higher frequencies, and that the ellipticity remains small over a substantial part of the air region throughout X band,(assuming that A is the width of the X band waveguide). Since the r.f. magnetic field is almost circularly-polarised over the whole of X band,and has a relatively high value at the dielectric-air interface, it appears that a suitable sample of ferrite material placed at the dielectric face would exhibit non-reciprocal attenuation with a low forward loss under the proper condition of d.c. magnetisation.

Experiments have been carried out with a small ferrite sphere, transversely-magnetised,at the dielectric face to confirm the calculated results by direct measurement.Another experiment is also described where the ferrite 'probe' is a long,thin slab against the dielectric where the reverse loss is of the same order as that in a practical isolator, (20db).

6.3. Ferrite Slab Loaded Waveguide.

The complexity of the mathematical difficulties involved in solving problems concerning propagation through ferrites is mainly due to the tensor property of the ferrite permeability. In certain simple cases, the tensor reduces to a scalar, e.g. in the propagation of electromagnetic waves in an infinite axially-magnetised ferrite medium where the normal modes have circularly polarised magnetic fields. In the case of the ferrite slab loaded waveguide, it is found[31] that the ferrite has an effective scalar permeability when the dominant H-mode propagates. The fields in this configuration are of interest in the design of field displacement isolators, resonance isolators and non-reciprocal phase shifters. The problem is capable of treatment by the finite-difference method and an indication of the technique to be used is described below.

The cross-section of the structure to be discusses is drawn in Fig. 6.3. Since the fields are independent of y (this condition is essential for H-mode propagation), a one-dimensional treatment can be used. As in the case of the dielectric slab, the line y = 0, is subdivided into small equal intervals, h, in the range $-A/2 \leqslant x \leqslant A/2$ In the special case where the ferrite is central, an axis of symmetry exists at x = 0 and only the region $0 \leqslant x \leqslant A/2$ need be considered.

The propagating fields in the air medium are given by:-

$$E_y = \emptyset$$

$$H_x = -\beta/\omega\mu\,\emptyset \qquad 6.3.1.$$

$$H_z = \frac{j}{\omega\mu}\frac{\partial \emptyset}{\partial x}$$

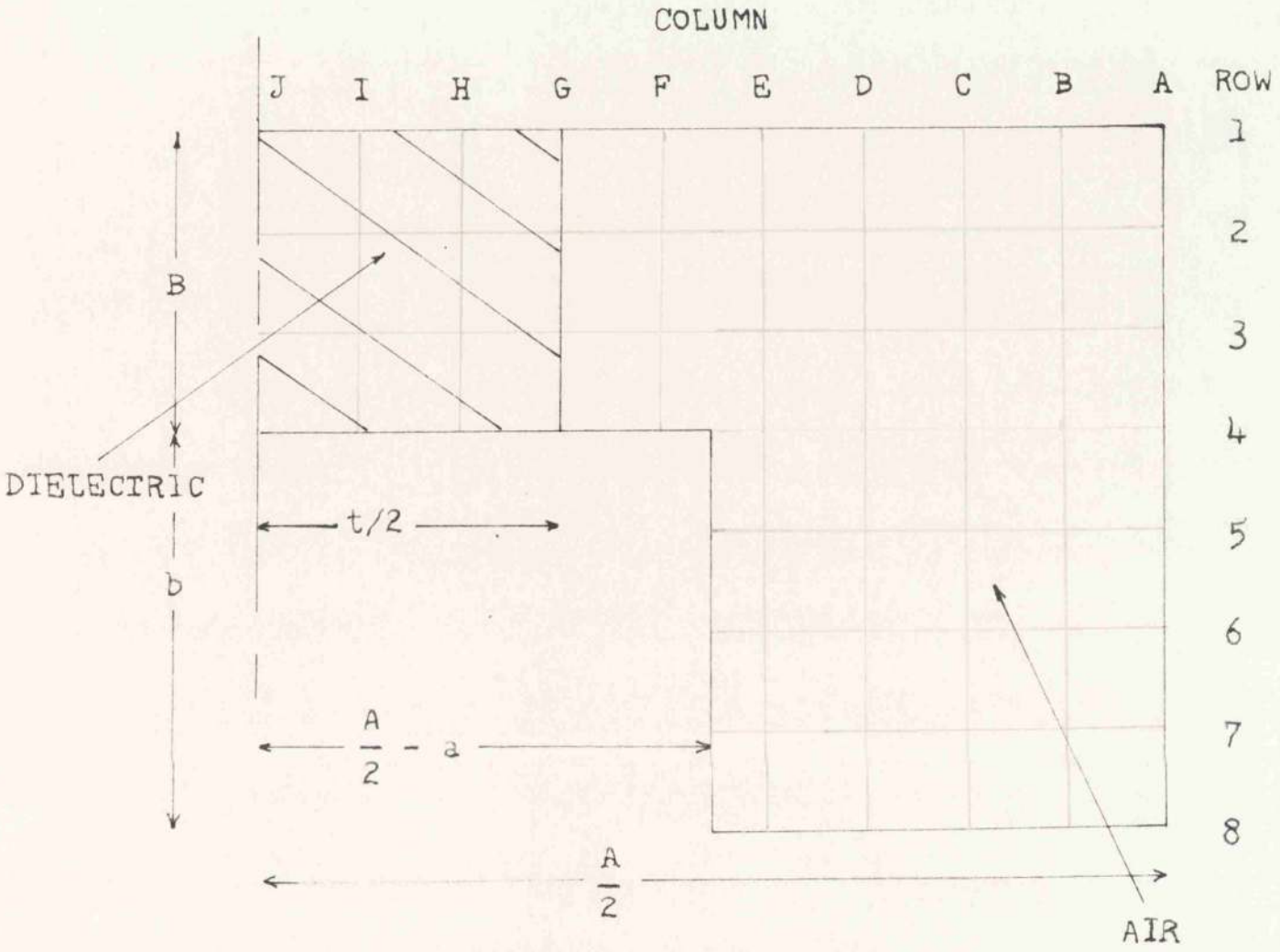

FIGURE 6.4.

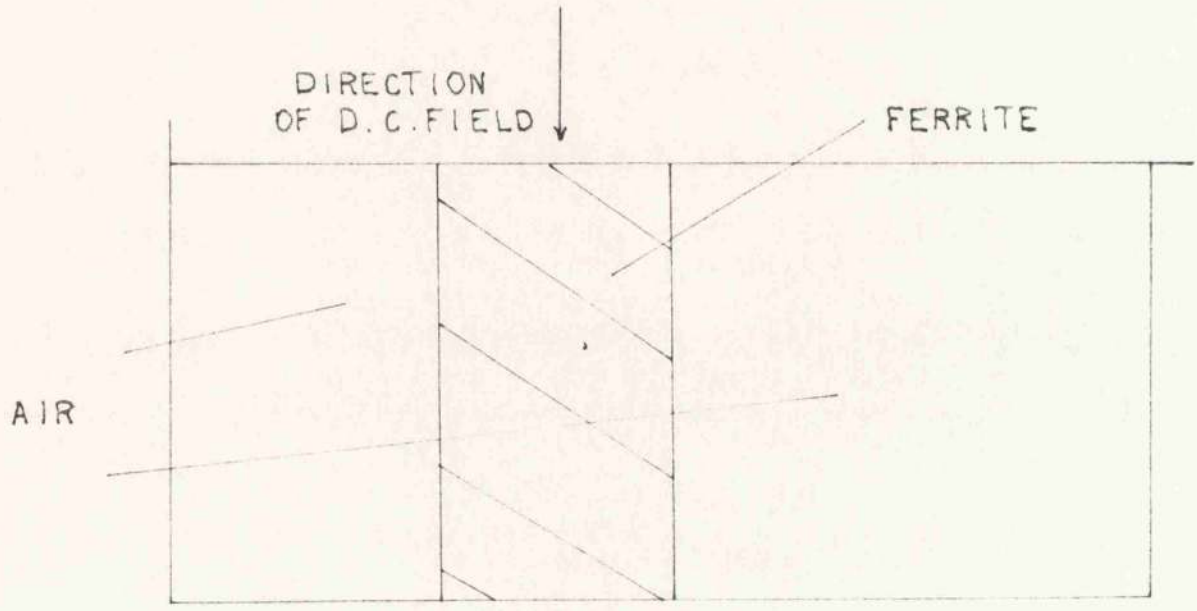

FIGURE 6.3.

Where ϕ is identified with E_y and satisfies the wave equation

$$(\nabla_t^2 + k_A^2)\,\phi = 0 \qquad 6.3.2.$$

$$k_A^2 = \omega^2 \mu_o \epsilon_o - \beta^2 \qquad 6.3.3.$$

It has been shown[32] that the field behaviour in the ferrite region, is given by:-

$$E_y \equiv \phi.$$

$$H_x = -\frac{1}{\mu_1^2 - \mu_2^2}\left(\frac{\beta \mu_1}{\omega}\phi + \frac{\mu_2}{\omega}\frac{\partial \phi}{\partial x}\right) \qquad 6.3.4.$$

$$H_z = \frac{j}{\mu_1^2 - \mu_2^2}\left(\frac{\mu_2 \beta}{\omega}\phi + \frac{\mu_1}{\omega}\frac{\partial \phi}{\partial x}\right)$$

where ϕ satisfies

$$(\nabla_t^2 + k_F^2)\,\phi = 0 \qquad 6.3.5.$$

$$k_F^2 = \omega^2 \mu_c \epsilon_r - \beta^2 \qquad 6.3.6.$$

$$\mu_c = \frac{\mu_1^2 - \mu_2^2}{\mu_1} = \text{ferrite 'effective' permeability} \qquad 6.3.7.$$

$$\epsilon_r = \text{ferrite permittivity.}$$

The ferrite tensor permeability is given by

$$\underline{\tilde{\mu}} = \begin{bmatrix} \mu_1 & -j\mu_2 & 0 \\ j\mu_2 & \mu_1 & 0 \\ 0 & 0 & \mu_0 \end{bmatrix} \qquad 6.3.8.$$

The finite difference equations applying at points lying in the air and ferrite region are found with little difficulty. In air,

$$\sum_1^2 \phi - 2\phi_0 = -h^2 k_A^2 \phi_0 \quad \text{(by equation 6.3.2.)} \qquad 6.3.9.$$

In ferrite

$$\sum_{1}^{2} \phi - 2\phi_o = -h^2 k_F^2 \phi_o \quad \text{(by equation 6.3.5.)} \qquad 6.3.10.$$

At the ferrite-air interface, the continuity conditions on E_y, B_x and H_z ensure that ϕ is continuous but $\partial\phi/\partial x$ is discontinuous. Employing 'image' functions values at the points 1 and 2 on either side of the interface point, as in section 6.1., we may express the continuity of H_z across the interface as follows:

$$\frac{1}{\omega \mu_o} \left(\frac{\partial \phi}{\partial x}\right)_A = \frac{1}{\mu_1^2 - \mu_2^2} \left(\frac{\mu_2 \beta}{\omega} \phi_o + \frac{\mu_1}{\omega} \left(\frac{\partial \phi}{\partial x}\right)\right)_F \qquad 6.3.11.$$

Hence,

$$(\phi_{1A} - \phi_2) = \frac{\mu_o \mu_2}{\mu_1^2 - \mu_2^2} \cdot 2\beta h . \phi_o + \frac{\mu_o \mu_1}{\mu_1^2 - \mu_2^2} (\phi_1 - \phi_{2F}) \qquad 6.3.12.$$

The double application of the FD_2 formula at the point O results in separate equations in ϕ_{1A} and ϕ_{2F}.

$$\begin{aligned} \phi_{1A} + \phi_2 - 2\phi_o &= -h^2 k_A^2 \phi_o \\ \phi_1 + \phi_{2F} - 2\phi_o &= -h^2 k_F^2 \phi_o \end{aligned} \qquad 6.3.13.$$

Eliminating ϕ_{1A} and ϕ_{2F} between equations 6.3.12. and 6.3.13., we have for the difference equation to be applied at the interface point,

$$2\phi_2 + 2\phi_1 F - 2\left(1 + F - \beta h . F \frac{\mu_2}{\mu_1}\right) \phi_o = -h^2 \phi_o (k_A^2 + k_F^2 F) \qquad 6.3.14.$$

Where $F = \dfrac{\mu_o}{\mu_c}$ 6.3.15.

The occurence of the term in β in equation 6.3.13 is to be expected since the fields are non-reciprocal with respect to the direction of propagation unless the ferrite is in the centre of the waveguide. For the purpose of expressing all the difference equations in matrix form, it is essential for the right-hand sides to be identical. It is possible to eliminate the term is β by taking advantage of the fact that under a reversal of the d.c. biassing magnetic field, the propagation constants in opposite directions differ only in sign. Thus, if

$$H_{d.c} = H_+ , \text{ then } \beta_+ = \beta \quad \text{and} \quad F = F_+ \qquad 6.3.16.$$

When $H_{d.c}$ is reversed,

$$H_{d.c} = -H_+ , \quad \beta_- = -\beta \quad \text{and} \quad F = F_- \qquad 6.3.17.$$

For the two conditions of opposite polarity of the d.c field, equations 6.3.13. may be written down and the term in β eliminated between them. In this way, the following equation is obtained for the interface point:-

$$\frac{1}{\frac{1+F_+}{F_+} + \frac{(\mu_1)_-}{(\mu_1)_+}\,\frac{1+F_-}{F_-}} \left\{ 2\phi_2 \left(\frac{1}{F_+} + \frac{(\mu_1)_-}{(\mu_1)_+} \cdot \frac{1}{F_-} \right) + 2\phi_1 \left(1 + \frac{(\mu_1)_-}{(\mu_1)_+} \right) \right.$$

$$\left. - 2\left(1 + \frac{(\mu_1)_-}{(\mu_1)_+}\right)\phi_0 + \left(\frac{\omega h}{c}\right)^2 \left[\frac{1+F_+}{1+F_+} + \frac{(\mu_1)_-}{(\mu_1)_+}\,\frac{1+F_-\,\epsilon_r}{1+F_-} \right] \phi_0 \right\}$$

$$= h^2\beta^2\phi_0 \qquad 6.3.18.$$

Equations 6.3.13. are rearranged to give the same right-hand side as 6.3.18.

$$\phi_1 + \phi_2 - \left(2 - \left(\frac{h\omega}{c}\right)^2\right)\phi_0 = h^2\beta^2\phi_0 \quad \text{(air)} \qquad 6.3.19.$$

$$\phi_1 + \phi_2 - \left(2 - \left(\frac{h\omega}{c}\right)^2 \frac{\epsilon_r}{F}\right)\phi_0 = h^2\beta^2\phi_0 \quad \text{(ferrite)} \qquad 6.3.20.$$

It is now possible by means of equations 6.3.18., and 6.3.19., and 6.3.20., to write down the elements of matrix B, equation 5.2.11. from which the latent root, $h^2\beta^2$ and vector can be found. The tensor elements, μ_1 and μ_2 are known once the d.c. biassing field, H_o, saturation magnetisation, M and the angular frequency, ω are prescribed. It follows from equations 6.3.15. and 6.3.7. that F_+, F_-, μ_- and μ_+ are known.

Having obtained the matrix equation, the derivation of the field distribution and propagation constants may be accomplished on a high-speed digital computer.

6.4. Dielectric loaded ridged waveguide.

One of the structures mentioned in section 6.2. which has been used[14] in conjunction with a magnetised ferrite as a broadband resonance isolator at C and S band, is the dielectric slab loaded ridged waveguide, shown schematically in Fig.6.4. Since the structure is not uniform in the y-direction, there is a dependence of electromagnetic field along the y-coordinate. It is found that attempts to satisfy the interface boundary conditions, assuming a pure H-mode leads to the conflicting condition that

$\frac{1}{k^2}\frac{\partial \phi}{\partial y}$ and $\frac{e_r}{k^2}\frac{\partial \phi}{\partial y}$ be continuous at the dielectric-air interface. Hence, pure H-modes cannot exist for the structure, and for the same reason, neither can pure E-modes. It is necessary, in order to satisfy all the boundary conditions, to consider a mode which is a combination of the fundamental H- and E-modes. Such a mode has a longitudinal component of both H and E and is commonly termed[33] a hybrid mode. It is true to state that, if a waveguide contains two media which are contiguous along a line parallel to one or both of the transverse coordinates, and there is a dependence of field along these coordinates, then the only propagating modes are hybrid. The interface couples the E- and H-modes.

Superposition of equations 5.1.1. and 5.1.2. gives the following expressions for the electromagnetic fields referred to a rectangular coordinate system,

$$k^2 H_x = -j\beta \frac{\partial \phi}{\partial x} + j\omega e_o e_r \frac{\partial \psi}{\partial y}$$

$$k^2 H_y = -j\beta \frac{\partial \phi}{\partial y} - j\omega e_o e_r \frac{\partial \psi}{\partial x}$$

$$H_z \equiv \phi$$

$$k^2 E_x = -j\beta \frac{\partial \psi}{\partial x} - j\omega\mu \frac{\partial \phi}{\partial y} \qquad 6.4.1.$$

$$k^2 E_y = -j\beta \frac{\partial \psi}{\partial y} + j\omega\mu \frac{\partial \phi}{\partial x}$$

$$E_z \equiv \psi$$

ϕ and ψ are solutions of equation 5.1.3. subject to the boundary conditions :-

$$\frac{\partial \phi}{\partial n} = 0 \; ; \qquad \Psi = 0 \quad \text{on the perfectly conducting walls} \qquad (6.4.2.)$$

according to the boundary conditions at the interface of the two dielectric media, all the H components and all the E components with the exception of E_x are continuous, (D_x is continuous at the interface). Expressing the derivatives of ϕ and ψ in terms of the fields from equations 6.4.1., we find that

$$(\omega\mu H_x - \beta E_y) = j \frac{\partial \psi}{\partial y}$$

$$(\beta H_x - \omega\epsilon E_y) = j \frac{\partial \phi}{\partial x}$$

$$(\omega\mu H_y + \beta E_x) = j \frac{\partial \psi}{\partial x} \qquad 6.4.3.$$

$$(\beta H_y + \omega\epsilon E_x) = -j \frac{\partial \phi}{\partial y}$$

From these equations and the known continuity conditions on

the field components, it is found that

$\frac{\partial \phi}{\partial x}$, $\frac{\partial \psi}{\partial x}$ are discontinuous at the interface and

$\frac{\partial \phi}{\partial y}$, $\frac{\partial \psi}{\partial y}$ are continuous at the interface.

The finite-difference equations derived in section 5 are invalid if the functions dealt with are discontinuous or if they have discontinuous first or second derivatives. It is necessary to reformulate the equations, as was done in section 6.1. Use is made, therefore, of image function values at points 1 and 3, (see Fig.6.1.) to resolve the difficulty of having discontinuous x-derivatives. The equations of continuity of H_x and H_y are written down with a numerical approximation, used in equation 5.6.2., substituted for the spatial derivatives of ϕ and ψ .

For H_x,

$$\frac{1}{u}\left\{\beta(\phi_1 - \phi_{3A}) - \omega e_o (\psi_2 - \psi_4)\right\} = \beta(\phi_{1D} - \phi_3) - \omega e_o e_r (\psi_2 - \psi_4) \qquad 6.4.4.$$

In the case of H_y,

$$\frac{1}{u}\left\{\beta(\phi_2 - \phi_4) + \omega e_o (\psi_1 - \psi_{3A})\right\} = \beta(\phi_2 - \phi_4) + \omega e_o e_r (\psi_{1D} - \psi_3) \qquad 6.4.5.$$

The FD_4 formula is again applied at the point 0 of Fig.6.1. to give separate equations in ϕ_{1D} and ϕ_{3A} :-

$$\phi_{1D} + \phi_2 + \phi_3 + \phi_4 - 4\phi_0 = -h^2 k_D^2 \phi_0 \qquad 6.4.6.$$

$$\phi_1 + \phi_2 + \phi_{3A} + \phi_4 - 4\phi_0 = -h^2 k_A^2 \phi_0 \qquad 6.4.7.$$

The image function values are eliminated between equations 6.4.4.,6.4.6.,and 6.4.7. to give the following equation for ϕ at the interface point O ;-

$$\phi_1 + \phi_3 + \tfrac{1}{2}(1+u)(\phi_2 + \phi_4 - 4\phi_0) + \tfrac{1}{2}(e_r u - 1)(\eta_2 - \eta_4)$$

$$= -h^2 k_A^2 \phi_0 \qquad 6.4.8.$$

where $u = (k_A / k_D)^2$ and $\eta = \frac{\omega}{\beta c}\left(\frac{\epsilon_o}{\mu_o}\right)^{1/2}\Psi$ 6.4.9.

The function η is introduced instead of Ψ for two reasons.It first allows equation 6.4.8. to be written in non-dimensional form and secondly absorbs the unknown phase velocity, $\frac{\omega}{\beta}$, of the travelling wave. When ϕ, η , and k_A are determined through the solution of the matrix equation for a given value of u, the phase velocity is determined through k_A and u, and hence, so is the function Ψ.

Using the equivalent formulation of equations 6.4.6. and 6.4.7. to eliminate the image functions η_{1D} and η_{3A} , the following equation is obtained for η at the point O on the interface :-

$$\frac{1}{1+e_r}\Big\{2\eta_1 + 2e_r u\eta_3 + (e_r u + 1)(\eta_2 + \eta_4 - 4\eta_0) + (1-u)(\phi_2 - \phi_4)\Big\} = -h^2 k_A^2 \eta_0 \qquad 6.4.10.$$

To solve a hybrid mode problem,the difference equations for ϕ and η must be set up separately at the 'n' field points in the cross-section. For points not lying on the interface,the FD_4 type formulae given in equations 6.1.3. and 6.1.4. are applied directly.Interface points

require the special procedure outlined above and summarised in equations 6.4.8. and 6.4.10. Thus, 2n linear algebraic equations are obtained, given u, for the ϕ_r, η_r values over the waveguide cross-section in terms of the unknown eigenvalue, k_A^2. These equations may again be written in the matrix form of equation 5.2.11. In this case, however, half the elements in the column vector are ϕ_r values and the remainder, η_r values. The matrix is conveniently written in partitioned form :-

$$B = \begin{bmatrix} \underline{H} & \underline{C}_1 \\ \underline{C}_2 & \underline{E} \end{bmatrix}$$

In this matrix, $\underline{H}$ is an H-mode matrix, $\underline{E}$ an E-mode matrix, and $\underline{C}_1$ and $\underline{C}_2$ are coupling matrices between the modes due to the field dependence on the transverse interface coordinates. With these modifications, the solution to the given problem is then obtained by the procedure described for homogeneous waveguides and H-modes in inhomogeneous waveguides. The method is, of course, capable of extension to cylindrical geometries and these are discussed in section 9.

As an example of the inhomogeneous waveguide structure which propagates a hybrid mode, the dielectric loaded ridged waveguide is chosen, Fig.6.4. The structure has been used together with two transversely magnetised ferrite slabs as a broadband resonance isolator. (A double ridge was used actually). The method for deriving the matrix equation has already been described in this section.

For simplicity in presentation, the field components and phase constants are given at one frequency for a particular structure. The

variation of the field components along row 2, (see Fig.6.4.),where the region of near circular polarisation of the r.f. magnetic field exists,is given in Table 6.4. The electric field components are normalise so that

$$E_t = \frac{\beta A}{(k_A A)^2} \cdot \frac{A}{2h} \bar{E}_t$$

$$E_z = \frac{\beta}{8 \omega e_o} \bar{E}_z$$

Table 6.4. Field components; $u = -2.5$ $2A/\lambda_o = 1.045$

Point	H_z	H_x	$-H_y$	$\bar{E}_z$	$-\bar{E}_x$	$\bar{E}_y$
A2	0.07411	0.00000	0.00843	0.00000	0.00810	0.00000
B2	0.08578	0.05248	0.01000	0.00003	0.00961	0.05052
C2	0.12460	0.12199	0.01431	0.00008	0.01372	0.11743
D2	0.20310	0.22958	0.02106	0.00020	0.02011	0.22096
E2	0.34530	0.40402	0.02566	0.00056	0.02425	0.38878
F2	0.59125	0.67724	0.01995	0.00162	0.01751	0.65150
G2	0.99519	1.09600		0.00490		
H2	0.72669	1.58231	0.00492	0.00192	0.00119	1.52522
I2	0.38319	1.88371	0.00164	0.00085	0.00048	1.81451
J2	0.00000	1.98767	0.00000	0.00058	0.00000	1.91440

The phase constants are given by ;

$(k_A A)^2 = -84.662 \quad (k_D A)^2 = 33.865 \quad (\beta A)^2 = 95.440$

The fields in Table 6.4. are normalised so that the axial magnetic component is unity at the point G1. Owing to the discontinuity in the normal derivatives of H_z and E_z at the interface, it is not possible to work out the transverse fields there by numerical differentiation. However, when the component varies smoothly acroes the interface it is possible to find the approximate value by interpolation. In this way, the value of H_x at the interface,(G2), which is necessary for the evaluation of the ellipticity of the r.f. magnetic field,is found. Interpolation is not possible with the value of E_x at the interface since it is discontinuous there.

It is observed from the figures in Table 6.4. that the propagating fields resemble closely those of an H-mode - H_y is small compared with H_x and H_z and similarly E_z and E_x are small compared with E_y. (In a rectangular waveguide propagating the dominant H-mode,only H_z,H_x and E_y are non-zero. This H-mode appearance is more pronounced in the dielectric region than in the air. Under these conditions, the r.f. magnetic field can be regarded as elliptically-polarised. In isolator applications the d.c. magnetic field acts in the y-direction and the y-component of r.f. magnetic field has second order effect on the precession anyway.

According to the figures in Table 6.4., the polarisation factor,P, at the location of the dielectric interface,is close to 1.11 and remains near this value over most of the waveguide region next to the top wall. It is found,as in the case of the dielectric loaded rectangular waveguide that the variation of P with frequency is small when the air region is well above transverse cut-off,i.e. k_A^2 is negative and large.

When the guide width is 0.90", the frequency range over which P remains close to unity extends throughout X band. The presence of the ridge in an empty waveguide has been shown to have little effect on the cut-off frequency of the H_{02} mode. Also, the cross-sectional area of the dielectric is much smaller than that used in the case of the dielectric loaded rectangular waveguide. It is to be expected, therefore, that in the case of the dielectric loaded ridged waveguide, the unwanted higher-order modes do not cause the complications in the design of a ferrite resonance isolator that arise in the dielectric loaded rectangular waveguide.

The behaviour of the axial magnetic field over the whole cross-section is shown in Fig.6.5. The values of H_z are printed at the relevant mesh points in the cross-section. Also shown in Fig.6.5. are the parameters of the ridged waveguide structure together with the normalised free-space wavelength.

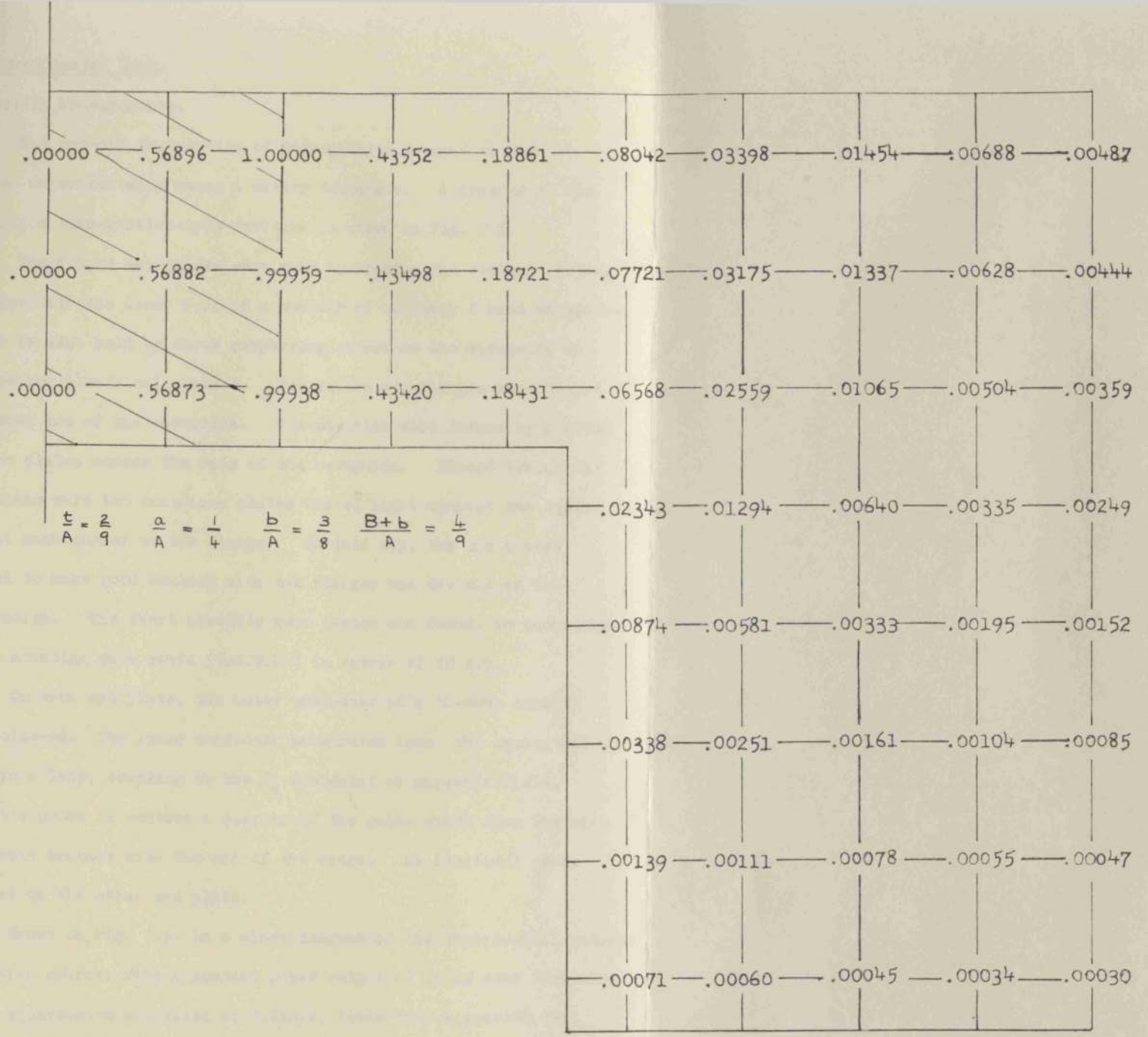
.00000 .56896 1.00000 .43552 .18861 .08042 .03398 .01454 .00688 .00487
.00000 .56882 .99959 .43498 .18721 .07721 .03175 .01337 .00628 .00444
.00000 .56873 .99938 .43420 .18431 .06568 .02559 .01065 .00504 .00359
.02343 .01294 .00640 .00335 .00249
.00874 .00581 .00333 .00195 .00152
.00338 .00251 .00161 .00104 .00085
.00139 .00111 .00078 .00055 .00047
.00071 .00060 .00045 .00034 .00030
t/A = 2/9 a/A = 1/4 b/A = 3/8 (B+b)/A = 4/9

FIGURE 6.5.

7. Experimental Work.

7.1. Cavity Measurements.

The cut-off frequencies of three ridged waveguides were determined experimentally using a cavity technique. A drawing of one of the ridged transmission-type cavities is shown in Fig. 7.1.

The ridged waveguides were made by brazing the central oblong brass ridge onto the lower face of a section of ordinary X band waveguide. The ridge is also held by three supporting screws on the waveguide to provide better electrical contact. Two square end flanges were brazed on at either end of the waveguide. The cavities were formed by placing two copper plates acress the ends of the waveguide. Placed behind the copper plates were two cast-iron plates bolted tight against the square flanges at each corner of the flange. In this way, the end plates were found to make good contact with the flanges and the end of the ridged section. The short circuits were tested and found, in each case, to give a standing wave ratio (V.S.W.R.) in excess of 28 d.b.

On each end plate, the outer conductor of a 50-ohm coaxial line is soldered. The inner conductor penetrates into the cavity and is formed into a loop, coupling to the H_x component of magnetic field. The magnetic probe is centred a quarter of the guide width from the side wall to avoid contact with the end of the ridge. An identical probe is situated on the other end plate.

Shown on Fig. 7.2. is a block diagram of the experimental set-up. A CW klystron source, with a nominal power output of 10 mw over frequency band, and square-wave modulated at 3.2kc/s, feeds into a coaxial tee

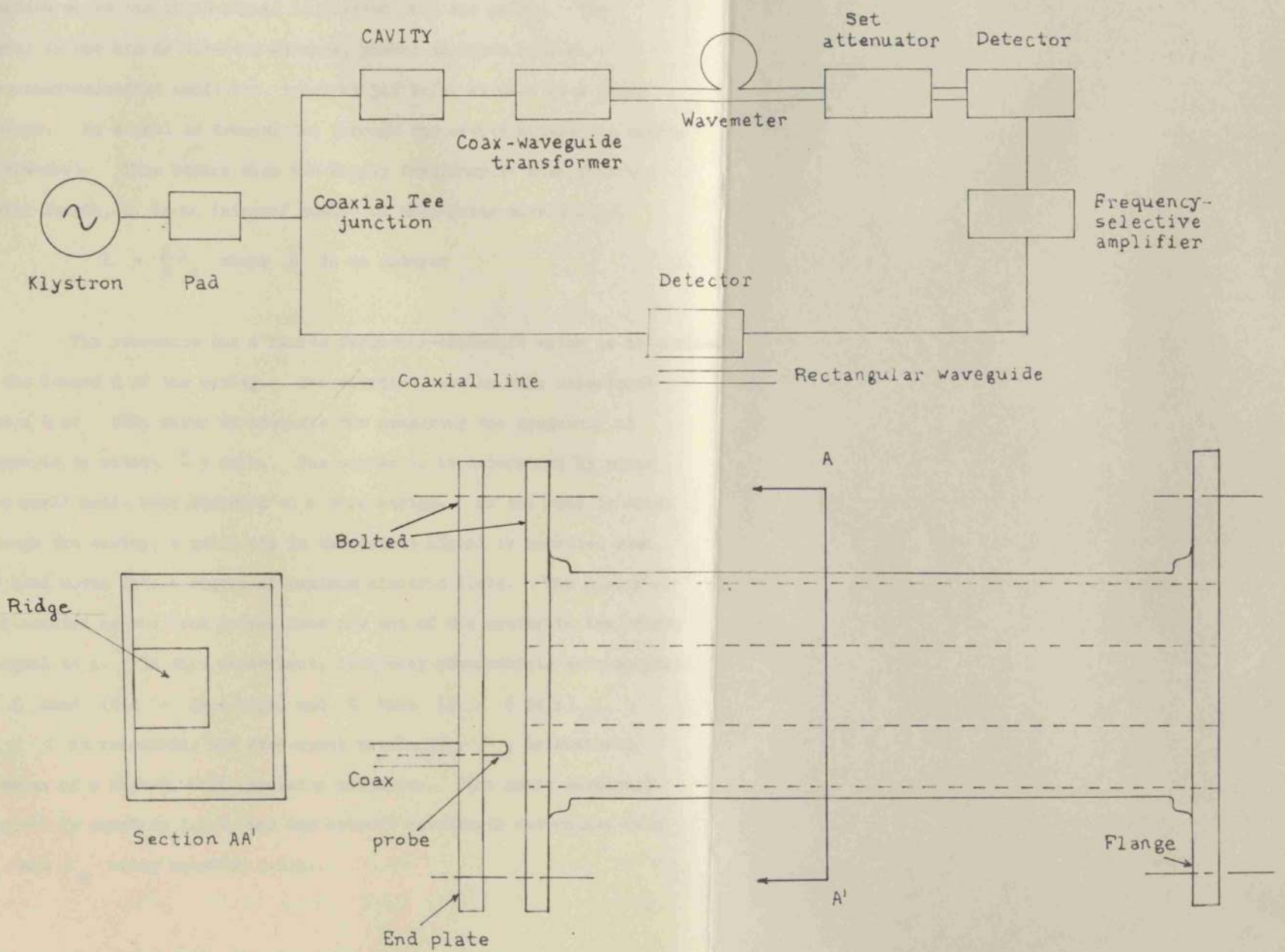
CAVITY
Set attenuator
Detector
Wavemeter
Coax-waveguide transformer
Coaxial Tee junction
Frequency-selective amplifier
Klystron
Pad
Detector
Coaxial line
Rectangular waveguide
A
Bolted
Ridge
Coax
probe
Section AA'
Flange
A'
End plate

FIGURE 7.1.

junction where the input signal is divided into two parts. The signal in one arm is detected at once, passed to input A of a frequency-selective amplifier, tuned at 3.2 kc/s, at used as a power monitor. No signal is transmitted through the cavity unless the cavity is resonant. This occurs when the supply frequency is such that the cavity length, L, is an integral number of half guide wavelengths,

$$L = \frac{n}{2}\lambda_g \quad \text{where } n \text{ is an integer} \qquad 7.11.$$

The resonance has a finite frequency-bandwidth which is determined by the loaded Q of the cavity. The cavities used in this experiment have a Q of 200, which is adequate for measuring the frequency at resonance to within $\pm$ 3 mc/s. The number n, is determined by means of a small metal bead attached to a thin string. As the bead is drawn through the cavity, a small dip in the output signal is detected when the bead moves into a region of maximum electric field. The number of dips counted as the bead passes from one end of the cavity to the other, is equal to n. In this experiment, frequency measurements were confined to X band (8.4 - 12.4 Gc/s) and C band (4 - 6 Gc/s).

At resonance, the free-space wavelength, λ_o, is measured by means of a high-Q, high precision wavemeter. The guide wavelength is given by equation 7.1.1. and the cut-off wavelength determined from λ_o and λ_g using equation 3.1.1.

Results.

The three ridged waveguides measured in the experiment have the following parameters:-

	Guide width	Ridge width	Guide height	Ridge height
Cavity 1	0.90"	0.45"	0.40"	0.135"
Cavity 2	0.90"	0.45"	0.40"	0.180"
Cavity 3	0.90"	0.45"	0.40"	0.225"

The measured λ_o, frequency and n are tabulated together with the calculated values of λ_c for each cavity.

Table 7.1. Cut-off wavelength by cavity measurement.

Cavity 1. L = 15.00 cms.						
n	1	2	3	4	7	8
f(Gc/s)	5.575	5.840	6.252	6.780	8.885	9.692
λ_o(cms.)	5.376	5.132	4.794	4.420	3.373	3.093
λ_c(cms.)	5.464	5.462	5.463	5.471	5.465	5.468

Cavity 2 L = 15.02 cms.							
n	2	3	4	7	8	9	10
f(Gc/s)	5.355	5.790	6.350	8.565	9.394	10.256	11.141
λ_o(cms.)	5.602	5.173	4.712	3.500	3.191	2 .923	2.691
λ_c (cms.)	6.034	6.043	6.051	6.049	6.055	6.053	6.054

Cavity 3 L = 15.00 cms.

Cavity 3	L = 15.00 cms.					
n						
f (Gc/s)	5.390	5.990	6.692	9.160	10.046	10.951
λ_o (cms)	5.560	5.003	4.478	3.275	2.986	2.739
λ_c (cms.)	6.689	6.715	6.728	6.723	6.721	6.720

The accuracy of the cavity-type measurement is extremely good because it depends on the accuracy with which the length of the cavity, and the frequency at resonance, can be measured. The high-precision wavemeter measures frequency to within $\frac{1}{2}$ Mc/s and the length of the cavity can easily be found to 0.010". The values of λ_c calculated for cavity 1 have a maximum deviation from the mean of 6 parts in 5000. The deviation in the other two cases is greater than this. This may be explained by the fact that, if there is a small gap between the ridge end and the short-circuiting end plate, the series capacitance of the gap has a much larger effect on the impedance at lower frequencies than at higher frequencies, ($X_c = \frac{1}{\omega C}$). For this reason, we might expect the calculated values of λ_c to differ more violently at smaller values of n. From the experimental Table 7.1., this effect is noticed. It is reasonable to expect, then, that the most accurate value of λ_c is found at the higher resonant frequencies. The effect of the wire probes on the cut-off frequency and loaded Q of the cavity has been ignored since both lie in a region of small electric field.

7. 2. Measurement of Ferrite Loss.

The object of the experiment is to measure the magnetic loss occuring in a ferrite loaded waveguide when the ferrite is biassed to resonance. The ferrite is transversely-magnetised in a uniform d.c. magnetic field provided by an electromagnet. For opposite senses of d.c. polarity, two such resonance losses are found. The smaller of these is called the forward loss, F, and the larger, the reverse loss, R.

The experimental set-up is shown in block diagram in Fig. 7.2. The power source used was a reflex klystron operating at 7 - 12 Gc/s with an average power output of 10 mW, CW, and square-wave modulated at 3.2 kc/s. The klystron has a built-in piston attenuator which controls the power output and gives the valve some protection from undesirable relections. At high frequencies, the attenuator has to be wound right in to give a reasonable signal level and an isolator is used to give added protection to the klystron. The signal from the klystron is fed by means of a coaxial line to waveguide transformer to a 4-port, 20 db directional coupler. Arm 3 is ended with a matched termination. The signal in arm 1 is used as a reference signal and is detected and fed to input A of a frequency-selective amplifier tuned to 3.2 kc/s. The 3-stup tuner in arm 1 is provided to match the crystal detector to give maximum power output. All actual measurements are taken in arm 2 where the input passed through a set-level attenuator, rotary-vane attenuator and the test waveguide to the detector. The rectified current is supplied along coaxial line to input B of the selective amplifier. The frequency of operation is measured with a high-Q absorption-type

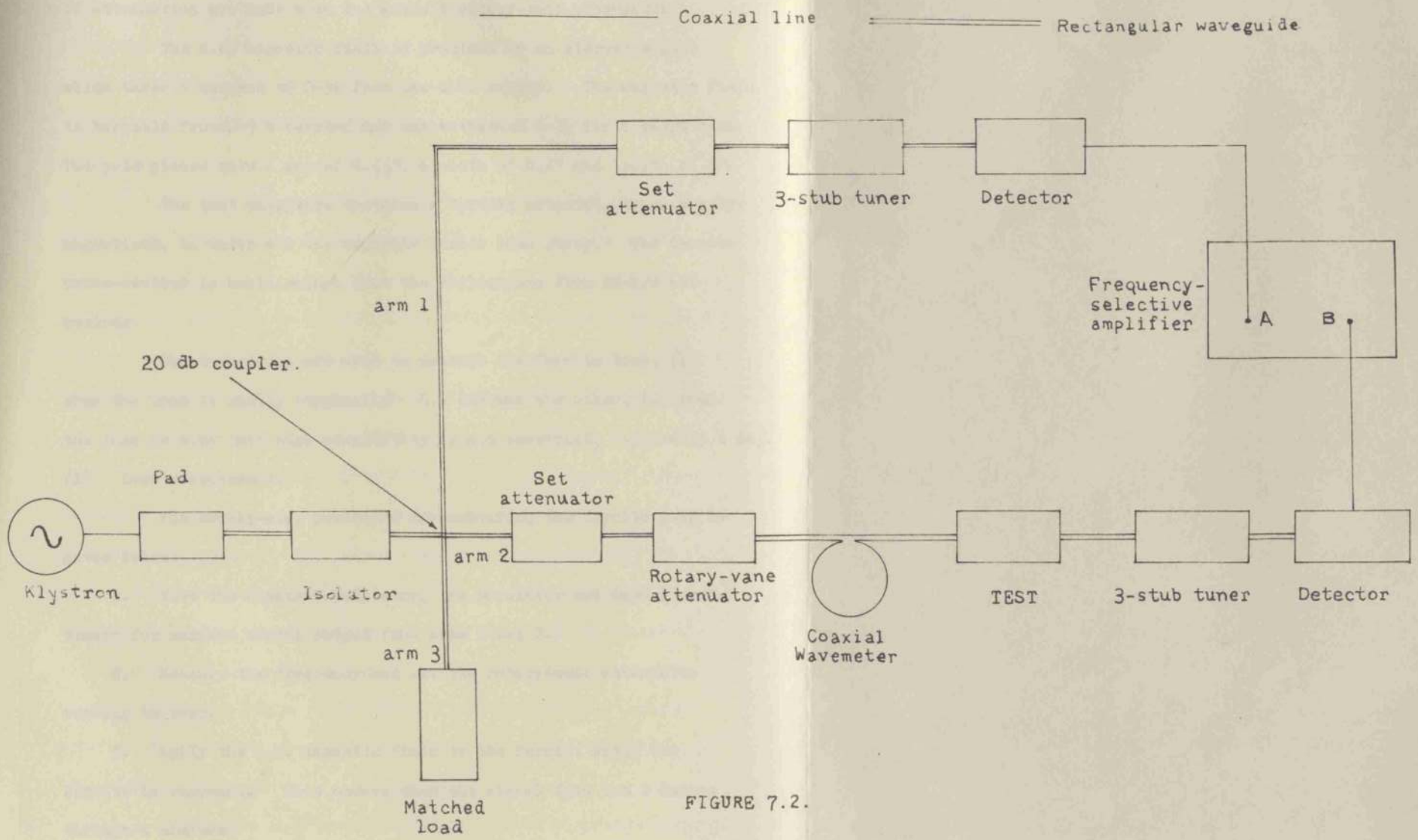
Coaxial line
Rectangular waveguide
Set attenuator
3-stub tuner
Detector
Frequency-selective amplifier
A
B
arm 1
20 db coupler.
Pad
Set attenuator
arm 2
Klystron
Isolator
Rotary-vane attenuator
Coaxial Wavemeter
TEST
3-stub tuner
Detector
arm 3
Matched load

FIGURE 7.2.

wavemeter, calibrated from 8 - 12 Gc/s, with a reset accuracy of $\frac{1}{4}$ Mc/s. A 3-stub tuner is used to match the arm at each frequency. All measurements of attenuation are made with the grade 1 rotary-vane attenuator.

The d.c. magnetic field is provided by an electro-magnet which takes a current of 0-5A from the d.c. supply. The magnetic field is variable from 0-5 k oersted and can withstand 6-7A for a short time. The pole pieces have a gap of 0.55", a width of 0.4" and length of 4".

The test waveguide contains a ferrite material, transversely-magnetised, in which all the magnetic losses take place. The ferrite cross-section is small enough that the reflections from it are not serious.

Two techniques are used to measure the ferrite loss, (1) when the loss is small, (typically 0.5 db) and the other, (2) when the loss is such that high sensitivity is not essential, (typically 1 db).

(1) Loss measurement.

The step-by-step procedure for measuring the ferrite loss is given below:

1. Tune the klystron reflector, the modulator and both 3-stub tuners for maximum signal output from arms 1 and 2.

2. Measure the frequency and set the rotary-vane attenuator reading to zero.

3. Apply the d.c. magnetic field to the ferrite until the ferrite is resonant. This occurs when the signal from arm 2 passes through a minimum.

4. Using opposite polarity crystals in the two detectors, switch the selective amplifier in the set-level attenuators in arem 1 and 2.

5. Remove the applied d.c. field and wind in the rotary-vane attenuator until the pointer again passes through a minimum.

6. Read the attenuator setting and reset to zero.

7. Reverse the direction of the d.c. magnetic field and repeat steps 3 - 6.

The two readings obtained on the attenuator in step 6 are the forward and reverse loss in the ferrite, F, and R, resepctively. By this method, attenuations of 0.03 db can be detected. This facility is necessary when trying to measure losses in the region 0.10 - 0.50 db. High accuracies could be obtained if the null found in step 4 could be brought nearer zero. This would make theswing in the number of scale divisions for a small change in attenuation, much larger. The limitation in how near to noise level the null can be set, is imposed by the summing network in the selective amplifier. Howevern the two outputs from arms 1 and 2 can be fed into a coaxial tee junction and the signal in the third arm sent into input A or B of the selective amplifier. In this way, attenuations of 0.01 db can be detected, and a change in attenuation of 0.1. db made to correspond to 100 scale divisions.

When the losses to be measured are greater than 1 db, an alternative procedure is used which is less sensitive than (1).

(2) Loss Measurement.

This method is commonly used in practice to measure losses in ferrites. The step-by-step procedure is given as follows:-

1. Tune the klystron, modulator and both 3-stub tuners for maximum signal in arm 2.

2. Measure the frequency and set the rotary-vane setting to zero.

3. Apply the d.c. magnetic field to the ferrite until the ferrite is resonant.

4. Adjust the setting on the selective amplifier until the pointer reads 50 scale divisions.

5. Remove the applied d.c. field and wind in the rotary-vane attenuator until the pointer again reads 50 scale divisions.

6. Read the setting on the rotary-vane attenuator and reset to zero.

7. Reverse the direction of the d.c. matnetic field and repeat steps 3 - 6.

The two readings obtained in step 6 are the forward and reverse losses in the ferrite. By this method, an attenuation of 5 db can be measured to within $\pm$ 0.1 db. The dielectric slab loaded rectangular waveguide considered in sections 3 and 6.2. has been shown to have the required characteristics for a structure to be used in conjunction with a ferrite as a broadband ferrite resonance isolator, viz., a magnetic field which is almost circularly polarised over the band and a high field strength in the ferrite position. The next higher order mode, H_{02}, can be shown to propagate in the upper half of X band for all the loadings considered in section 3. It was decided to carry out an experiment to determine how the magnetic field polarisation behaves with frequency. For this purpose, a magnetic field probe is required. A small sphere

of Yttrium-Iron Garnet (YIG) was chosen as the probe because (a) a spherical shape is necessary to ensure that the fields inside the ferrite are uniform, (b), the cross-section of the sample must be small compared with the guide cross-section to reduce the initial field perturbation and (c) the loss in the smaple must be large enough to measure. The last reason, (c), follows because the ferrite loss depende on the saturation magnetisation of the ferrite and the resonance linewidth, ΔH.A polycrystalline YIG material having a linewidth of 55 oersteds and $4\pi M$ of 1750 oersteds was chosen. Most ordinary ferrite materials have linewidths much in excess of the YIG linewidth, and are therefore unsuitable. The single crystal YIG has narrower linewidth than the polycrystalline material (typically 5 oersted) but also has a preferred axis of magnetisation and anisotropic internal fields which affect the uniformity of the internal r.f. fields. These factors as such as to debar the use of single crystal material. An indication of the amount of loss to be expected in the polycrystalline sphere is given in section 8.1. The loss calculated for the dielectric configuration in Fig. was calculated to be 1.23 db in the reverse direction at 10 Gc/s, when the ferrite properties are as given in section 8.1. The forward loss is calculated to be less than 0.01 db. It would be possible to use more than one YIG sphere so that the ferrite diameter could be reduced to give less perturbation. However, since the loss in the YIG depends on its volume, a reduction in the ferrite diameter by a factor of 2, for the same loss, could only be achieved by using 8 ferrite spheres. Obviously some compromise has to be made,and it was decided to use a YIG sphere of diameter 0.050".

When the ferrite is biassed to resonance,it absorbs the component of r.f. magnetic field which is circularly polarised in the same sense as the ferrite electron precession. This component is called the positive wave. The negative wave,i.e. the component of circularly polarised field which rotates in the opposite direction to the ferrite precession, is unattenuated. Also, if the r.f. field is elliptically polarised, both forward and reverse losses are non-zero and the ratio of the two is small if the ellipticity of the r.f. field is small. In this way, the ferrite is used as a probe for detecting circular polarisation of an r.f. magnetic field.

The ferrite YIG material supplied by Microwave Chemicals, was ground into a spherical shape by a carborundum powder. The YIG was first cut into approximately cubic shape and the frinding done in a cylindrical metal box. The cubes were circulated by a jet of air blown in tangientially through a hole in the rim of the box. By this method, it was possible to make spheres of diameter 0.02" - 0.08".

The dielectric slab loaded waveguide shown in Fig.6.2. was assembled with a small YIG sphere placed against the dielectric face. The dielectric, Stycast HiK, of permittivity 12, thickness 0.12" and height 0.40" was provided with 3-step Tchebyscheff quarter-wave matching transformers[35] at either end. The matching sections to rectangular waveguide ensure that the standing-wave ratio does not exceed 1.14 over the frequency band, (8 - 12 Gc/s). The dielectric slab was supported in the centre of the waveguide by two polyzote sections. In one of the polyzote slabs, the YIG sphere was placed contiguous with the dielectric. Polyzote

has a very low microwave loss and permittivity close to unity and consequently does not interfer in the measurement.

Experimental results are given in Fig.7.3. of the maximised forward and reverse loss in the ferrite as a function of frequency. The theoretical reverse loss is included for the purposes of comparison. The reverse loss, as indicated by equation 8.1.14. increase with frequency, the theoretical and experimental values agreeing well. The forward loss is low throughout the measured band, indicating that near circular polarisation of the r.f. magnetic field exists in the ferrite over the frequency range. However, the forward loss predicted by the theory is significantly less than the experimental. One cause for this effect is that the presence of the ferrite at the dielectric interface produces a perturbation of the original field configuration. The pertuebation, assumed to be small, has a much larger relative effect on the forward loss than on the reverse loss because the forward loss is very small. Also, irregularities in the spherical shape of the ferrite cause a distortion of the fields, setting up an elliptically polarised wave. The positive component of this wave couples to the ferrite electron precession and suffers absorption. At a frequency of 11.5 Gc/s, an absorption effect was observed in the forward direction different from that at lower frequencies. As the magnetic field was increased from zero, the ferrite began to absorb energy immediately. The loss increased to a value of 3db at a d.c. field of 5 k oersted. No resonance effect was noticed. Two loss peaks were observed with the d.c. field in the reverse direction which were of the same order of magnitude - 4db. It was presumed

FIGURE 7.3.

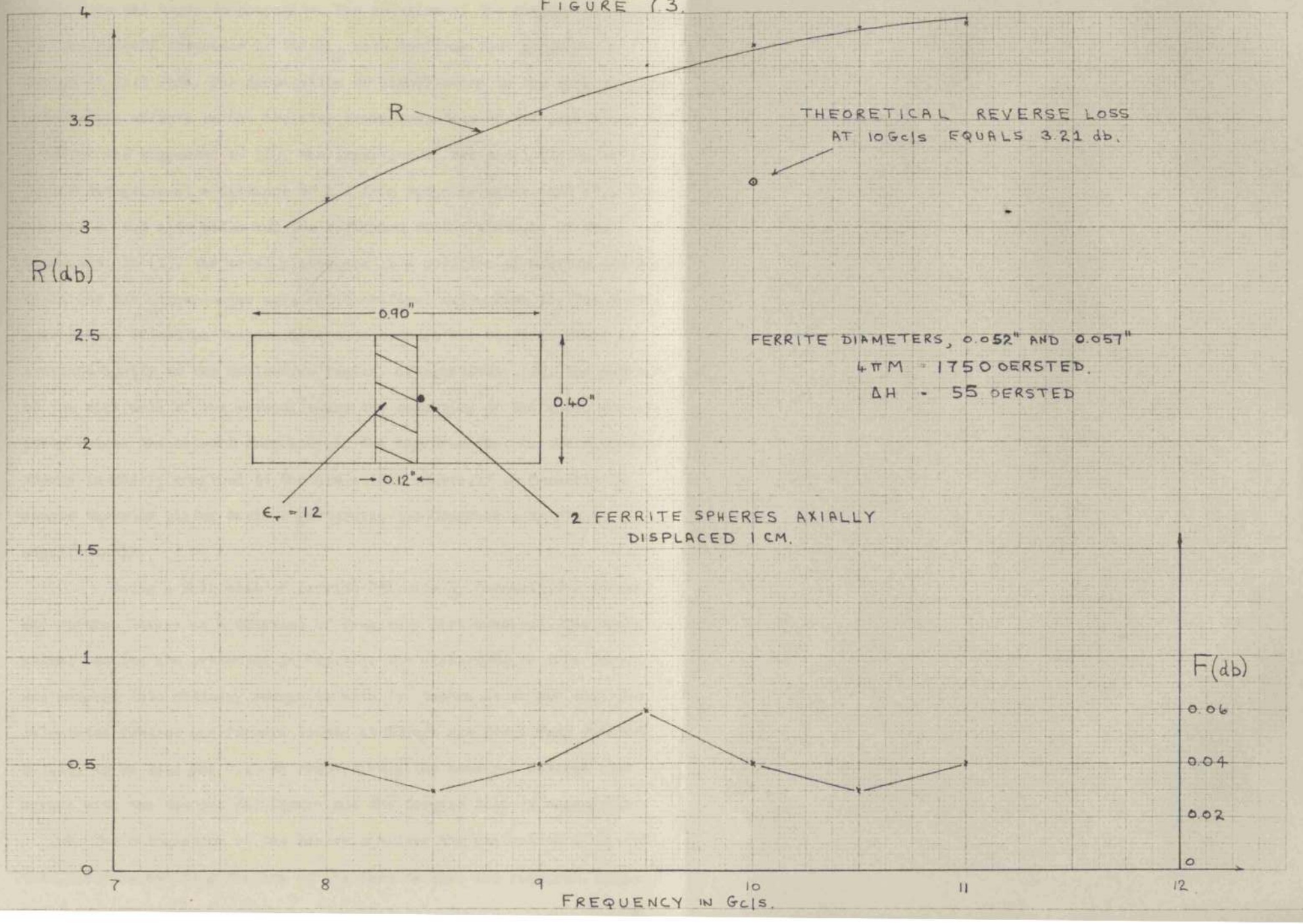
R
THEORETICAL REVERSE LOSS
AT 10Gc/s EQUALS 3.21 db.
R(db)
0.90"
0.40"
0.12"
ϵ_r = 12
2 FERRITE SPHERES AXIALLY
DISPLACED 1 CM.
FERRITE DIAMETERS, 0.052" AND 0.057"
4πM = 1750 OERSTED.
ΔH = 55 OERSTED
F(db)
0.06
0.04
0.02
0
4
3.5
3
2.5
2
1.5
1
0.5
0
7
8
9
10
11
12
FREQUENCY IN Gc/s.

that the loaded waveguide was 'multi-moding',i.e. that the next higher-order mode had begun to propagate. The solution of the dispersion equation for the cut-off frequency of the H_{02} mode confirms that propagation begins at 11.3 Gc/s. The propagation of higher-modes in the structure has undesirable effects on the isolator characteristics of the structure. Two remedies are suggested :- (1), the insertion of two metal plates in the loaded waveguide at a distance of A/4 from the side walls, and (2), the removal of the side walls and the reduction of the width,A, of the waveguide. In (1), the metal plates are in a position of maximum electric field for the higher-order mode and,therefore, extinguish it. The plates have little effect on the dominant mode because the electric field is confined mostly to the dielectric region. Alternatively,(2), the removal of the side wall of the waveguide and the reduction of the width effectively raises the cut-off frequency of the higher-modes. As the microwave energy is mainly confined to the dielectric region,it is feasible to remove the side plates without perturning the dominant mode fields significantly.

Using a thin slab of ferrite F5X,made by Ferranti,the forward and reverse losses as a function of frequency were measured. The experimental results are presented in Fig.7.4. The dielectric,in this case, was matched into ordinary waveguide with $7\frac{1}{2}^{o}$ tapers at either end. The calculated reverse and forward losses at 10Gc/s are found from equation 8.1.14. to be 24.4 and 0.45 db respectively.The measured reverse loss agrees with the theoretical figure but the forward loss is measured at 2db. The calculation of the losses involves the evaluation of ς.For this,the demagnetising factors of the ferrite slab are required. Since

FIGURE 7.4.

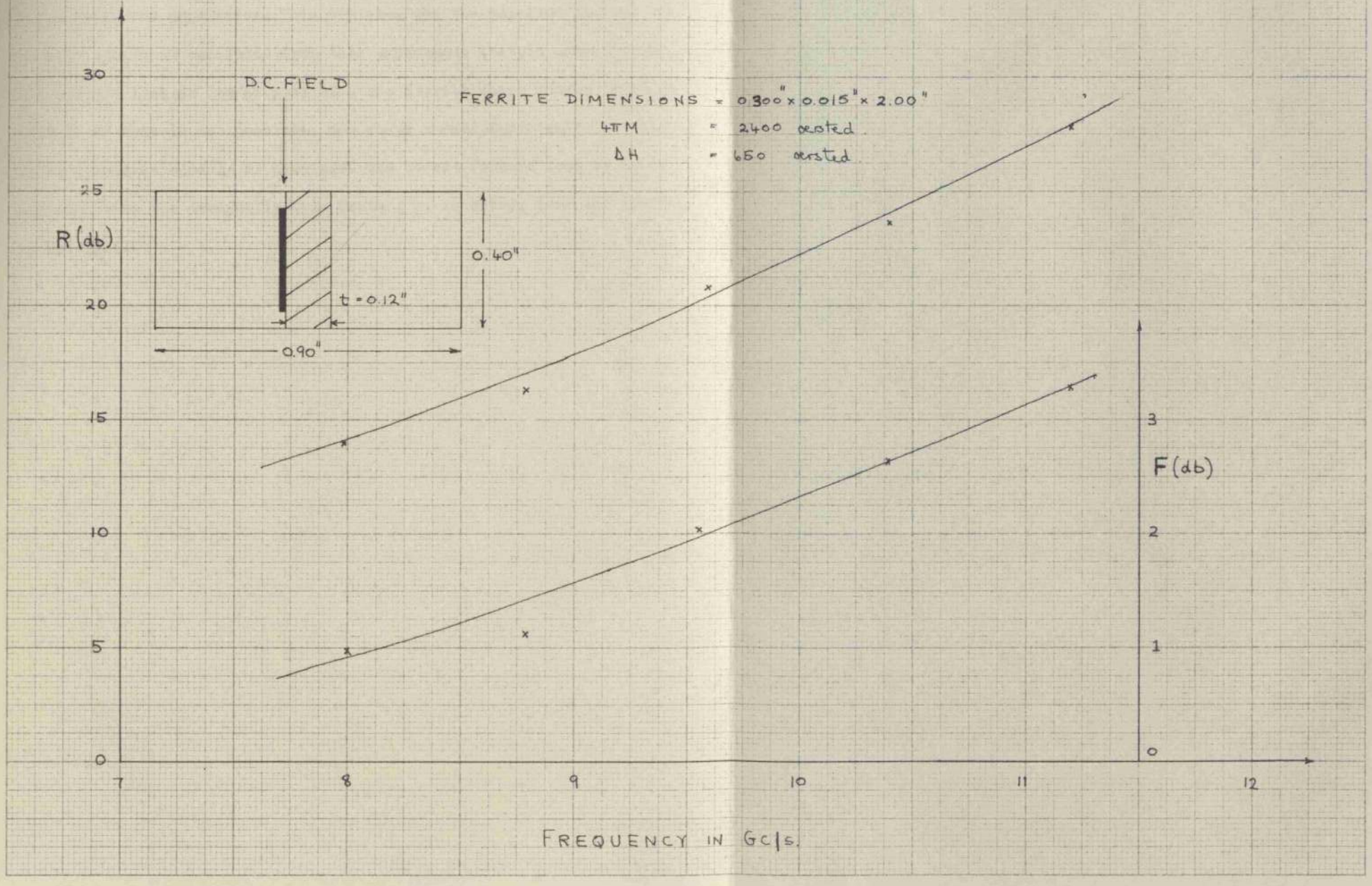
D.C. FIELD
FERRITE DIMENSIONS = 0.300" × 0.015" × 2.00"
4πM = 2400 oersted
ΔH = 650 oersted
0.40"
t = 0.12"
0.90"
R (db)
F (db)
30
25
20
15
10
5
0
3
2
1
0
7
8
9
10
11
12
FREQUENCY IN GC/S.

the ferrite shape is not ellipsoidal, it is not stricly true to say that the demagnetising factors have any meaning because the fields in the ferrite are non-uniform.This explains why the measured forward loss is high and it is concluded from this experiment that,in order to keep the forward loss as low as possible, the ferrite shape should be ellipsoidal. If this is not possible, the shape should approximate to that of an ellipsoid as closely as possible. The lowest forward loss is to be expected when the demagnetisation factor, ς, is unity, i.e. the ferrite is spherical.

Ridged waveguide.

The measurement of magnetic field polarisation in the ridged waveguide by means of a ferrite slab, is described in this section. The method used in measuring the forward and reverse losses in the ferrite is identical with that used in the case of the dielectric loaded waveguide and described at the beginning of section 7.2. In this case, however, the ferrite has a rectangular cross-section and a long axial length. This choice of ferrite is made rather than the spherical sample because the fields are weak at the position of the ferrite and a substantial volume of ferrite is required to produce a measureable loss. The slab was positioned on the top waveguide wall where the fields are calculated to be circularly polarised. Three locations were tried ; D = 0.13", 0.15", 0.17". D is the distance of the ferrite centre plane from the side wall. The corresponding frequencies of circular polarisation at the centre plane are calculated by the methods described in 5.7. to be:- f = 9.8 Gc/s, 8.5 Gc/s and 7.1 Gc/s respectively. The maximised reverse and forward losses for these three cases are plotted in Fig.7.5. as a function of frequency.

The forward losses pass through minima at frequencies close to those given above. The forward losses do not become zero at the centre frequency because the polarisation is only circular at one section of the ferrite and becomes more elliptical further away from this section. An averaging effect takes place over the ferrite cross-section which results in a non-zero forward loss. On either side of

FERRITE DIMENSIONS, 0.100" × 2.75" × 0.0 "

$4\pi M$ = 2400 oersted

ΔH = 650 oersted

FIGURE 7.5

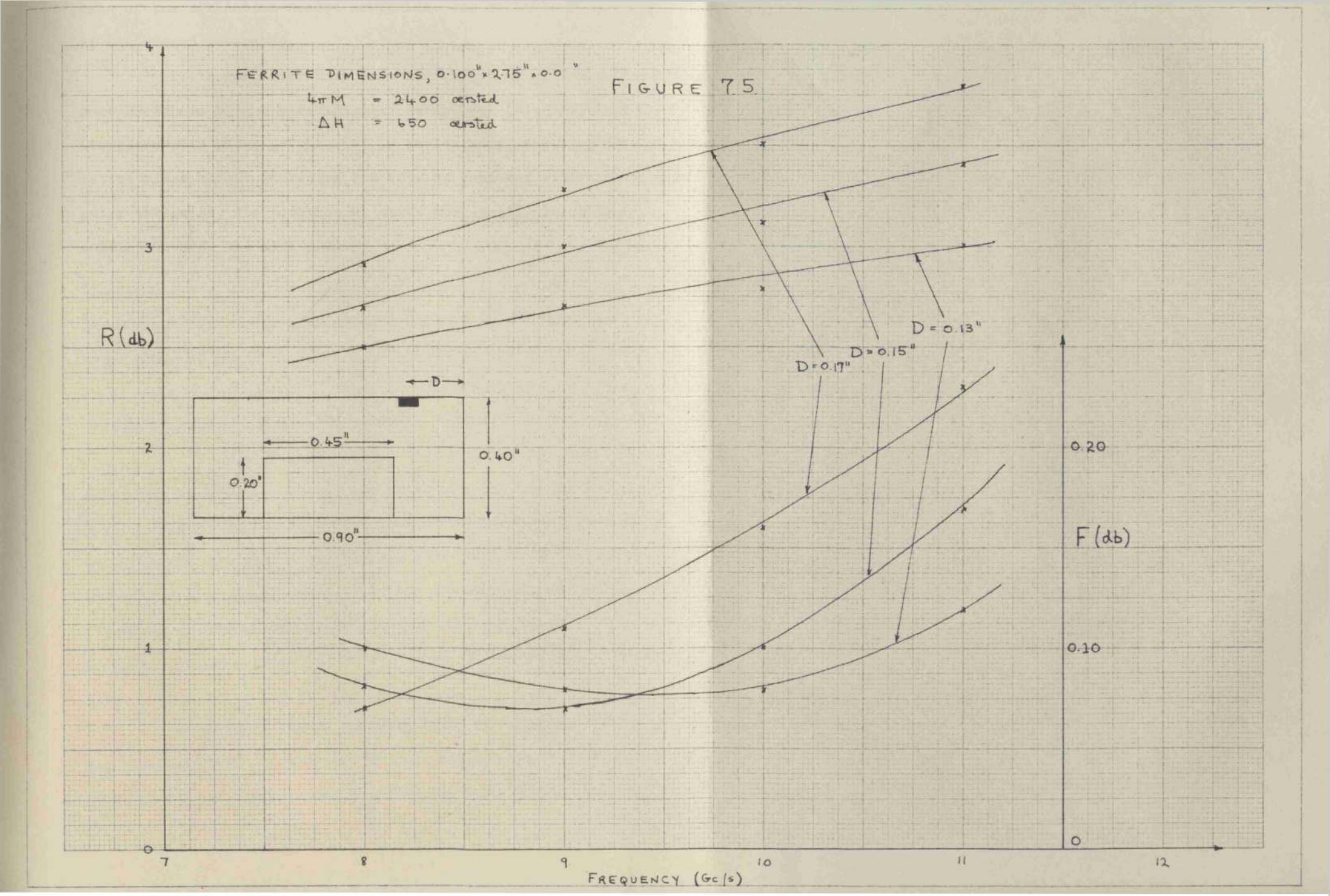

case of the dielectric loaded waveguide, and in Table 5. . in the case of the ridged waveguide.

It is concluded that (a), the ridged waveguide is inherently more broadband than the rectangular waveguide, (b), the bandwidth increases with ridge height, (c), P varies more sharply with position as the ridge height increases and (d), as compared with the rectangular waveguide, the position at which $P(x_0,y_0,f_0)$ is unity, is shifted towards the side wall.

7.3. Insertion loss measurement.

A loss occurs when a dielectric is placed in a waveguide which may be due to (a) reflections caused by a mismatch or (b),an absorption in the dielectric. This loss is called the insertion loss. In resonance isolators,the insertion loss is usually classed as part of the forward loss and for this reason, it is necessary to reduce the insertion loss as far as possible. By using a dielectric of small cross-section and low loss,it is relatively simple to produce a good match and low insertion loss. However, in the dielectric loaded rectangular waveguide discussed in sections 3 and 6.2., the dielectric has full guide height and large cross-sectional area. Two methods have been used to match the loaded guide to the air section, (1), tapering of the dielectric and (2), using stepped transformer sections. It has been found that the latter method gives,by far, the best results. It has been shown by Cohn[35] that, for a given bandwidth, the minimum standing-wave ratio over the band is achieved by using a matching section with a Tchebyscheff response. Following Parkes and Sullivan[36], a 3section transformer has been built to cover a bandwidth of 40% centred at 10 Gc/s with a maximum standing-wave ratio of 1.07. A drawing of the transformer is made in Fig.7.6. together with a block diagram of the experimental arrangement used to measure the insertion loss.

The klystron source,operating CW in the frequency range 7 - 12 Gc/s, and modulated at 3.2.kc/s, is protected by an isolator and piston attenuator which is also used to control the level of the output power.

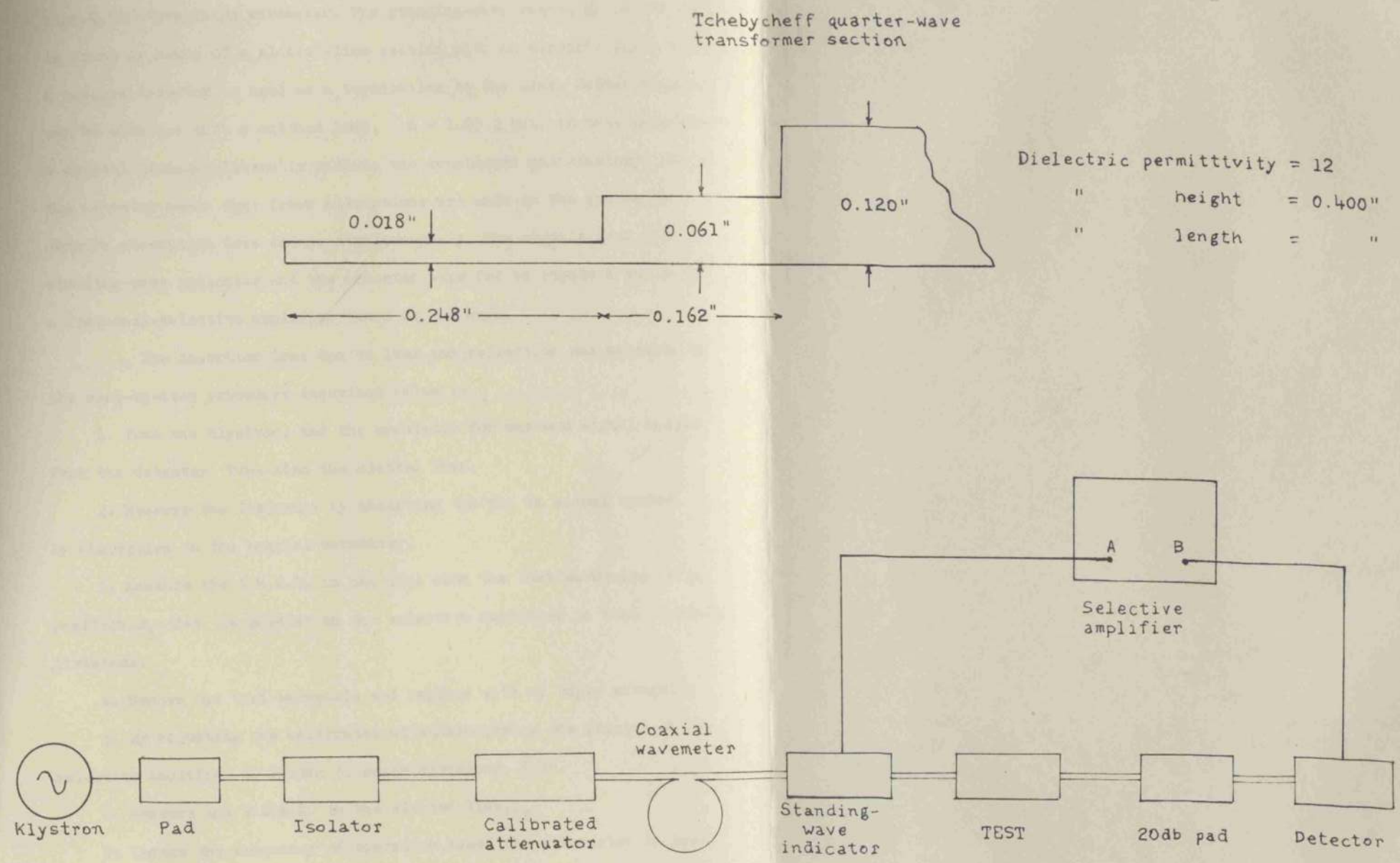
Tchebycheff quarter-wave transformer section
0.018"
0.061"
0.120"
0.248"
0.162"
Dielectric permitttvity = 12
" height = 0.400"
" length = "
A
B
Selective amplifier
Coaxial wavemeter
Klystron
Pad
Isolator
Calibrated attenuator
Standing-wave indicator
TEST
20db pad
Detector

FIGURE 7.6.

The frequency at which the measurement took place was measured with a high-Q,high-precision wavemeter. The standing-wave ratio, S, in the line is found by means of a slotted-line section with an electric field probe A matched detector is used as a termination to the line. Better accuracy can be obtained with a matched load, (S = 1.03) but, in this experiment a crystal detector,liberally padded, was considered satisfactory. Use of the detector means that fewer alterations are made to the system to measure absorption loss and S. simultaneously. The signals from the standing-wave indicator and the detector were fed to inputs A and B of a frequency-selective amplifier tuned at 3.2 kc/s.

The insertion loss due to loss and reflection was measured by the step-by-step procedure described below :-

1. Tune the klystron, and the modulator for maximum signal output from the detector. Tune also the slotted line.

2. Measure the frequency by observing the dip in signal caused by absorption in the coaxial wavemeter.

3. Measure the V.S.W.R. in the line when the test waveguide is in position,S_1. Set the pointer on the selective amplifier to read 50 scale divisions.

4. Remove the test waveguide and replace with an empty waveguide.

5. By adjusting the calibrated attenuator,bring the pointer on the selective amplifier to reread 50 scale divisions, L db.

6. Measure the V.S.W.R. in the slotted line,S_2.

7. Change the frequency of operation,reset the attenuator to zero and repeat steps 2-6.

The attenuator reading, L db, is the total loss in the test waveguide due to reflection and absorption. The reflected portion of the measured loss can be found by calculating, from the V.S.W.R., the reflected loss. When the test waveguide is matched, ($S < 1.20$), the loss due to reflection is neglected in comparison with the absorption loss.

A comparison is made in Fig.7.7. between the measured absorption loss and the loss calculated in section 8.2. The V.S.W.R. due to the dielectric loading is drawn on the same Figure. The insertion loss in the loaded waveguide considered is typically 0.3 db, which is rather high. This is one of the reasons why the dielectric loaded ridged waveguide is used in isolator applications because the dielectric cross-sectional area is reduced and, consequently, the insertion loss is lower.

FIGURE 7.7.

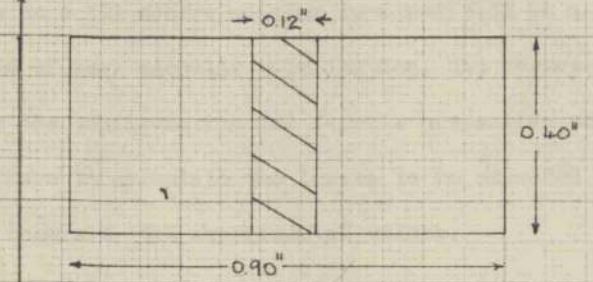

DIELECTRIC ϵ_r = 12

" tan δ ~ 0.002

EXPERIMENTAL

THEORETICAL

L (db)

0.5

0.4

0.3

0.2

0.1

0.0

V.S.W.R.

1.20

1.10

1.00

7 8 9 10 11 12

FREQUENCY (Gc/s)

8. Loss Calculations.

8.1. Ferrite Magnetic Loss.

In the experiment described fully in section 7.2. to measure the loss in a YIG sphere sitting in a position in a dielectric loaded waveguide of near circular polarisation, the reverse loss is typically 2 db for the configuration and ferrite properties considered. An attempt is made here to calculate the losses to be expected in the system and to compare them with the experimental values.

The loss occuring in a ferrite medium are of two kinds - those due to the finite conductivity of the ferrite, (dielectric loss) and those entirely due to energy transfer from the travelling wave to the electron spin precession (magnetic loss). For the small samples of ferrite usually used in waveguides the latter loss is the more significant especially as the dielectric loss tangent of the ferrite is small. The resonance loss in a small ferrite sphere is calculated below by means of the Poynting vector theorem:-

Maxwell's equations written for a ferrite medium are

$$\nabla \times \underline{E} = -j \underline{B} \omega = -j\omega(\mu_o \underline{H} + \underline{M}) \qquad 8.1.1.$$

$$\times \underline{H} = j \underline{D} \omega = j\omega\varepsilon \underline{E} + \sigma \underline{E} \qquad 8.1.2.$$

The complex Poynting vector is given by:-

$$2\nabla.(\underline{E} \times \underline{H}^*) = -\sigma|E|^2 + j(\varepsilon|E|^2 - \mu_o|H|^2) - j\omega(\underline{M}.\underline{H}^*) \qquad 8.1.3.$$

The power dissipated in the ferrite medium due entirely to the magnetic loss is given by:-

$$P_{dis} = + \tfrac{1}{2}\omega \mathrm{Re} \int_V j \underline{M}.\underline{H} \cdot dV. \qquad 8.1.4.$$

where V is the ferrite volume.

Assuming that the fields are uniform and unperturbed over the ferrite sample, the magnetic loss becomes

$$P_{dis} = \tfrac{1}{2}\omega V. \mathrm{Re} \ (j\underline{M}.\underline{H}) \qquad 8.1.5.$$

The magnetisation vector and the internal field in the ferrite are related through the Landau-Lifshitz equation,

$$\frac{dM}{dt} = - |\gamma| \ (M \ X \ H) + \frac{\alpha}{M} \ (M \ X \ \frac{dM}{dt}) \qquad 8.1.6.$$

where γ is the gyromagnetic ratio (= 2.8 Mc/s/oersted) and α is a parameter determining the magnitude of the damping action. Since we assume that the d.c. magnetic filed acts in the z-direction and the r.f. field in the xy-plane, the magnetisation vector and the internal magnetic field in the ferrite may be written down:-

$$\underline{M} = M_o \underline{u}_z + m_x \underline{u}_x + m_y \underline{u}_y \qquad 8.1.7.$$

$$\underline{H} = (H_o - N_z \frac{M_o}{\mu_o}) \underline{u}_z + (h_x - N_x \frac{m_x}{\mu_o}) \underline{u}_x + (h_y - N_y \frac{m_y}{\mu_o}) \underline{u}_y \qquad 8.1.8.$$

where $\underline{u}_x$, $\underline{u}_y$, $\underline{u}_z$ are unit vectors in the x,y and z directions respectively. N_x, N_y, N_z are the ferrite demagnetising factors.

By substituting equation 8.1.8. in equation 8.1.6. and re-arranging, we obtain the following expressions for m_x and m_y.

$$m_x = \frac{\omega_M (\omega_o \S h_x + j\omega h_y)}{\omega + \omega_o (\omega_o - \omega + \frac{1}{2} j|\gamma| \Delta H)} \qquad 8.1.9.$$

$$m_y = \frac{\omega_M (-j\omega h_x + \omega_o/\varrho \cdot h_y)}{\omega + \omega_o (\omega_o - \omega + \tfrac{1}{2} j|\gamma| \Delta H)} \qquad 8.1.10.$$

where ΔH is the ferromagnetic linewidth.

$$\varrho^2 = \frac{H_o + (N_y - N_z) \frac{M_o}{\mu_o}}{H_o + (N_x - N_z) \frac{M_o}{\mu_o}} \qquad 8.1.11$$

and ω_o is the Kittel resonance frequency defined by :-

$$\omega_o^2 = |\gamma|^2 (H_o + (N_x - N_z) \frac{M_o}{\mu_o})(H_o + (N_y - N_z) \frac{M_o}{\mu_o}) \qquad 8.1.12.$$

$$\omega_M = |\gamma| \frac{M_o}{\mu_o} \qquad 8.1.13.$$

$$j . (M.H^*) = j (m_x h_x^* + m_y h_y^*) \qquad 8.1.14.$$

$$M.H^* = \frac{\omega_M (\omega_o \varrho |h_x|^2 + \omega_o/\varrho \cdot |h_y^2| + j\omega (h_y h_x^* - h_y^* h_x)}{(\omega + \omega_o) (\omega_o - \omega + \tfrac{1}{2} j|\gamma| \Delta H)} \qquad 8.1.15.$$

The expression for the power dissipated in the ferrite can now be evaluated by means of equations 8.1.5. and 8.1.15.

$$P_{dis} = \tfrac{1}{2} \omega V \frac{M}{\omega + \omega_o} \cdot \frac{\tfrac{1}{2}|\gamma| \Delta H}{(\omega_o - \omega)^2 + (\tfrac{1}{2}|\gamma|\Delta H)^2} \left\{ \omega_o (\varrho |h_x|^2 + \frac{1}{\varrho} |h_y|^2) \pm 2\omega |h_x h_y| \right\} \qquad 8.1.16$$

At resonance, $\omega = \omega_o$ and the dissipated power is :-

$$P_{dis} = \tfrac{1}{2} \omega V (\frac{M_o}{\mu_o \Delta H}) \left\{ \varrho |h_x^2| + \frac{1}{\varrho} |h_y^2| \pm 2 |h_x h_y| \right\} \qquad 8.1.17.$$

The power flow in a rectangular waveguide propagating the dominant H-mode is

$$P = \frac{AB}{4}\left(\frac{\omega\mu_o}{\beta}\right) h^2 \qquad 8.1.18$$

where h is the amplitude of the h_x component.

Therefore

$$\frac{P_{dis}}{P} = 2\frac{V\beta}{AB}\left(\frac{M_o}{\mu_o \Delta H}\right) \sin^2\frac{\pi a}{A}\left(\varsigma + \frac{1}{\varsigma} X^2 \pm 2X\right) \qquad 8.1.19.$$

where $X = \frac{h_y}{h_x}$

The power flow in the dielectric loaded waveguide is given by equation 3.3.6.

$$P = \frac{bA}{2}\left(\frac{\mu_o}{\epsilon_o}\right)^{\frac{1}{2}} H_x / g^2 \qquad 8.1.20.$$

where g has already been computed and H_x is the value of the transverse magnetic field at the dielectric wall. Combining equations 8.1.17. and 8.1.20., we have the ratio between the power dissipated in the ferrite and the total power flow:

$$\frac{P_{dis}}{P} = \frac{\omega A}{c} \cdot \frac{V}{A^2 B} \cdot \left(\frac{M_o}{\mu_o \Delta H}\right) g^2 \left(\varsigma + \frac{1}{\varsigma} X^2 \pm 2X\right) \qquad 8.1.21.$$

The reverse and forward losses occuring in a small ferrite sphere placed against the dielectric wall in a dielectric loaded rectangular waveguide may be calculated by means of equation 8.1.21.

Sample calculation.

The ferrite properties and dielectric parameters used in the experiment described in section 7.2. are given below:-

Ferrite diameter = 0.057" Dielectric constant = 12

Saturation magnetisation = 1750 oe " thickness = 0.12"

Ferrite linewidth = 55 oe. Frequency = 10 Gc/s.

g, and X are obtained from the results of section 3. For a sphere, ς = 1, since the demagnetising factors are the same in all directions.

The calculated reverse loss = 1.79 db

" " forward " 0.01 db

For ferrite shapes other than spherical, ς may be calculated once the demagnetising factors are known. In cases where the shape is not ellipsoidal, the demagnetising factors are only approximate. The demagnetising factors for several different shapes, e.g. the this disc, long rod, and the this slab, have been given in the literature.[18]

8.2. Dielectric Loss.

The attenuation to be expected by placing a dielectric sample in a rectangular waveguide, is calculated by means of the Poynting vector theorem. The loss derived is due solely to the non-zero concuctivity of the dielectric medium and is called dielectric insertion loss. The power dissipated per unit length of a uniform sample of dielectric, assumed to be matched, is defined as P_d.

$$P_d = \omega e \tan \delta \int_{S_1} |E|^2 \, dS_1 \qquad 8.2.1.$$

where S_1 is the cross-section of the dielectric in the waveguide, and $\tan \delta$ is the dielectric loss tangent.

The total power flow along the waveguide is given by

$$P = \frac{\beta}{\omega \mu} \int_{S_2} |E|^2 \, dS_2 \qquad 8.2.2.$$

where S_2 is the waveguide cross-section.

The loss in the dielectric causes an exponential decrease in the amplitude of the fields in the axial direction, $e^{-\alpha z}$. According to Lamont,

$$2\alpha = \frac{P_d}{P} \qquad 8.2.3.$$

Over a length of dielectric, L, the loss in the dielectric in decibels, is

$$\text{Loss (db)} = 4.34 \left(\frac{\omega A}{c}\right)^2 \mu_r e_r \frac{L}{A} \frac{\pi}{\beta A} \frac{\tan \delta . F}{\pi} \qquad 8.2.4.$$

where A is the rectangular waveguide broad dimension and

$$F = \frac{\int_{S_1} |E|^2 \, dS_1}{\int_{S_2} |E|^2 \, dS_2} \qquad 8.2.5.$$

$\frac{\beta A}{\pi}$ is determined from the dispersion curve at any frequency. The energy factor, F, is found graphically from the electric field distribution over the cross-section.

9.Further applications of the finite-difference method.

9.1.Homogeneous cylindrical waveguides.

So far,the treatment of propagation down waveguides has been restricted to those waveguides which have rectilinear boundaries.However,in practice,the use of waveguides having cylindrical boundaries is also extensive,e.g.,the circular waveguide and the coaxial line. (The coaxial line is treated here as a type of circular waveguide). In both cases,the boundaries of these transmission lines are most conveniently described in cylindrical polar coordinates with the origin on the longitudinal axis of symmetry.

The propagating fields and the cut-off frequencies of the dominant H_{11} mode and other higher-order modes in circular waveguide have been known[37] for some time.This is also true for the TEM mode and higher-order waveguide modes in coaxial line.As an introduction to the topic of the application of finite-difference methods to waveguides having cylindrical boundaries,it is proposed to show how the fields and cut-off wavelength of waveguide modes in a homogeneous circular waveguide are found.A somewhat different procedure is necessary for the dominant TEM mode in coaxial line because the equation satisfied by the field components is not the wave equation but Laplace's equation. The general method is then applied to deal with more complicatde cylindrical waveguides and finally to a section on inhomogeneously-loaded waveguides where conventional analytical methods are very cumbersome

As in the case of the rectilinear waveguide,the electromagnetic fields of the travelling wave may be shown to be derived from

a scalar wave function ϕ which satisfies the two-dimensional wave equation

$$\nabla_t^2 \phi + k^2 \phi = 0 \qquad 9.1.1.$$

The field components are given in the case of H-mode and E-mode propagation by equations 5.1.1. and 5.1.2. respectively. By the finite-difference method, half of the circular waveguide cross-section is subdivided into a number of curvilinear meshes by lines drawn with constant radius, r, and angle, θ, see Fig. 9.1a. The basic finite- difference approximation to the Laplacian operator at any point 0 in the cross-section is given in the literature[38] and quoted here:-

$$h^2 \nabla_t^2 \phi = \phi_1 + \phi_2 + \phi_3\left(1 + \frac{h}{2r_o}\right) + \phi_4\left(1 - \frac{h}{2r_o}\right) - 4\phi_0 = -h^2 k^2 \phi_0 \qquad 9.1.2$$

where h is the mesh length, r_o is the radius from the origin to the point 0, and the points 0-4 refer to the drawing in Figure 9.1b. At each point in the subdivided cross-section, the difference approximation to the wave equation is applied with the boundary conditions incorporated in the equations holding at the points on the waveguide boundary. The 'n' linear equations obtained at the 'n' mesh points are written in the matrix form of equation 5.2.11. In contrast to the case of the homogeneous rectilinear waveguide, the elements of the band matrix are not all integers owing to the presence in the difference equation of the fractional term $\frac{h}{r_o}$ in the coefficients of ϕ_3 and ϕ_4. This fact causes a certain amount of difficulty in the preparation of the matrix data for computation where it is simple and quick to punch all the elements in binary. Non-integer elements must be punched in decimal and

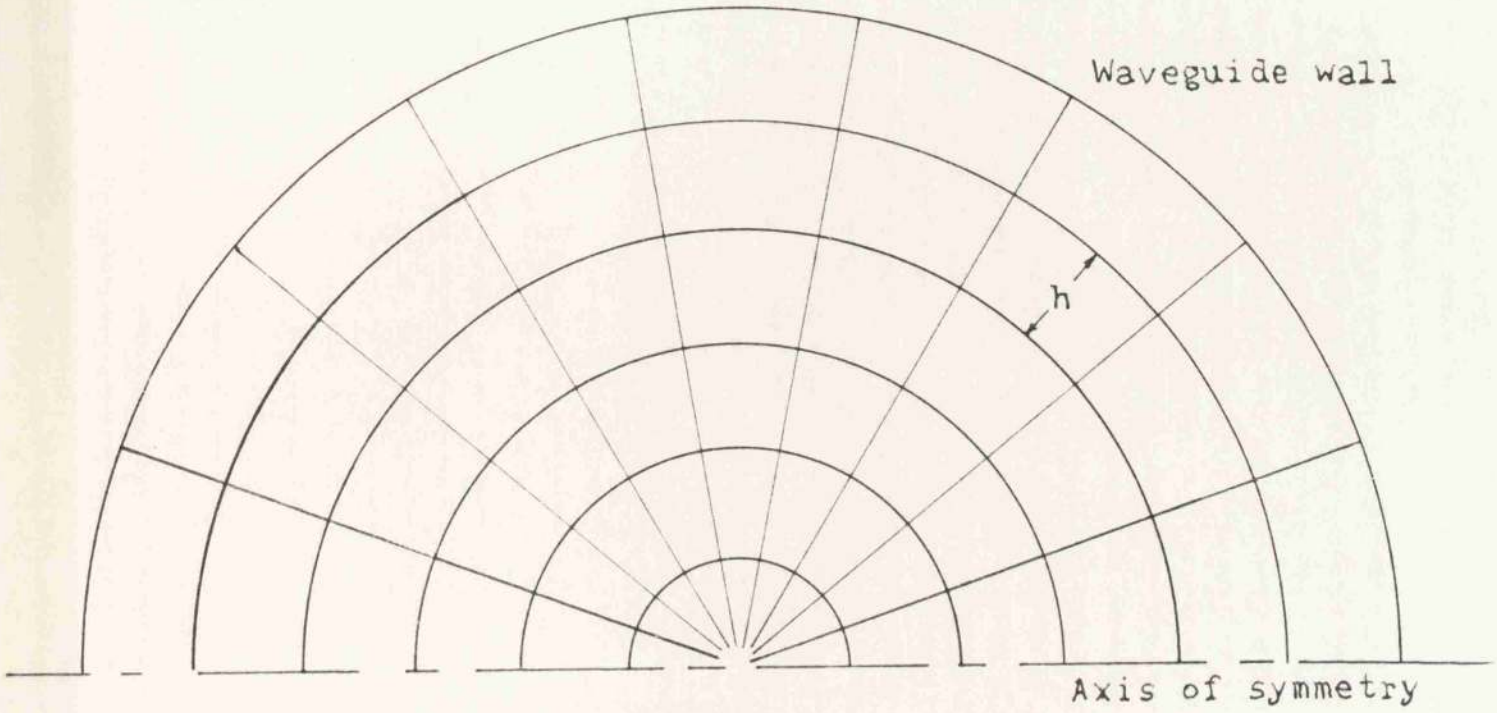

FIGURE 9.1a.

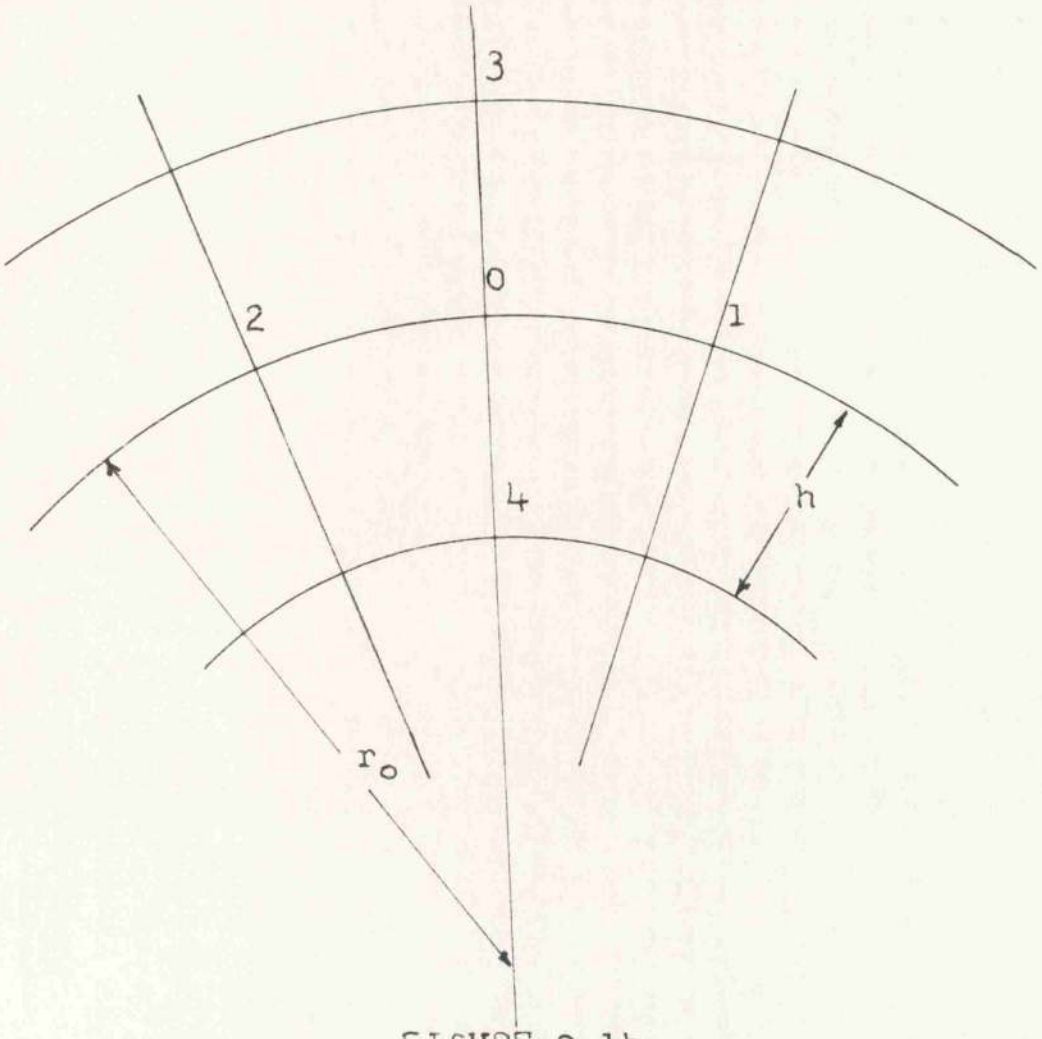

FIGURE 9.1b.

thus,it requires two separate programmes to read the data into the computer.

The solution of the matrix equation gives the cut-off condition and the longitudinal field distribution from which the remaining field components may be derived.When the mode considered is H-type,the longitudinal field is magnetic,and when E-type,the longitudinal field is electric.The type of mode is determined by the boundary conditions on the wave function.Higher-order modes of the system are dealt with as before,by considering the appropriate latent roots and vectors of the matrix.

The coaxial transmission line is treated in the same manner as the circular waveguide,the only difference in the two cases being the extra boundary condition on the inner conductor of the coaxial line.As pointed out earlier,the finite-difference procedure only applies to the waveguide modes of the coaxial line.An alternative method of solution is possible in the case of the coaxial line by transforming the circular boundaries and the wave equation into rectangular co-ordinates and solving the resulting problem by finite-differences.This method will be referred to as the 'transformation' method.Under the conformal transformation

$$y = \log r \quad ; \quad x = \theta$$ (see Fig.9.2.)

the tubular cross-section of the coaxial line transforms into a rectangle.If H-modes are considered,the boundary conditions on the rectangle are known - there are electric walls at $y = 0$ and $y = \log a$, and magnetic walls at $x = 0$ and $x = \pi$. The inner radius of

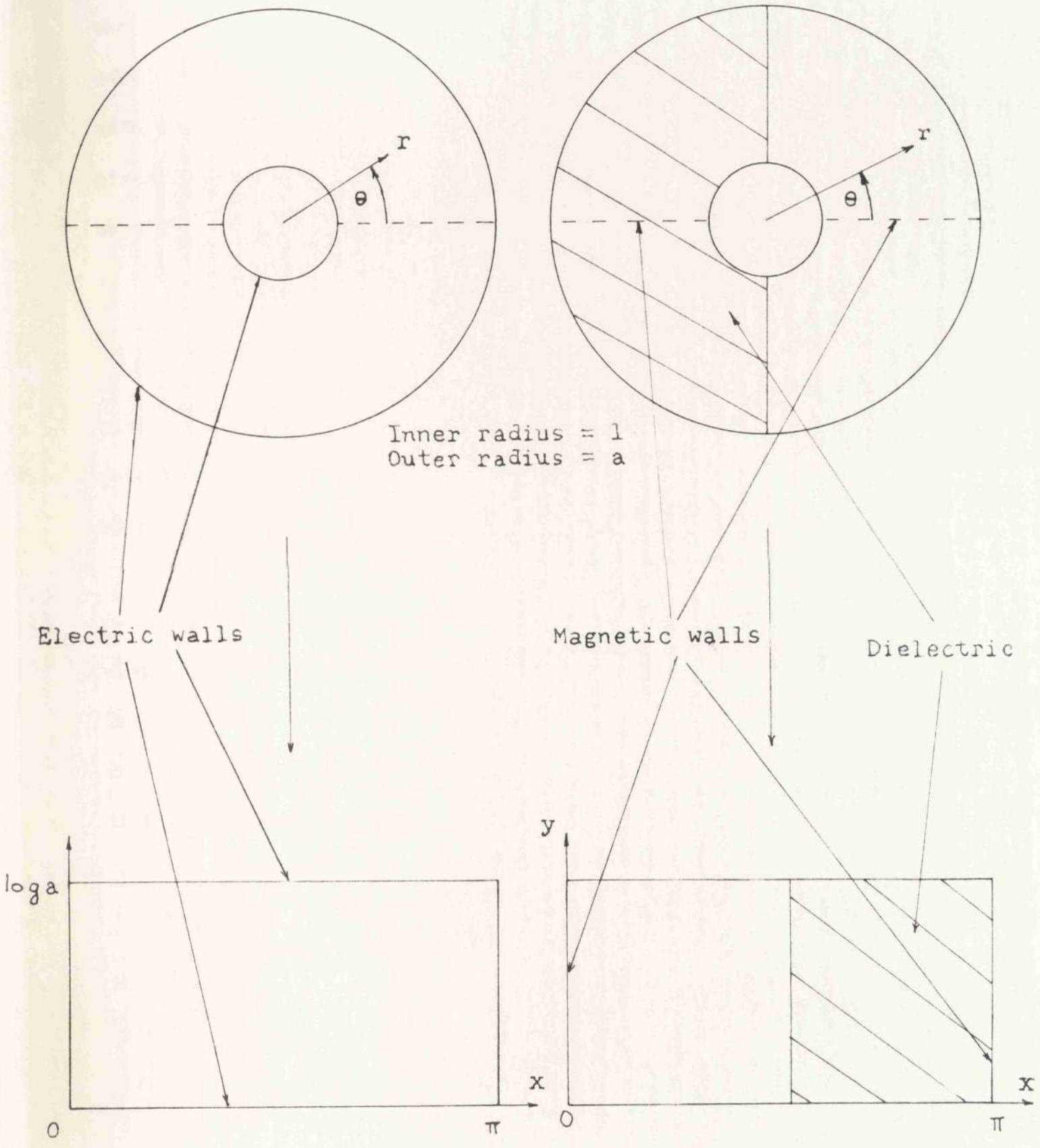

FIGURE 9.2.

FIGURE 9.3.

the coaxial line is normalised to be unity and the plane of symmetry taken at $\theta = 0$ so that the origin of the rectangular axes coincides with a corner of the rectangle.Analagous boundary conditions to those given above hold when the mode considered is E-type.The two-dimensional wave equation transforms into

$$e^{-y^2} (\nabla_t^2 + k^2) \phi = 0 \qquad 9.1.4.$$

In the transformed cross-section,square meshes are drawn which cover the whole region exactly as in the case of the rectangular waveguide.It is advisable to arrange that the width of the rectangle, ,is an integral number of half mesh lengths,h,

$$= \frac{rh}{2} \qquad \text{where r is an integer.}$$

so that,if there is a mesh point at x = 0,there is either a mesh point at $x = \pi$,or two mesh points which straddle the point at $x = \pi$. In this case,the expression of the boundary condition in terms of the function values at the boundary is much simplified.Since a square mesh is normally employed,then

$$\log a = \frac{sh}{2} \qquad \text{where s is an integer.}$$

Consequently,it is preferable to choose the outer radius of the coaxial line to satisfy this equation rather than to deal with an arbitrary radius.This condition on 'a' is not essential but more convenient.

From symmetry conditions on particular modes,it may be possible to consider only one half of the rectangular cross-section,i.e. one quadrant of the coaxial line.The finite-difference representation of

of equation 9.1.4. is simply

$$e^{-y^2}\left(\sum_{1}^{4} \phi - 4\phi_0\right) = -h^2 k^2 \phi_0 \qquad 9.1.5.$$

Applying equations 9.1.5. at each point in the cross-section the matrix formulation of the resulting equations is obtained again. As in the case of the circular waveguide, the elements of the matrix are complicated by the presence of non-integer terms which, in this case arise from the exponential factor in equation 9.1.5.

The cylindrical ridged waveguide has found use, in practice, in the development[38a] of a broadband circular waveguide Faraday rotator. In order to maintain constant rotation of the linearly-polarised electric field, it is desirable to make the axial propagation constant insensitive to change in frequency. For this reason, the ridged waveguide is chosen rather than the empty waveguide. A quantitative idea of the behaviour of the fields and propagation constants are necessary for the design of the broadband rotator. The actual configuration used in reference [38] is not suitable for an analysis by finite-differences because the ridge shape is rectangular. However, the situation most convenient for the difference method, (where the ridge edges lie parallel to r and θ) is similar to the above case.

The direct method of applying the finite-difference equations 9.1.2. to the mesh points in the subdivided cross-section, is used to determine the propagating fields and cut-off frequency of the dominant mode. The only difference in treatment between this structure and the ridged rectangular waveguide is in the derivation of the matrix B. The transformation method described earlier in this section may not be

applied in this case because the transformed cross-section is not rectangular.

9.2. Inhomogeneous cylindrical waveguides.

Attempts [39] to build a resonance isolator in coaxial transmission line has led to the use of unsymmetrical loading of the line with a high-permittivity dielectric. The dominant mode in coaxial line is the well-known TEM mode which has no component of field in the direction of propagation. The transverse magnetic field is linearly-polarised and consequently, there can never be any condition of circular polarisation in the air-filled structure. In order to create a longitudinal component of magnetic field, the region between the two conductors is loaded with a dielectric in one half of the cross-section. The other half remains air-filled. Owing to the disconuity in field caused by the dielectric, an axial component of $\underline{H}$ is set up with the result that the total magnetic field vector is, in general, elliptically polarised. It is surmised from the results of intense dielectric loading in other waveguide structures, that the ellipticity of the magnetic field close to the dielectric-air interface, is small. In order to determine the dependence of circular polarisation on frequency, it is necessary to investigate the propagating fields in the structure. In addition, a knowledge of the wave impedance and the dependence of guide wavelength on frequency is most valuable in determining the design of Tchebyscheff quarter-wave matching sections into the ordinary homogeneous circular waveguide.

As was pointed out in section 6.4., only hybrid modes can

propagate in a wavguide structure which contains a dielectric when there is a dependence of field along the transverse dielectric face. The dielectric loaded ridged circular waveguide is such a structure. By transforming the boundaries of the structure according to equation 9.1.3.,the cross-section becomes that of a dielectric loaded rectangular waveguide,see Fig.9.3. As in the case of the air-filled coaxial line,the wave equation transforms into equation 9.1.4.Since the propagating modes are hybrid,it is not possible to describe the fields by means of a single wave function.Instead,two wave functions are used whose solutions are identified as H_z and E_z respectively.The field expressions are found by combining the separate terms due to H_z and E_z alone.The finite-difference solutions of the wave equations are accomplished in a similar manner to that used in the case of the dielectric loaded ridged rectangular waveguide.The vector,ϕ, in the matrix equation consists of half ϕ_r values and half η_r values.By comparison with a structure propagating only H or E modes,the matrix size needs to be doubled to gain the same degree of accuracy.With the computer programmes available at present,this is a stringent condition on the accuracy of the solution.

When the hybrid mode propagates,all three components of r.f. magnetic field are non-zero.However, since the propagating dominant mode is predominantly H-type,(see the section on the dielectric loaded ridged rectangular waveguide),it may be assumed that the radial component of H,viz.,H_r, is small in comparison to H_z and H_θ.To a first approximation,the fields may be regarded as being elliptically-polarised.

The finite-difference solution may also be found by direct application of equation 9.1.2. together with the relevant modifications at points on the dielectric interface. Just as in the case of the dielectric loaded ridged rectangular waveguide, the normal component of electric field at the interface, E_x, is discontinuous, so is the component E_ϕ in dielectric loaded coaxial line.

The circular waveguide axially-loaded with a dielectric is sometimes used as a reciprocal phase-shifter. The dispersion curve for the dominant mode is useful as the first stage in a perturbation calculation of the curve for a magnetically-saturated ferrite rod. The analysis of the most interesting modes of the structure by finite-differences is carried out by the direct method described for the empty circular waveguide, with modifications of the difference equations at points in the dielectric region and at the interface. In the case of modes having independence of the azimuthal coordinate, θ, the propagating modes are not hybrid and the solution is relatively simple. The transformation method doed not work for circular waveguides since the transformed cross-section is not a bounded rectangular region. Clarricoats has studied a number of the possible propagating modes in the structure and it seems that the finite-difference method has a particular advantage here over other procedures in that all the modes of one type can be considered simultaneously.

9.3. Conclusions.

The finite-difference method described in this thesis, has been applied to propagation in various types of homogeneous and inhomogeneous rectilinear waveguides and the extension of the method

to include cylindrical structures pointed out.In all cases,a matrix equation is derived from the finite-differences representation of the wave equation at mesh points in a bounded waveguide region.As compared with conventional methods of solving propagation problems in waveguides, the finite-difference technique produces the longitudinal electromagnetic field and the transverse wavenumbers in a single matrix operation. It is also possible by finite-differences,to give similar information about the higher-order modes of the system.This is done simultaneously if the requisite computer programmes are available which give all the latent roots and vectors of a matrix.It is pointed out,however,that the computed latent roots and associated vectors diverge further from the physical quantities which they represent as the order of the higher mode increases.This is simply explained by the fact that the fields in the higher-order modes vary more rapidly across the waveguide cross-section than for the dominant mode.As a consequence,the finite-difference representation to the Laplacian becomes less accurate. Detailed information on the higher modes can only be obtained by taking a sufficiently large number of mesh points in the waveguide cross-section.

In a waveguide configuration where any one dimension is small compared with the others,the finite-difference method is unsuitable.As an example of this situation,the case of the dielectric loaded rectangular waveguide is considered where the slab thickness is small comparde with the guide width.Due to the small area of the dielectric section,the proportion of mesh points in it is small. Since the finite-difference method can only be accurate when there

a sufficient number of mesh points in any region to describe the physical situation adequately,it is to be expected that inaccuracies crop up.Subdivision of the mesh length to increase the number of points in the dielectric region leads to large matrices which cannot be dealt with by the computer.Similar difficulties arise in the case of the ridged waveguide when the ridged height is small in comparison with the guide height and also when the ridge height is very close to the guide height.It is concluded that perturbation or variational techniques are most suitable in these situations.

The lack of high-speed large-capacity computers to deal with large matrices is the most important single factor determining the accuracy available with the finite-difference method.In the case of the ridged waveguide,it has only been possible to use a matrix of order 140 which gives the eigenvalue with an error of less than 5%. In the case of the dielectric loaded ridged waveguide where the fields vary more rapidly,it is not expected that the eigenvalue is accurate to less than 10%.

The finite-difference method is capable of dealing with a wide range of problems in the field of microwave propagation.For the most part,it is simple and fast and flexible in that only minor modifications to the general method are necessary to deal with widely-different waveguide configurations.The application of the method to propagation in ferrite-loaded structures has only been investigated in the relatively simple case of H-mode propagation in a ferrite slab loaded rectangular waveguide.

Another more complicated range of problems than hitherto discussed is concerned with microwave devices employing electromagnetic modes that owe their existence to the presence of a magnetised ferrite. These have been partially explored by Seidel[41], Clarricoats[40,42] and Trivelpiece[43] but much work remains to be done. It may well be that finite-difference techniques will find considerable future application in this direction.

10. Conclusions.

The magnetic field polarisation in several waveguide structures has been calculated and the theoretical results compared with experimental values. The ridged waveguide has been shown to be more broadband than the rectangular waveguide as far as frequency is concerned but the positional dependence of the circular polarisation somewhat obscures this effect. Dielectric loading techniques have been shown to improve this situation by creating a region close to the dielectric where the r.f. magnetic field remains substantially circularly polarised throughout a large frequency band. Higher-order modes may be dealt with by techniques which all depend on keeping the cut-off frequency beyond the upper limit of X band.

The measurement of magnetic field polarisation, accomplished by ferrite probes in the waveguide, is made difficult by the necessity of using a ferrite which suffers a measureable loss and at the same time does not perturb the fields appreciably. Moreover, it is also necessary to use a ferrite sample which is ellipsoidal so that the internal fields are uniform. To satisfy these requirements, it is best to employ a spherical ferrite. with a very narrow linewidth. It is possible with present-day garnets, (YIG), to obtain a linewidth of around 40 oersteds with a polycrystalline sample. For the purpose of measuring the magnetic polarisation, the small sphere of narrow linewidth gives satisfactory results although, ideally, it would be preferable to use a material of extremely narrow linewidth.

Employing the methods described in this work for the

determination of the fields and wavenumbers in propagating waveguides, it would be possible to use the results as a basis for the design of a resonance isolator. The large bandwidth requirement of a resonance isolator can be obtained in two ways. Firstly, by using a narrow linewidth material with d.c. field tapering employed to resonate different sections of the ferrite at different frequencies in the band, it is possible to obtain a large reverse-to-forward loss ratio over a large bandwidth. At any single frequency, the portion of the ferrite not at resonance acts as a dielectric . Secondly, the broadband effect can be obtained by using a ferrite of extremely large linewidth with uniform d.c. field biassing in a structure where the circularly polarised r.f. field is insensitive to frequency,e.g., the dielectric loaded waveguide.

The work on magnetic field polarisation in waveguides may be applied to structures other than resonance isolators, e.g. the non-reciprocal phase shifter, where constant rotation of a linearly polarised wave is required over a frequency band. In this case, it is necessary to look for a structure which has a propagation constant independent of frequency. The propagation constant is often difficult to determine due to the complexity of the transcendental equations which naturally occur. In these circumstances, the finite-difference method is extremely useful since, in most cases, the wavenumbers and fields of the dominant mode are simply determined. The longitudinal propagation constant is also of interest in the design of Tchebyscheff matching transformers to the empty waveguide.

11. Appendix.

11. 1. Inversion and Iteration Programme.

The inversion procedure is carried out on the computer (DEUCE) by the standard LVO1 programme on a square matrix whose order is restricted to 83. The output of the inversion, $(B^{-1})_t$, is used as the input for a G.I.P. programme which performs the iteration. G.I.P. uses standard 'bricks' to perform matrix and scalar operations. The use of the bricks is controlled by a set of codewords which are presented below. The number of the brick is given under the 'r' column. The brick operates on matrices stored at 'a' and 'b' and stores the result at 'c'. In this programme, the vector obtained in each iteration is normalised by dividing the vector by the ratio of the root mean squares of the elements of the current vector and the previous vector.

CODEWORDS

No.	a	b	c	r	
0	0	0	16	1	Read inverted matrix, $(B^{-1})_t$.
1	16	0	16	2	Standardise (B^{-1}).
2	16	0	16	3	Transpose matrix (B^{-1}).
3	0	0	10	1	Read guess vector, x_n.
4	16	10	13	5	Multiply - $B^{-1}x_n = x_{n+1}$.
5	10	10	0	4	Form $x_n^2 = k_n^2$.
6	13	13	1	4	Form $x_{n+1}^2 = k_{n+1}^2$.
7	0	0	0	9	Divide k_n^2 by $k_{n+1}^2 = K_n^2$.
8	1	1	10	8	Expand K_n^2 as a 1X1 matrix.
9	10	0	13	10	Form K_n.

10	11	0	0	11	Punch K_n.
11	11	13	10	5	Form $K_n.x_{n+1}$ and replace x_n.
12	10	2	0	13	Convert to scheme A.
13	0	0	0	12	Reverse sign of matrix.
14	0	1	10	13	Convert to scheme B.
15	10	0	0	11	Punch out vector $K_n x_{n+1}$.
16	0	0	4	33.	Jump to instruction 4 and obey.

Bricks

No.		
1	Read matrix	LR07B/2
2	Standardise matrix	LZ69B
3	Transpose matrix	LT03
4	Scalar product	LM07B
5	Matrix multiply	LM05B (3 sections)
8	Expand scalar as matrix	LZ19B/1
9	Scalar divide	LZ06A
10	Matrix square root	LZ18B/1
11	Punch matrix	LP15BT
12	Reverse signs	LZ04A
13	Convert to scheme A or B	LZ20B

11. 2. Linear Equations and Iteration.

The whole operation of solving the linear equations and performation is done by a G.I.P. programme. The normalisation of the vectors is done by dividing by the largest element in the vector. The codewords and bricks for this programme are given below:

Codewords

No.	a	b	c	r	
0	0	0	170	1	Read guess vector, x_i, 1 X n.
1	0	0	40	1	Read band matrix B, n X n.
2	170	n	1	7	Change parameters to n X 1.
3	40	170	40	2	Compound matrices, B and x_i.
4	40	1	164	48	Plant auxialary codeword.
5	29	6	22	3	Obey LEO 7B and form x_{i+1}.
6	164	1	n	7	Change parameters to 1 X n.
7	164	0	162	8	Find maximum element of x_{i+1}.
8	162	0	0	9	Punch out maximum element, c.
9	4	0	0	48	Plant divide codeword.
10	164	162	170	10	Divide x_{i+1} by c and replace x_i.
11	170	0	0	9	Punch out x_{i+1} / c.
12	170	n	1	7	Change parameters to n X 1.
13	0	0	1	33	Jump to codeword 1 and continue.

Bricks

No.		
1	Read binary matrix	LR16BT
2	Compound matrices	LZ08B / 1

3	Solve linear equations	LE07B
7	Change parameters of matrix	LZ51B
8	Find maximum element	LZ21B/1
9	Punch matrix	LP15BT
10.	Term by term arithmetic	LZ61B

12. References.

1. D.Polder, Phil.Mag.,Vol.40, pp.99-115, 1949.
2. N.G.Sakiotis, H.N.Chait, Trans.I.R.E.,MTT-1, pp.11-16, 1953.
3. C.L.Hogan, B.S.T.J.,Vol.31, pp.1-31,Jan., 1952.
4. P.H.Vartanian, J.L.Melchor, W.P.Ayres,
   Trans.I.R.E.,MTT-4, p.8, 1956.
5. S.Weisbaum, H.Boyet, Proc.I.R.E.,Vol.44, pp.554-555, Apr., 1956.
6. S.Weisbaum, H.Seidel, B.S.T.J.,Vol.35, pp.877-898, July, 1956.
7. S.Weisbaum, H.Boyet, Trans.I.R.E.,MTT-5, pp.194-198, 1957.
8. A.G.Fox, S.E.Miller, M.T.Weiss,
   B.S.T.J.,Vol.34, pp.5-103, Jan., 1955.
9. M.T.Weiss, Trans.I.R.E.,MTT-4, pp.240-243, Oct., 1956.
10. B.J.Duncan, B.Vafiades, Trans.I.R.E.,MTT-6, p.411, 1958.
11. B.Lax, Trans.I.R.E.,MTT-6, p.5, 1958.
12. W.W.Anderson, M.E.Hines, Trans.I.R.E.,MTT-9, pp.63-67,Jan., 1961.
13. P.H.Vartanian, W.P.Ayres, A.L.Helgesson,
   Trans.I.R.E.,MTT-6, pp.215-222, 1958.
14. E.S.Grimes, D.D.Bartholomew, D.C.Scott, S.C.Sloan,
   Trans.I.R.E.,MTT-8, pp.489-492, 1960.
15. E.Schlomann, Trans.I.R.E.,MTT-8, pp.199-206, 1960.
16. J.A.Stratton, 'Electromagnetic Theory',McGraw-Hill, p.12, 1941.
17. F.Young, J.Hohmann, Appl.Sci.Res.,Sect.B,Vol.8, pp.321-336.
18. R.F.Soohoo, 'Theory and Application of Ferrites',
   Prentice Hall, p.171, 1960.
19. L.G.H.Huxley, 'Principles and Practice of Waveguides',
   C.U.Press, p.27, 1947.
20. L.G.Lewin, 'Advanced Theory of Waveguides',Iliffe, p.147, 1951.
21. S.B.Cohn, Proc.I.R.E.,Vol.34, P.783, 1947.
22. P.N.Butcher, R.R.E. Memorandum No.1055,
23. N.Marcuvitz, 'Waveguide Handbook', M.I.T.10, p.1, 1951.
24. R.E.Collin, 'Field Theory of Guided Waves',McGraw-Hill,p.172,1960.
25. R.V.Southwell, 'Relaxation Methods in Engineering Science',
   O.U.Press, 1960.

26. D.S.I.R. Notes, 'Modern Computing Methods', p.29, 1960.
27. A.Thom, C.J.Apelt, G.F.J.Temple, 'Field Computations in Engineering and Physics',Van Nostrand, pp.23-24, 1961.
28. N.Marcuvitz, 'Waveguide Handbook',M.I.T.10, p.399, 1951.
29. S.Hopfer, Trans.I.R.E.,MTT-3, pp.20-29, 1955.
30. T.S.Chen, Trans.I.R.E.,MTT-5, pp.12-17, 1957.
31. B.Lax, K.J.Button, L.M.Roth,J.Appl.Phys.,Vol.25,pp.1413-1421,1954.
32. P.J.B.Clarricoats, 'Microwave Ferrites',Chapman-Hall,p.114, 1951.
33. D.G.Kiely, 'Dielectric Aerials',Methuen Mono.,p.20, 1953.
34. D.Doughty, G.E.C. Research Report, 'Garnet-structure yttrium ferrite'.
35. S.B.Cohn, Trans.I.R.E.,MTT-3, pp.16-21, 1955.
36. D.J.Sullivan, D.A.Parkes, Trans.I.R.E.,MTT-8,pp.212-217, 1960.
37. S.A.Schelkunoff,'Electromagnetic Waves',Van Nostrand,Ch.8, 1956.
38. D.N.de G.Allen,'Relaxation Methods',McGraw-Hill,p.90, 1955.
38a. H.N.Chait, N.G.Sakiotis, Trans.I.R.E.,MTT-7,pp.38-41, 1959.
39. B.J.Duncan, L.Swern, K.Tomiyasu, J.Hannumacher, Proc.I.R.E.,Vol.45, pp.483-490, 1957.
40. P.J.B.Clarricoats, Proc.I.E.E.,Monograph 410E, 1960.
41. H.Seidel, Proc.I.R.E.,Vol.44, p.1410, 1956.
42. P.J.B.Clarricoats, Proc.I.E.E., Monograph 409E, 1960.
43. A.W.Trivelpiece, A.Ignatius, P.C.Holscher, J.Appl.Phys.,Vol.32,No.2, pp.259-267.